Stanford Geothermal Program
Tnterdisciplinary Research
in Engineering and Earth Sciences
Stanford University
Stanford, California

# A LABORATORY MODEL OF STIMULATED GEOTHERMAL RESERVOIRS

by
A. Hunsbedt
P. Kruger
A. L. London

February 1975

This research was carried out
under Research Grant GI-34925
by the National Science Foundation

## ABSTRACT

A laboratory model (the chimney model) of a fractured rock chimney created by artificial stimulation of geothermal reservoirs has been constructed. The model has been used to study the behavior of a water/rock system resembling that created by fracturing of an originally dry hot rock geothermal region at maximum initial temperature and pressure of 500°F and 790 psia, respectively. The water/rock system is contained inside a steel vessel which constitutes an artificial environment, therefore, initial efforts were directed at obtaining calibration data to be used in correcting this "wall effect." A detailed presentation of this effort is given in the present report. The results show that the wall effect can be accounted for and meaningful experiments can be run with the model. Fluid production/pressure depletion tests were run for two systems, one had water only in the chimney and the other had a granite rock loading consisting of rocks with an average equivalent diameter of approximately one inch with drainage porosity of 43.7 percent. One run was made with partial recharge of cool water. Preliminary results of these experiments show that the thermal energy stored in the hot rock can be extracted efficiently by reducing system pressure and letting the flash front recede into the rock matrix. More than 90 percent of the energy in the rocks available between the temperature limits during these tests was extracted. The energy extracted from the rock increased the fraction of original water in the system that could be produced by roughly a factor of two for the water/rock system under the conditions of these experiments.

## ACKNOWLEDGMENTS

The support by the National Science Foundation under Grant No. GI-34925 during both the construction phase and early experimental phase of this program is gratefully acknowledged.

TABLE OF CONTENTS

LIST OF FIGURES

LIST OF TABLES

## NOMENCLATURE

English Letter Symbols

$A$ = area ($ft^2$)

$a$ = length dimension of rock (cm)

$a_1, a_2, a_3$ = parameters in transient model--defined in text (1/hr)

$b$ = breadth dimension of rock (cm)

$C$ = specific heat capacity ($Btu/lb_m$ °F)

$C_{ij}$ = multipliers in system transient solution--defined in text (°F)

$c$ = thickness dimension of rock (cm)

$D \triangleq d/dt$ = differential operator (1/hr)

$d$ = rock equivalent diameter (cm)

$e$ = specific internal energy ($Btu/lb_m$)

$e$ = 2.71...basis of natural logarithm (dimensionless)

$H$ = height dimension (in)

$h$ = heat transfer coefficient ($Btu/hr\ ft^2$ °F)

$h$ = height of rock matrix (in)

$i$ = specific enthalpy ($Btu/lb_m$)

$k$ = statistical parameter - peakedness (dimensionless)

$\ell$ = true flash front position measured from top (in)

$\ell'$ = indicated flash front position (in)

$M$ = mass ($lb_m$)

$M^*$ = mass fraction - normalized to initial mass (dimensionless)

$\dot{m}$ = mass flow rate ($lb_m/hr$)

$m_{1,2}$ = inverse time constants, defined by Eq. (A.10) (1/hr)

$n$ = statistical sample size (dimensionless)

$P$ = pressure (psia)

$P^*$ = nondimensional pressure - normalized to initial pressure (dimensionless)

$Q_m$ = total external heat transfer from metal chimney (Btu)

$q_m$ = specific external heat transfer parameter ($Btu/lb_m$)

$S_1$ = electric power supply - circulation heater (Btu/hr)

$S_2$ = electric power supply - tape heaters (Btu/hr)

$Sk$ = statistical parameter - skewness (dimensionless)

$s$ = specific entropy ($Btu/lb_m$ °F)

$s$ = Laplace transform variable (1/hr)

$s^2$ = statistical parameter - variance ($cm^2$)

$T$ = temperature (°F)

$t$ = time (hr)

$t^*$ = dimensionless time, defined in text (dimensionless)

$u(t-\tau)$ = unit step function, defined in text (dimensionless)

$V$ = volume ($ft^3$)

$v$ = specific volume ($ft^3/lb_m$)

$X$ = steam quality (dimensionless)

$\bar{X}$ = statistical parameter - mean value (cm)

Greek Letter Symbols

$\alpha$ = void fraction (dimensionless)

$A$ = characteristic matrix (dimensionless)

$\eta$ = rock energy extraction efficiency, defined in text (dimensionless)

$\varphi$ = drainage porosity of rock matrix (dimensionless)

$\psi$ = roundness factor of rock, defined in text (dimensionless)

$\rho$ = density ($lb_m/ft^3$)

$\sigma$ = statistical parameter - standard deviation (cm)

$\tau_{11}$ = time when electric heater is turned on (hr)

$\tau_{12}$ = time when electric heater is turned off (hr)

$\tau_{21}$ = time when heater tapes are turned on (hr)

$\tau_{22}$ = time when heater tapes are turned off (hr)

$\theta = T - T_\infty$ = excess temperature ($^\circ F$)

$\theta^* = (T - T_\infty)/(T_o - T_\infty)$ = nondimensional temperature (dimensionless)

Subscripts

C = cool side of heat exchanger

c = chimney

d = drainage from outlet line

e = exit conditions

f = saturated liquid

f = final - quantity at end of production cycle

fg = vaporization

g = saturated vapor

G = vapor in any state

H = hot side of heat exchanger

i = injection or recharge

in = inlet of heat exchanger

L = liquid of any state

o = initial - quantity at start of production cycle (t = 0)

out = outlet of heat exchanger

p = production

r = rock

SC = steam cap

SG = sight glass

w = water in chimney

1 = lumped mass of water and rock of (1) total system, or (2) chimney only

2 = lumped mass of (1) total system metal, or (2) of chimney metal

$\infty$ = surroundings

Special Symbols

$\bar{\ }$ = average value

$( )'$ = derivative with respect to pressure

$\hat{\ }$ = Laplace transformed variable

$\cdot$ = quantity on a rate basis

$( )_o$ = quantity at start of production cycle (t = 0)

$\bar{( )}$ = mean value of enclosed quantity

# CHAPTER 1

## INTRODUCTION

Geothermal energy stored in the earth's crust has been utilized on a limited scale for centuries. However, its conversion for electric power production initiated in **1913** is currently receiving considerable attention in view of the shortages of conventional energy sources and the environmental concerns and construction problems associated with nuclear power stations. The existence of vast energy potentials in the earth's crust can easily be demonstrated (Kruger and Otte, 1973), however, the problem is how to extract the energy economically. White (in Kruger and Otte, **1973)** predicts that only an insignificant amount of the available geothermal energy sources will be developed over the next two decades with present technologies. If this energy source is to become a significant portion of the energy supply development of new technologies is needed. One promising technology is the stimulation of geothermal resources.

Stimulation of natural resources is not a new concept, for example experiments on stimulation of natural gas resources have been underway for several years (Atkinson and Ward, **1967).** However, the application of this technology to geothermal resources has only recently been considered (Kruger and Otte, **1973).** Geothermal resources containing hot water with low porosity and permeability may be made more productive by artificial fracturing of the host rock (stimulation) using proposed stimulation techniques such as nuclear or conventional explosives, hydrofracturing, or thermal fracturing. **Also,** artificial fracturing of dry hot rock and introduction of water which is heated by the cracked rock may greatly enlarge potential geothermal resources.

How much of the thermal energy stored in the rock can be extracted by resource stimulation is not clear. To help provide answers to this question and other related questions a laboratory model of a stimulated geothermal reservoir (chimney model) was constructed.

The chimney model project is part of the Stanford Geothermal Program which comnenced as an interdisciplinary program at Stanford University

during the 1972-1973 academic year. The initial phase of the project involved the design and construction of the laboratory model with associated auxiliary loops and equipment for heatup and production operations. The major test objectives of the program are to obtain experimental data on the processes of in-place boiling, moving flash fronts, and two-phase flow in hot porous media, as well as chemical and radiochemical data for fluids production. Specifically the studies include: (1) optimum rock energy extraction, (2) cyclic and continuous recharge, (3) heat transfer characteristics, (4) water quality aspects, and (5) experimental data for analytic models.

The design and construction of the chimney model test system occurred during 1973 and the system was placed in operation in March of 1974. Initial testing was directed at obtaining calibration data prior to loading the chimney with rock. In August 1974 testing with the first load of granite rock of approximately one inch equivalent diameter rocks was initiated. Experimental data have been obtained for conditions similar to those of fractured hot rock systems, mostly without recharge. This report presents the first results from the chimney model experiments to disseminate the information at the earliest possible time. The report reviews the following achievements:

1. Design, procurement, and construction of the chimney model system and associated instrument systems;
2. Initial checkout of the system and the acquisition of calibration data with water only in the chimney;
3. Analysis of the system calibration data and establishment of the system's limitations with respect to providing useful test information.

Documentation for item (1) above is available (Kruger and Ramey, 1973; Kruger and Ramey, 1974) and therefore only a description of the current chimney model system is included here. The analysis of the experiments for items (2) and (3) are considered as preliminary. Further analysis will be needed before a final reporting can be completed.

CHAPTER 2

# DESCRIPTION OF TEST APPARATUS

## 2.1 Chimney Model System

The chimney model and associated equipment, hereafter referred to as the chimney model system or simply as the system, is located in the Lloyd Noble Laboratory of Petroleum Engineering at Stanford University, California.

The piping and instrumentation diagram of the system is given in Fig. 2.1. Figure 2.2 shows a side view of the chimney model system, while Fig. 2.3 shows a view of the chimney model and associated support structure. The system is constructed primarily from low carbon steel and is designed to ASME standards. The system includes a high pressure safety relief system to vent the high pressure fluid to the atmosphere in case of accidental overpressurization. Additionally, a blowdown system that can be operated manually from a remote location is included. The operating parameters of the chimney system model are listed in Table 2.1.

**TABLE 2.1**

**Chimney Model System Operating Parameters**

| | |
|---|---|
| Operating pressure (max) | 800 psig |
| Operating temperature (max) | 500°F |
| Chimney water/rock inventory | ~ 15 $ft^3$ |
| Total system water/rock inventory | ~ 19 $ft^3$ |
| Average heating rate | ~ 40°F/hr |
| Condenser cooling flow rate (max) | 2 gpm |
| Circulation flow rate during heatup (max) | 15 gpm |
| Recharge flow rate (continuous) | 0-1 gpm |
| Electric heater capacity | 23 kW |
| Tape heater capacity (chimney) | 4 kW |
| Tape heater capacity (water inlet) | 2 kW |

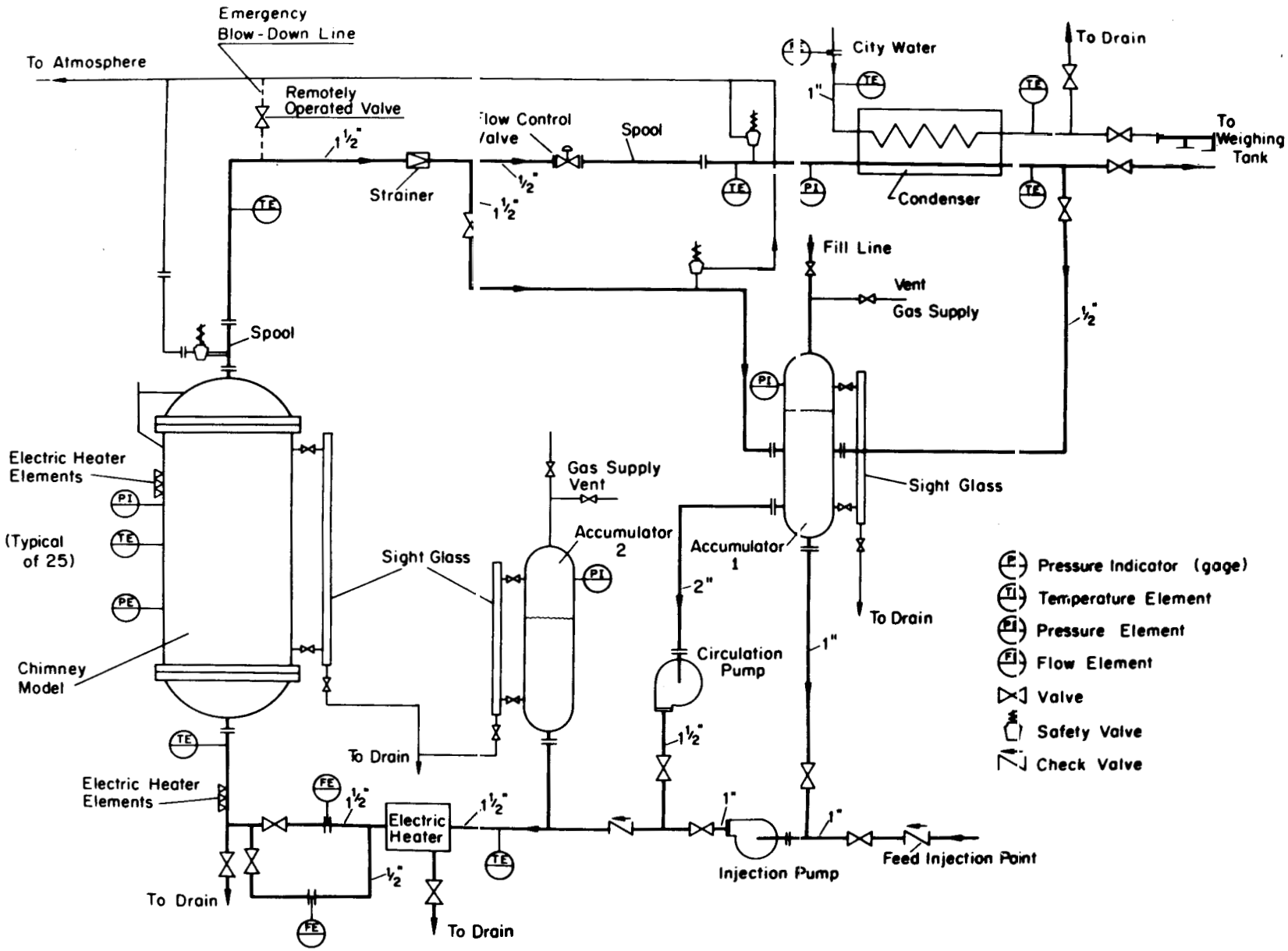


Figure 2.1 Piping and instrumentation diagram for chimney model system

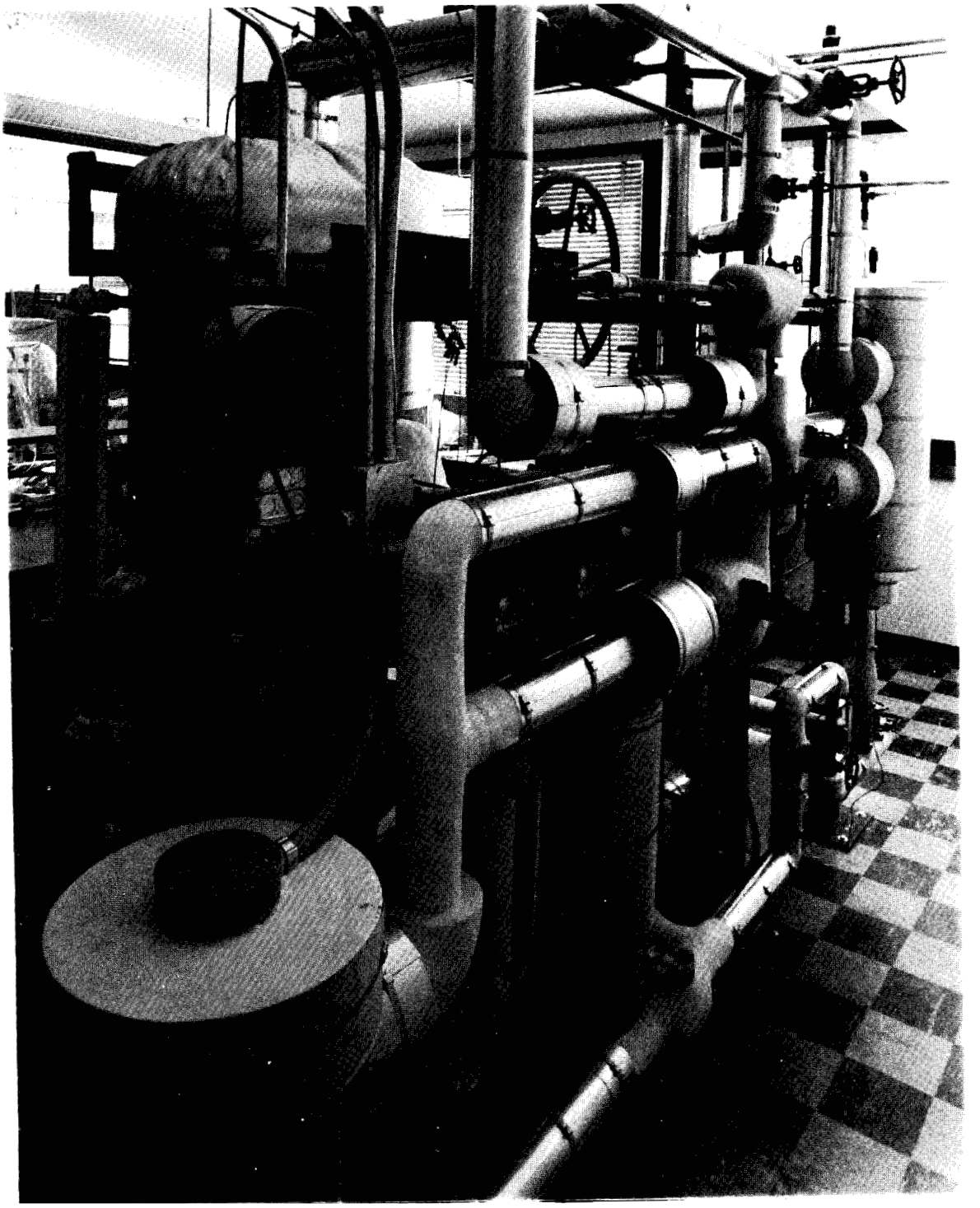

**Figure 2.2** View **of chimney model system upon construction completion**

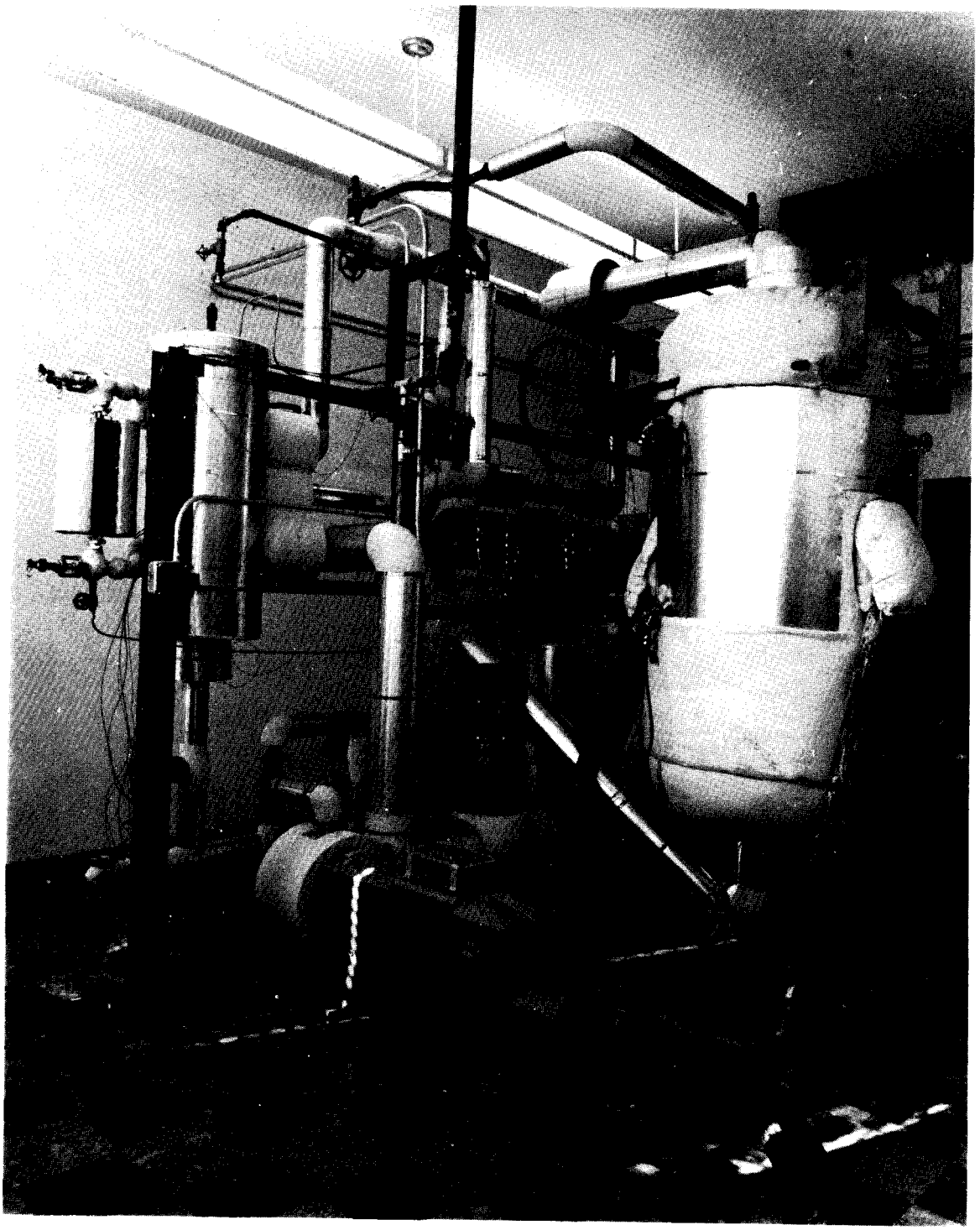

Figure 2.3 View of chimney and support structure upon construction completion

### 2.1.1 Chimney Model

The chimney model or steel vessel which simulates a fractured rock chimney produced by explosive, hydraulic, or thermal-stress fracturing is 2 feet I.D. and approximately 5 feet high. The lower head is connected to the vessel shell by standard bolted flanges while closure at the top end is accomplished using a "quick opening" head (Tube-Turn). The vessel shell has numerous nozzles for instrumentation entry for measurement of chimney temperatures and pressures. A sight glass is installed on the shell to observe water/steam level movements during operation of the system.

The vessel is supported on an axis through its approximate center of gravity by brackets which allow the vessel to be rotated 90 degrees from a vertical position to a horizontal position after inlet and outlet piping, instrumentation, and other connections are disconnected from the vessel. This provides easy access to the lower section of the vessel during rock loading and instrumentation of the rock load. The vessel shell has tape heaters wrapped around the outside diameter with heating power control sufficient to compensate for heat losses, or to provide energy to the water/rock system at a desired rate. The vessel is insulated with approximately 4 inches of insulation.

To assure uniform flow distribution at the lower end of the vessel (inlet), a flow distribution baffle is installed in the lower head. A diagram of the flow distribution baffle arrangement is shown in Fig. 2.4 and a view of the low side of the baffle prior to installation is shown in Fig. 2.5.

### 2.1.2 Auxiliary Components

An electric heater in the circulation piping supplies the thermal energy necessary to establish the initial temperature/pressure conditions of the chimney system in an acceptable length of time. It is also used to preheat the recharge water to desired temperature conditions. The circulation heater, prior to installation of electrical supplies and insulation, is shown in Fig. 2.6. The heater is controlled by an on/off thermostat. A continuous automatic power control system is being installed which will enhance the utility of the heater.

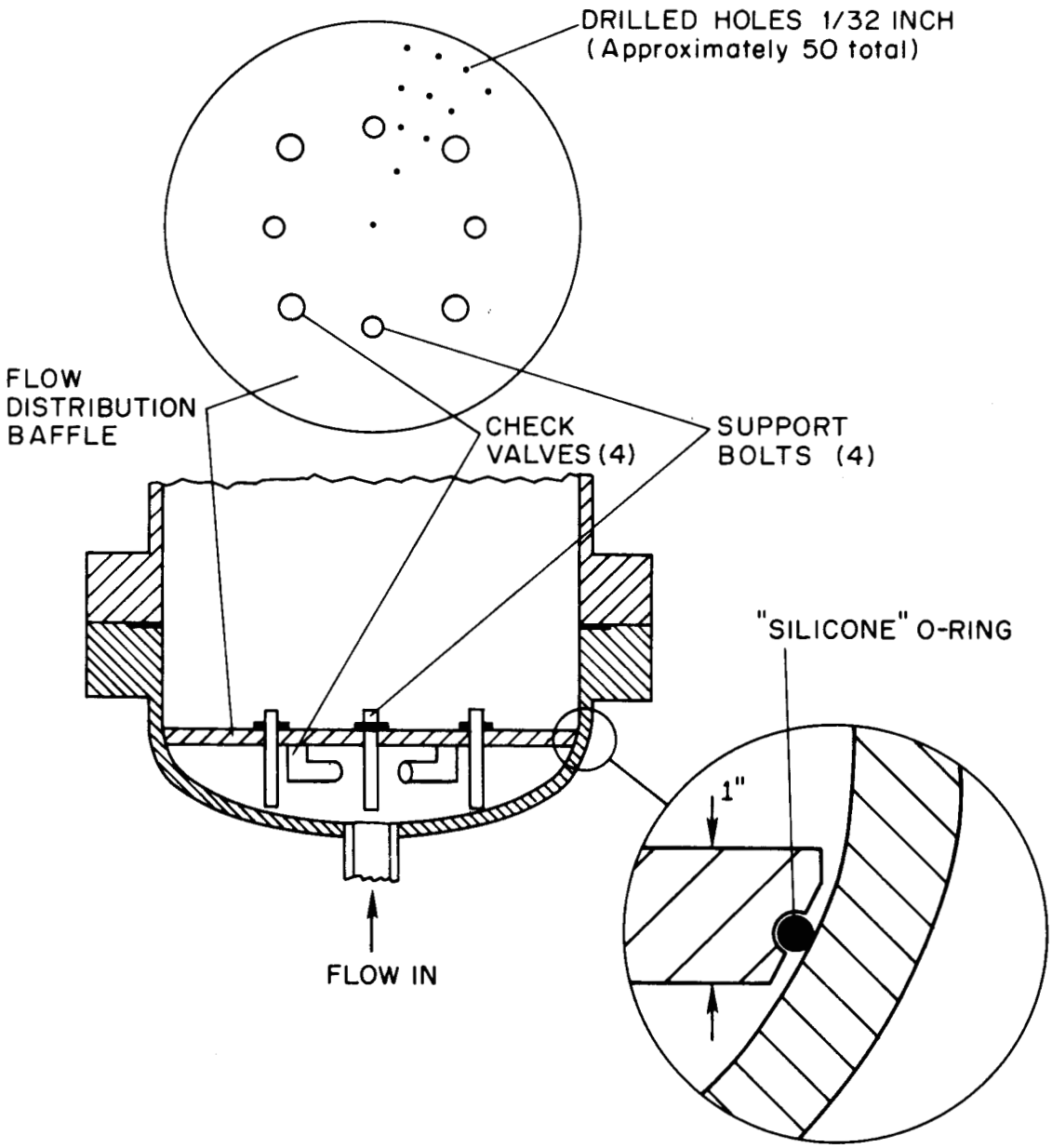


**Figure** *2.4* **Diagram of flow distribution baffle arrangement**

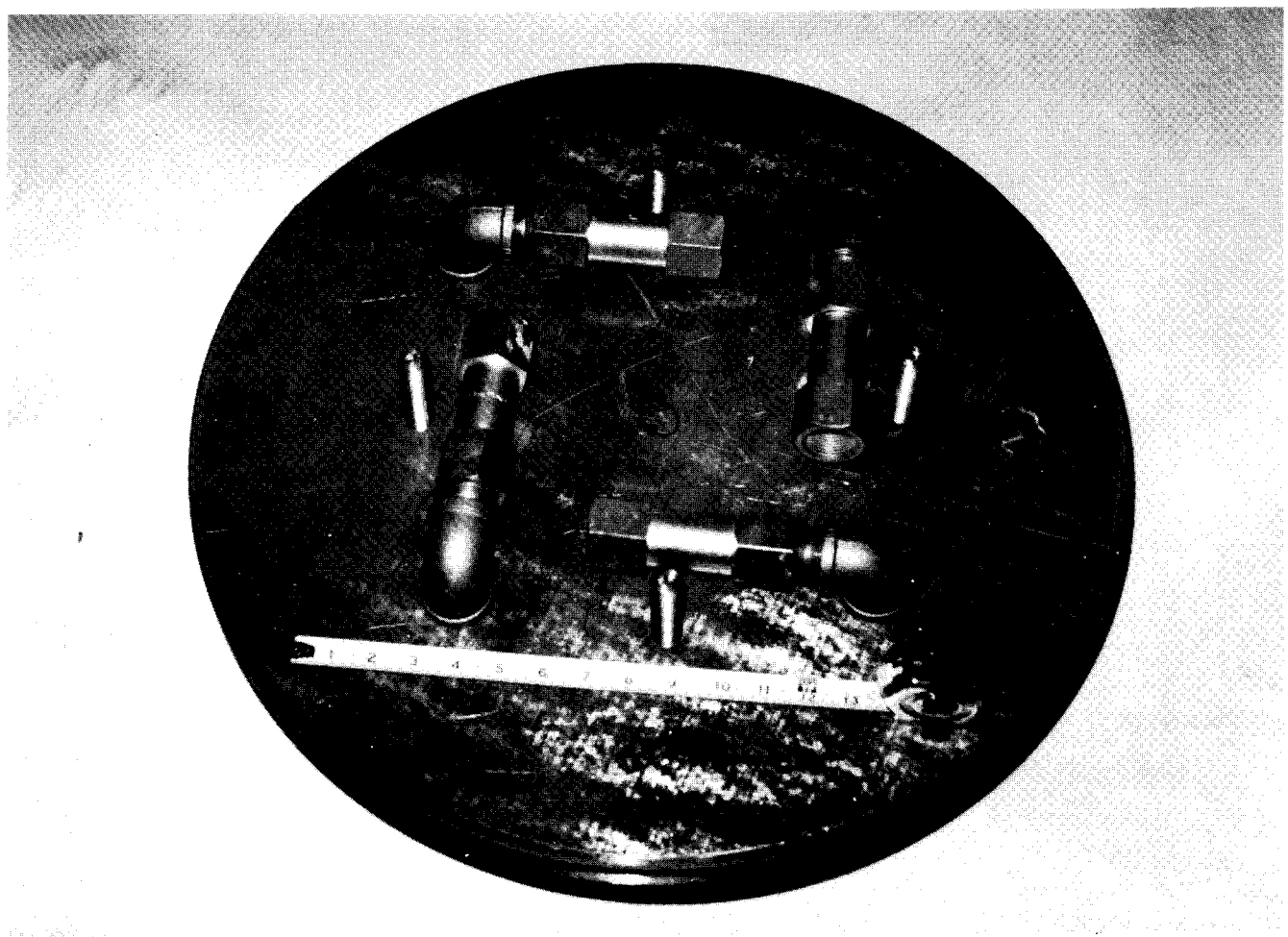

Figure 2.5 View of low side of flow distribution baffle

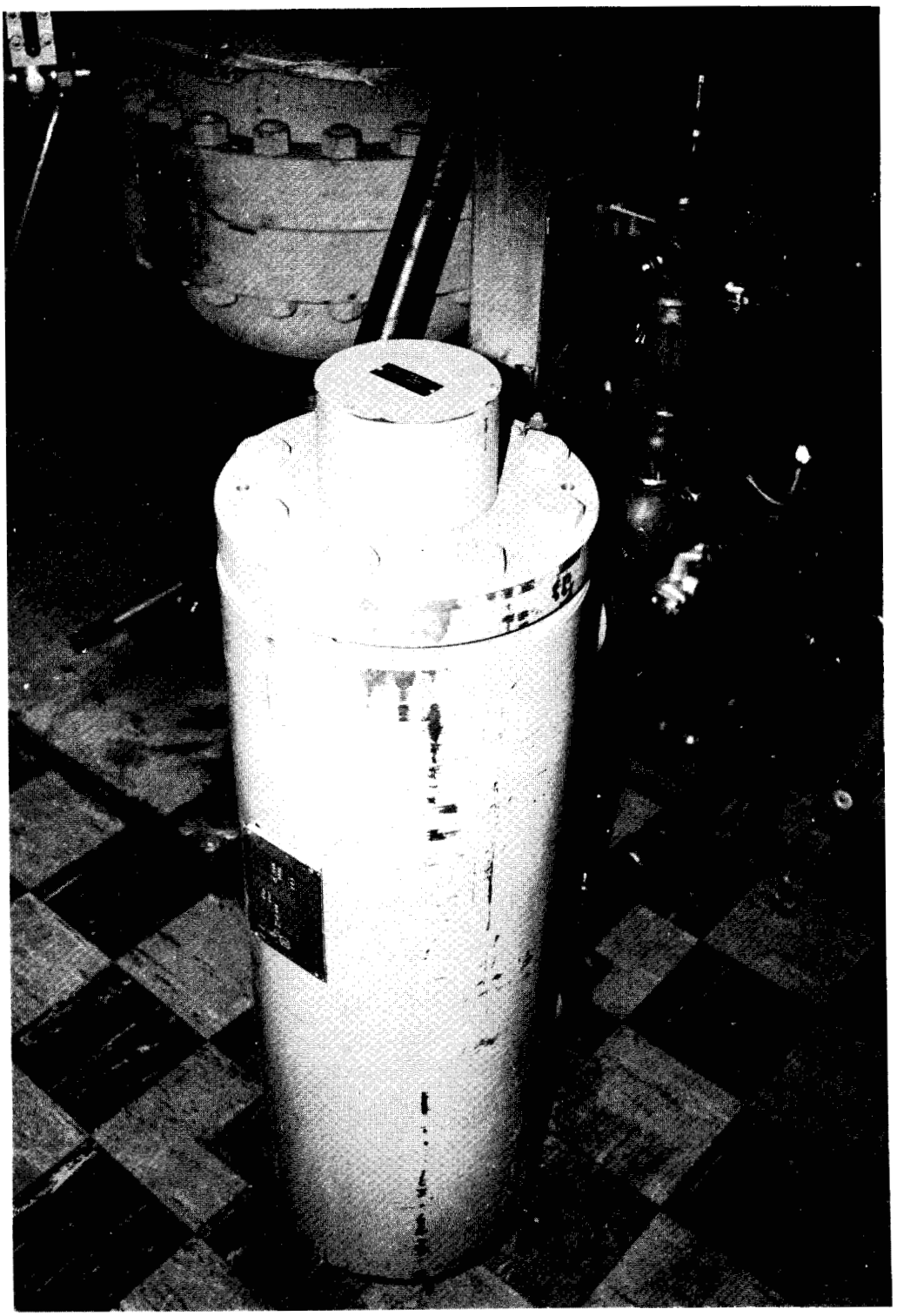

Figure 2.6 Side view of chimney model system with the electric circulation heater in the foreground prior to installation of insulation

A 15 gpm centrifugal pump provides 9 feet head for the circulation flow. A view of this pump prior to installation of insulation is shown in Fig. 2.7. The pump housing and parts in contact with water are made from stainless steel. The 1 gpm injection pump used to recharge the chimney is a positive displacement pump delivering a maximum head of 800 psi. The injection pump is shown as the component in the foreground in Fig. 2.3 and in the background in Fig, 2.7. The flow rate can be controlled continuously by adjustment of the piston displacement in the range 0-1 gpm. Parts in contact with water are made from stainless steel.

The system has two accumulators fabricated from low carbon steel, each with a water level sight glass. Accumulator 1 has a volume of approximately 1.5 $ft^3$. Its primary functions are to provide, (1) an expansion volume during heatup, (2) a free gas surface for inert gas pressurization of system to avoid flashing during heatup, and (3) a head tank suction supply for the circulation and injection pumps. Accumulator 2 has a volume approximately 0.5 ft3. Its functions are: (1) damping of pulses originating in the positive displacement injection pump, (2) inert gas pressurization of recharge water to avoid flashing in the electric heater during recharge, and (3) expansion volume during heatup.

The circulation loop is constructed from schedule 80 low carbon steel piping (sizes 1/2, 1, 1-1/2, and 2 inch). Except for connections to chimney, pumps, electric heater and various other components, the piping is all welded (140 high pressure welds). The system can be emptied at two low points by the drain valves which release approximately 99 percent of the system fluids. The piping system, accumulators and other pertinent components are covered with 1-1/2 to 2 inches of insulation.

### 2.1.3 Chimney Model System Operation

The system operates in two primary modes; the "heating mode" (see Fig. 2.8) which establishes the initial reservoir temperature and pressure conditions in a relatively short time, and the "fluid production mode" (see Fig. 2.9) during which production from a fractured geothermal system is simulated. A summary of these modes helps describe the system operation. The system is filled with water to desired levels through the make-up water line. Pressurization of the system to 100-200 psig is accomplished by addition of argon gas to accumulators 1 and 2. The

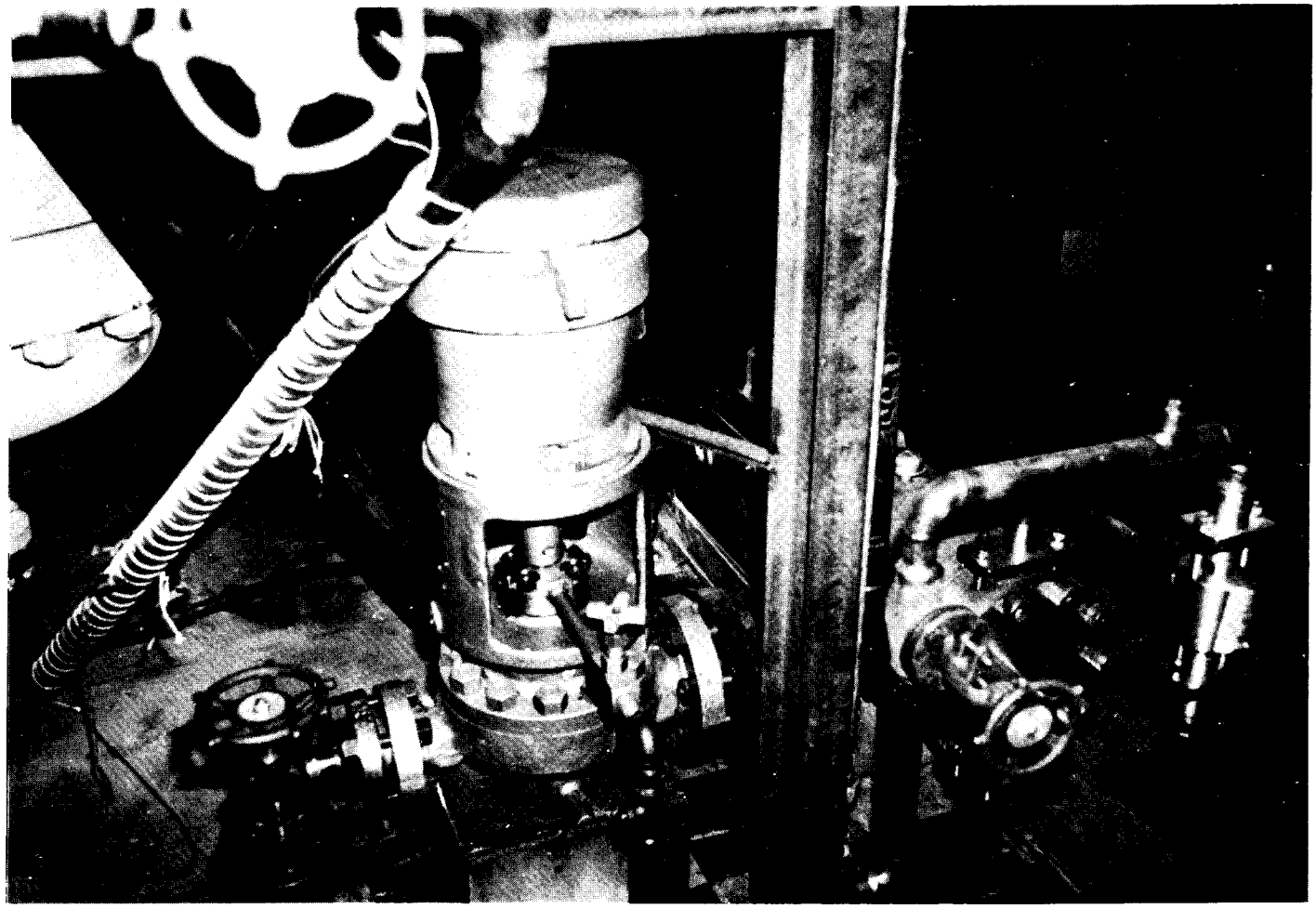

Figure 2.7 View of circulation pump prior to installation of insulation

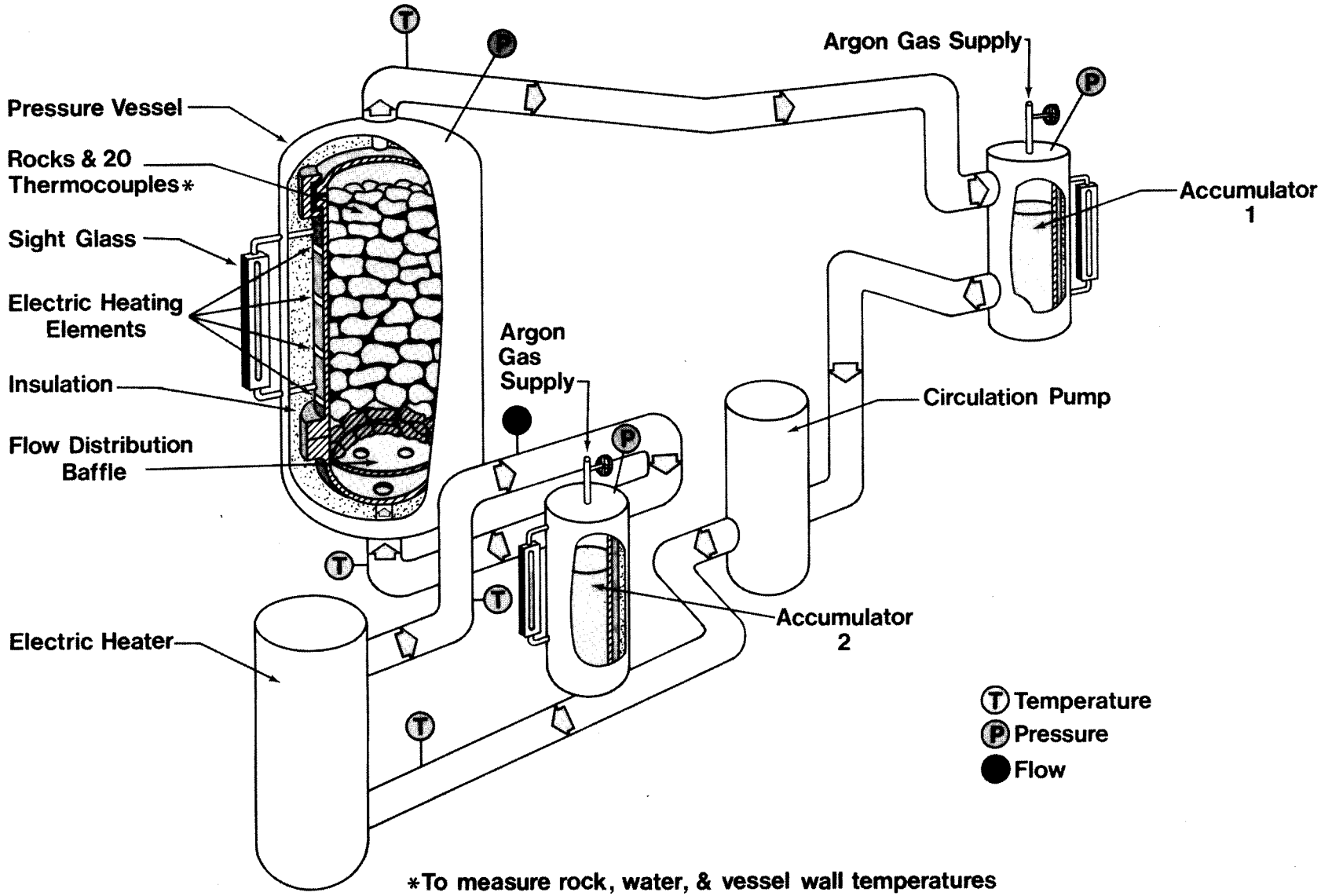


Figure 2.8 Diagram of chimney model system - heating mode operation

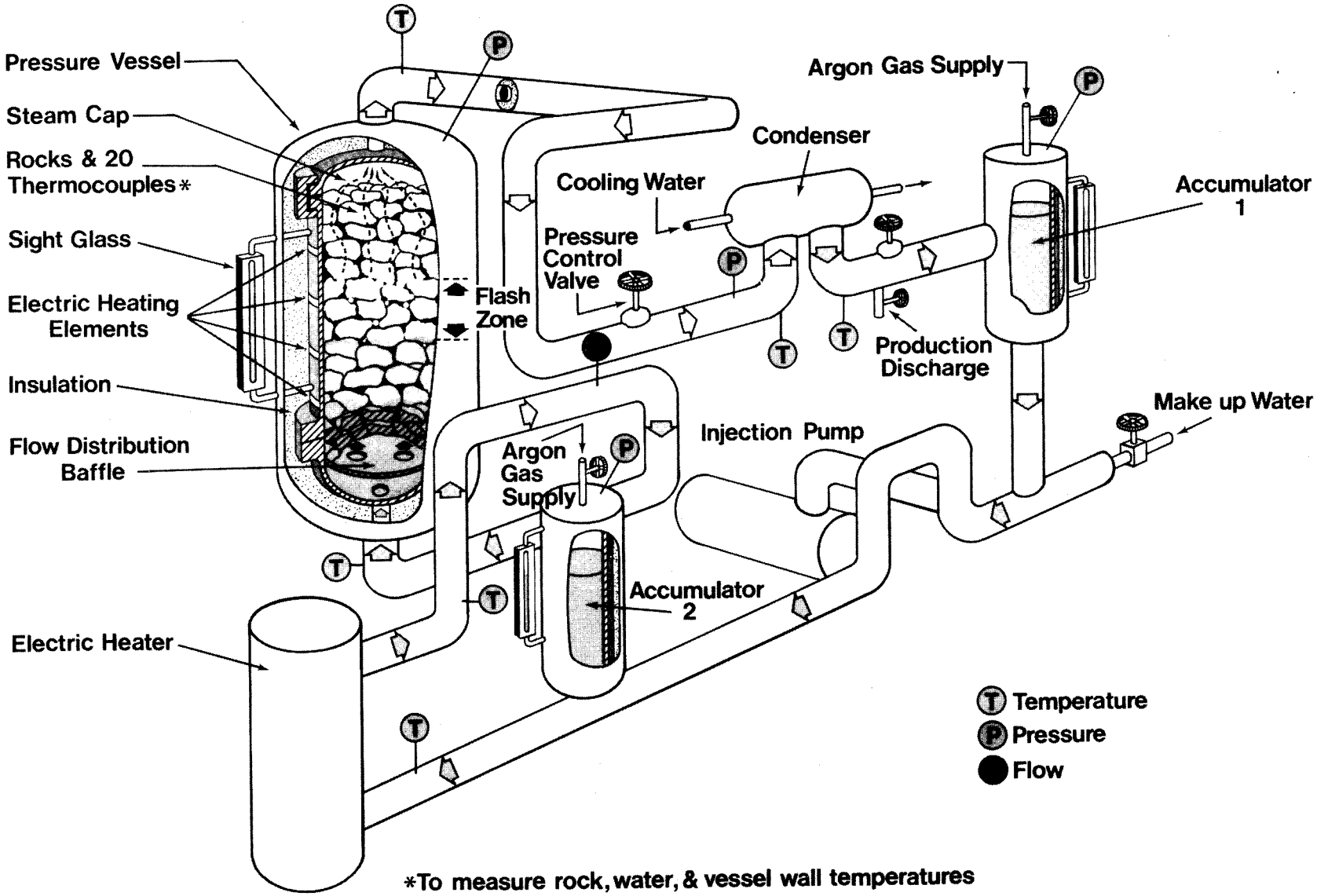


Figure 2.9 Diagram of chimney model system - fluid production mode operation

circulation pump starts the flow of water through the electric heater where it acquires its thermal energy with an approximately 10°F increase in temperature. The water from the heater circulates through the chimney where some of its energy is transferred to the vessel and the rock loading. Water at the chimney water mixture temperature is then returned via accumulator 1. Heatup circulation is continued until the desired temperature and pressure conditions are achieved and temperature equilibrium of the rock/water/metal system is established.

Fluid production is initiated by opening the pressure control valve. The produced fluids are passed through the condenser and subsequently either: (1) removed from the system through the production discharge line into a weighting system, or (2) returned through accumulator 1. Recharge of the system is accomplished by the injection pump which draws fluids from: (1) a make-up water line, or (2) accumulator 1, depending on the choice of production scheme.

The recharge water is preheated in the electric heater to the desired recharge temperature and enters the chimney uniformly through the flow distribution baffle.

## 2.2 Instrumentation

The parameters measured during operation of the system are summarized in Table 2.2.

TABLE 2.2

Summary of Measured Parameters

| | |
|---|---|
| Temperature | Terminal temperatures for chimney model, electric heater, condenser |
| | Water temperature distribution in chimney |
| | Rock temperature distribution |
| | Metal temperature distribution |
| Pressure Sensors | Chimney |
| | Accumulators |
| | Condenser |
| Flow Rate Meters | Circulation |
| | Injection |
| | Condenser cooling water |
| | Production flow rate (gravimetric measurement) |

The locations of the loop pressure, temperature and flow measurement sensors are indicated in Figs. 2.1, 2.8, and 2.9. Pressure indicators are installed on components according to ASME code requirements, and are not intended to be used for obtaining primary experimental data. Sensors for acquiring experimental data are discussed individually in the following.

### 2.2.1 Temperature and Pressure Measurements

The thermocouples used for loop temperature measurement are all 1/8 inch diameter stainless steel sheathed (grounded) iron/constantan thermocouples (type J). The positions of the thermocouples used to measure the chimney water, rock and metal temperature conditions are shown in Fig. 2.10. The thermecouples used for water and rock temperature measurement are 1/16 inch in diameter (type J). Holes are drilled in typically shaped rocks to the approximate center of the rock, and the thermocouples are cemented in place with a high temperature porcelain-like cement. The water temperatures are measured adjacent to the "instrumented" rocks to obtain rock/water temperature differences, and at other points to obtain axial and radial profiles. All thermocouples are inserted through the vessel wall by Conax high pressure fittings. The metal temperatures are measured using unsheathed fine-gage (type J) thennocouples cemented to the metal surface with high temperature cement. All thermocouple measurements are recorded on multipoint recorders. The loop metal temperatures are measured at accumulators 1 and 2. The pressure in the chimney is measured with an electronic pressure transmitter employing a Bourdon-tube as the primary sensing element.

### 2.2.2 Flow Measurements

The circulation flow rate during heating is measured using an orifice designed to ASME standards and installed in a 1-1/2 inch line. The measured pressure difference is converted to an electrical signal by an electronic differential pressure transmitter which is fed to the multipoint recorders. The recharge flow is measured using another orifice installed in a 1/2 inch line. The condenser cooling water flow rate is measured using an orifice installed in the 1 inch water line. The recording of the measurements is the same as for the circulation flow measurements. The produced fluid is weighed in the collection tank as a function of time from which the fluid production rate can be computed.

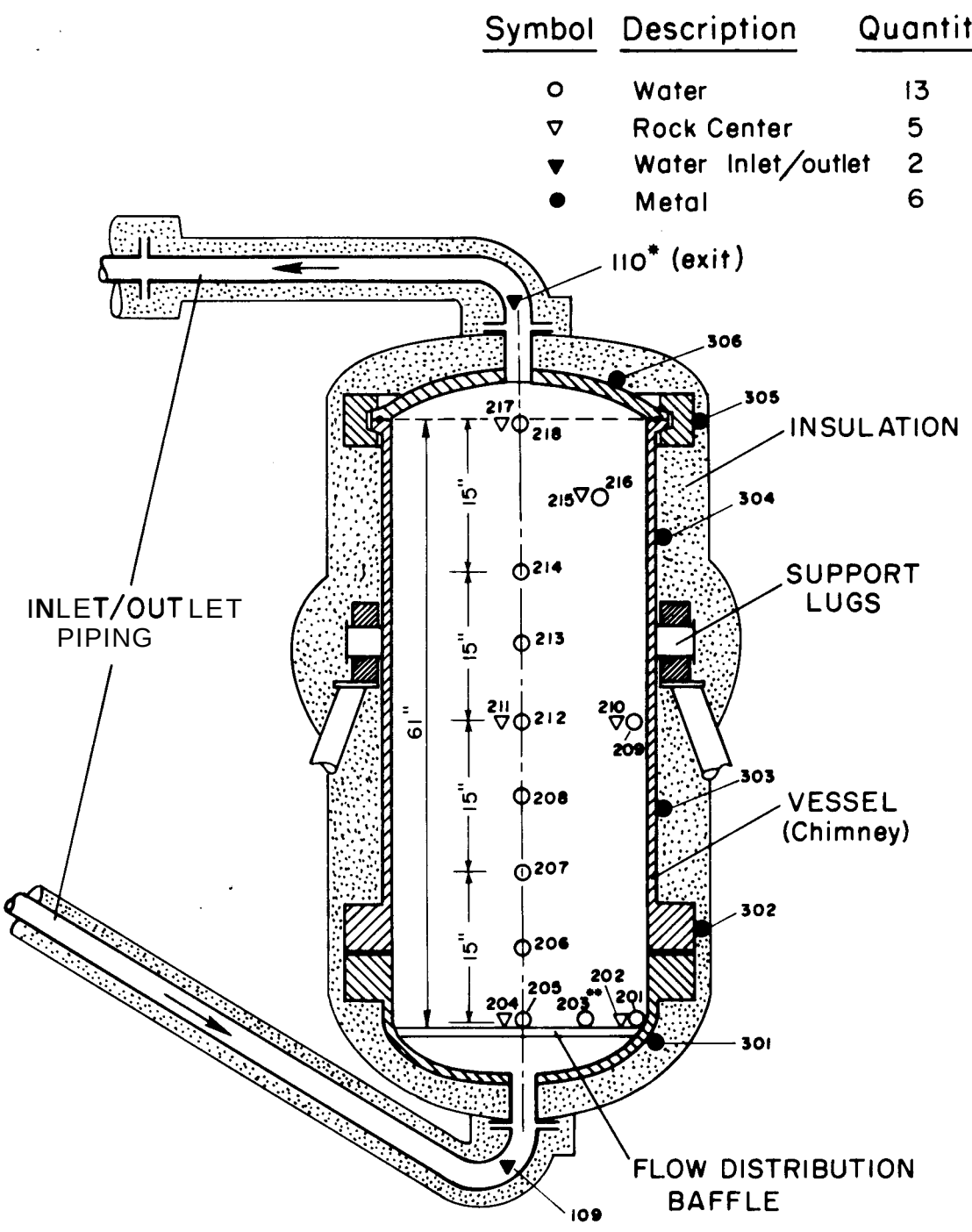


* Numbers refers to thermocouple numbers

**Located in the 45° plane relative to paper plane where all other T/c's are located

Figure 2.10 Diagram showing locations of thermocouples for measurement of chimney model temperature conditions

# CHAPTER 3

## TRANSIENT ANALYSIS AND CALIBRATION OF MODEL

The thermal characteristics of the steel vessel (chimney model) are substantially different from those of a fractured rock system located underground. In the natural system the heat transfer by convection and conduction from the formation (region not cracked) rock to the fractured rock/water system would in general be small. On the other hand the combined effect of heat losses to the environment from the chimney metal can result in considerable energy transfer. These differences may complicate the interpretation of the fluid production and pressure decline behavior of the simulated water/rock system. Therefore, it is important to determine the magnitude of this "wall effect" and, if possible, offset it by supplying energy at appropriate rates by artificial means.

The magnitude of the internal energy stored in the chimney metal can be expressed in terms of the mass, specific heat, and temperature product as

$$e = M \cdot C \cdot T ,$$

where the temperature is measured with respect to some reference level. The temperature readings from the six thermocouples located on the outside wall of the chimney (see Fig. 2.10) can be used to compute a mean temperature of the metal with an appropriate weighting scheme. The specific heat of low carbon steel is well known but the mass of the chimney is not known. The "mass" of the chimney model cannot be determined with great accuracy because the chimney cannot be weighted in place conveniently, and some of the mass in the supporting structures are not part of the "effective" mass, thus the internal energy cannot be measured directly.

The heat losses to the surrounding from the chimney can be expressed in terms of the heat transfer coefficient, surface area, and temperature product as

$$Q = h \cdot A \cdot \theta ,$$

where again the temperature of the chimney is the weighed average of six measurements with respect to a reference level (the ambient temperature). The heat loss conductance given by the hA product represents the combined effects of radiation and convection from the outside surface and conduction through the chimney model insulation and support structure; thus, it is an effective heat loss conductance. This conductance cannot be calculated with an adequate accuracy because of the complexity of the system.

However, both the effective chimney mass and the effective heat loss conductance can be estimated from such calibration experiments as cool-down and heatup transients. A number of such tests were made prior to loading the rock into the chimney during the early phases of the experimental program and a few have been made subsequent to loading the chimney. The results of these calibration experiments are given with the discussion of the following transient analytic description of the chimney model system.

## 3.1 General Transient Model

The chimney model is a complex system of tanks, pumps, piping, and other components, and a detailed analysis of the heatup and cooldown transients would require a substantial effort. Therefore, one has to look for a simplified physical system which can be analyzed and which represents the behavior of the real system to an adequate degree. Lumped parameter models of the system consisting of four masses and two masses were examined previously (Kruger and Ramey, 1974). The adequacy of the lumped parameter approach was also discussed and it was found to be satisfactory for all metal portions in contact with water and for small rocks (equivalent diameter of 1 inch or less) subjected to slow transients. Comparisons showed that the 2-mass model represented the behavior of the physical system just as well as the 4-mass model, and was more convenient to use.

The 2-mass model is shown schematically in the upper portion of Fig. 3.1. It consists of one tank representing all metal (and insulation) in the system undergoing temperature changes. The temperature of this metal lump is $T_2$ and is the mean temperature of all metal parts and insulation. The tank contains water and rock at mean temperature $T_1$.

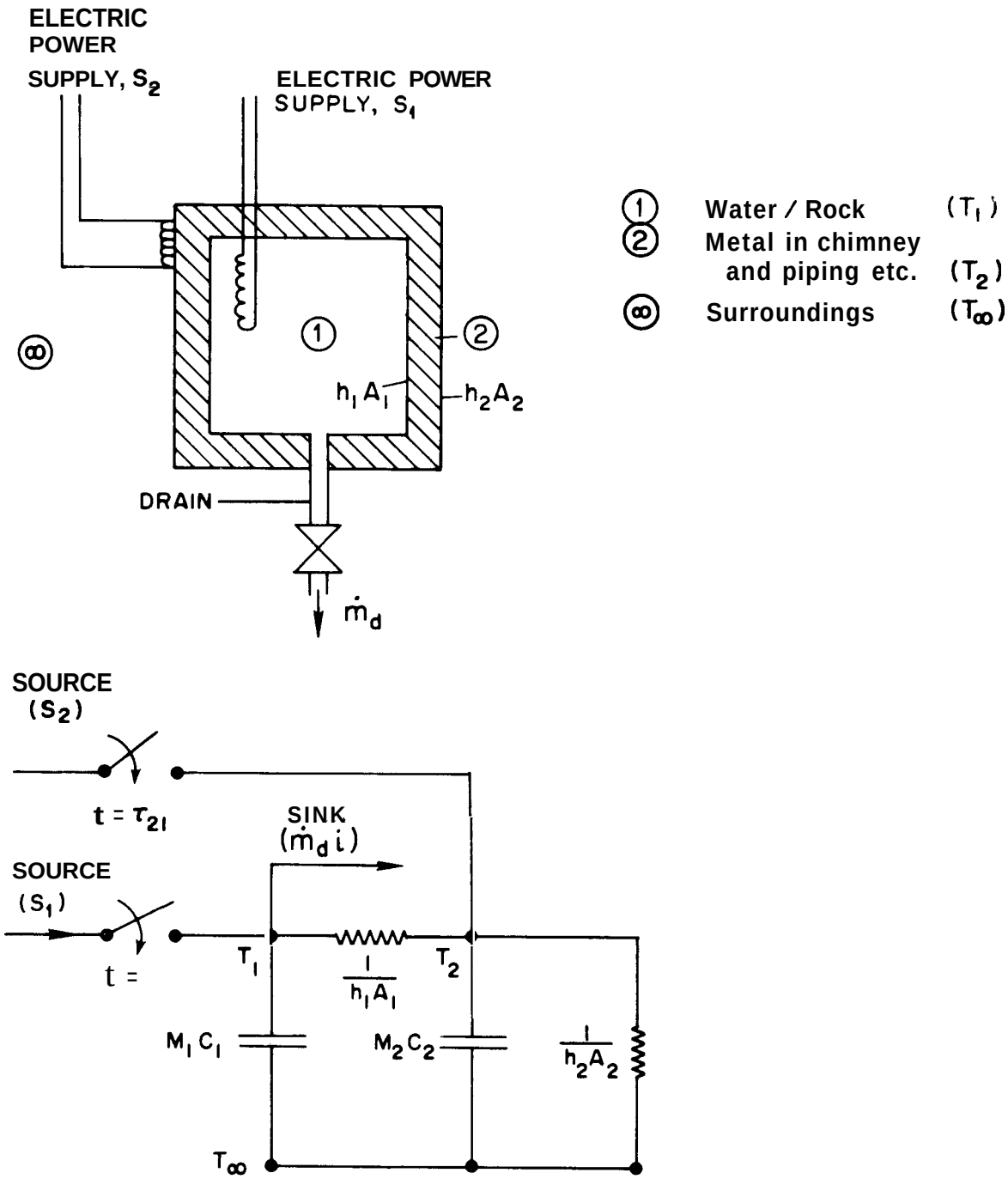


Figure 3.1 Diagrams of 2-mass lumped parameter model

Energy exchange occurs between the system and its surround ngs at constant temperature $T_\infty$, as follows: (1) heat transfer by convection conduction and radiation from the outside surface, (2) electric power supply, $S_1$ representing the electric circulation heater, (3) electric power supply, $S_2$ representing the tape heater elements on the outside wall of the chimney, and (4) hot water drainage during heatup (required due to thermal expansion of the water).

The electrical analog of the idealized chimney model system is shown on the lower portion of Fig. 3.1. Further discussion of the model, assumptions, and the derivation of the general solution are given in Appendix A. A summary of the assumptions are presented below:

1. All water and the rock are at a uniform temperature, $T_1$;
2. All metal (and insulation) is at a uniform temperature, $T_2$;
3. The temperature of the surroundings is constant at $T_\infty$;
4. The electric power ($S_1$ and $S_2$) is supplied as rectangular pulses;
5. The specific heats of rock, water and metal are constant;
6. The heat transfer conductances are constant.

The general solution for the transient temperature behavior of the system are presented below with $\theta_1 = T_1 - T_\infty$ and $\theta_2 = T_2 - T_\infty$.

$$\begin{aligned}\theta_1 = {} & C_{11}e^{m_1 t} - C_{12}e^{m_2 t} \\ & + \left[C_{13}\left(e^{m_1(t-\tau_{11})} - 1\right) - C_{14}\left(e^{m_2(t-\tau_{11})} - 1\right)\right] u(t - \tau_{11}) \\ & - \left[C_{13}\left(e^{m_1(t-\tau_{12})} - 1\right) - C_{14}\left(e^{m_2(t-\tau_{12})} - 1\right)\right] u(t - \tau_{12}) \\ & + \left[C_{15}\left(e^{m_1(t-\tau_{21})} - 1\right) - C_{16}\left(e^{m_2(t-\tau_{21})} - 1\right)\right] u(t - \tau_{21}) \\ & - \left[C_{15}\left(e^{m_1(t-\tau_{22})} - 1\right) - C_{16}\left(e^{m_2(t-\tau_{22})} - 1\right)\right] u(t - \tau_{22}) \quad (3.1a)\end{aligned}$$

$$\begin{aligned}\theta_2 = {} & C_{21}e^{m_1 t} - C_{22}e^{m_2 t} \\ & + C_{23}\left(e^{m_1(t-\tau_{21})} - 1\right) - C_{24}\left(e^{m_2(t-\tau_{21})} - 1\right)\Big] u(t - \tau_{21})\end{aligned}$$

$$- \left[C_{23}\left(e^{m_1(t-\tau_{22})} - 1\right) - C_{24}\left(e^{m_2(t-\tau_{22})} - 1\right)\right] u(t - \tau_{22})$$

$$+ \left[C_{25}\left(e^{m_1(t-\tau_{11})} - 1\right) - C_{26}\left(e^{m_2(t-\tau_{11})} - 1\right)\right] u(t - \tau_{11})$$

$$- \left[C_{25}\left(e^{m_1(t-\tau_{12})} - 1\right) - C_{26}\left(e^{m_2(t-\tau_{12})} - 1\right)\right] u(t - \tau_{12}) \quad (3.1b)$$

Explanations of the symbols are given in the Nomenclature and in Appendix A.

The above solution is specialized further for two cases following a discussion of how the mean or weighted lump temperatures can be obtained from experimental temperature data. These data are then compared to model predictions.

3.1.1 Definition of Weighted Metal Temperatures

It was observed during the heatup experiments with only water in the system that the water in the chimney remained at essentially uniform temperature. Since, the mass of water in the chimney constitutes about 80-90 percent of the water in the system an adequate representation of the water temperature ($T_1$) is obtained from the measured chimney exit temperature (see Fig. 2.10). Similar observations were made during the heatup experiments with the water/rock load.

On the other hand the six chimney metal temperature measurements on the outside wall (see Fig. 2.10) showed variations of 10-20°F depending on conditions. Therefore a weighting procedure was required to obtain a representative mean chimney metal temperature ($T_2$). The chimney and connecting inlet and outlet piping extending to nearest isolation valves were therefore divided into six sections corresponding to the six thermocouple locations. The mass of each section was estimated using measured dimensions and metal density. The best estimate of these masses and the corresponding mass fractions are given in the first and second columns of Table 3.1.

The chimney model mass cannot be determined directly; only the total chimney model system mass can be determined experimentally from heatup transients. However, the chimney model mass is a large fraction of the total system mass. The masses of the piping and other components were estimated

TABLE 3.1

Tabulation of Chimney Metal Mass Fractions--
Estimated from Dimensions and Adjusted Using Experimental Thermal Behavior

| Section | Estimated | | Experiment |
|---|---|---|---|
| | Mass, $M_{2,i}$ ($lb_m$) | Mass Fraction $M_{2,i}/M_2$ | Mass, $M_{2,i}$ ($lb_m$) |
| Lower head and inlet piping to closest isolation valve | 248 | 0.0629 | 216 |
| Lower flanges with bolts | 1435 | 0.3637 | 1246 |
| Lower section of shell including 1/2 support structure plus 1/2 sight glass | 480 | 0.1217 | 417 |
| Upper section of shell including 1/2 support structure plus 1/2 sight glass | 656 | 0.1664 | 570 |
| Jocks (closure device) | 756 | 0.1916 | 657 |
| Upper head and outlet piping to closest isolation valve | 370 | 0.0938 | 322 |
| Total Mass $M_2$ = 3945 $lb_m$ | | | = 3428 $lb_m$ |

and divided into sections where temperature measurements were available. From these and metal temperature measurements a mean system metal temperature ($T_2$) was estimated. The estimated system masses and the corresponding mass fractions are tabulated in the first and second columns of Table 3.2.

TABLE 3.2

Tabulations of System Metal Mass Fractions
Estimated from Dimensions and Adjusted Using Experimental Thermal Behavior

| Section | Estimated | | Experiment |
|---|---|---|---|
| | Mass, $M_{2,i}$ ($lb_m$) | Mass Fraction $M_{2,i}/M_2$ | Mass, $M_{2,i}$ ($lb_m$) |
| Chimney including inlet and outlet pipe sections | 3945 | 0.7543 | 3428 |
| Accumulator 1, connecting piping, and circulation pump | 690 | 0.1319 | 600 |
| Accumulator 2 and connecting piping | 165 | 0.0315 | 144 |
| Electric heater and connecting piping | 430 | 0.0822 | 375 |
| System Mass = 5230 $lb_m$ | | | = 4547 $lb_m$ |

### 3.1.2 Heatup Transient Experiments

A number of heatup transients were made both before and after loading of rock and a few of these have been evaluated. A typical heatup transient with water and rock in the chimney is shown in Fig. 3.2. The water temperature represents the chimney exit temperature and the mean system metal temperatures were derived using the mass fractions given in Tables 3.1 and 3.2 and experimental temperature data.

It is observed from Fig. 3.2 that during the first hour of heating there is a short time transient during which an adjustment of the mean temperatures of the two "lumps" takes place. Once this initial adjustment has occurred, the mean temperature difference between the lumps remains essentially constant indicating that the derivatives $d\theta/dt$ for both lumps are the same at each point in time. Evaluation of this slope from heatup transient data can be used to determine the total system heat capacitance using the following equation (see Appendix A for derivation)

$$MC \frac{d\theta}{dt} + h_2A_2\theta = S_1 \ , \qquad (3.2a)$$

from which

$$MC = \frac{S_1 - h_2A_2\theta}{d\theta/dt} \qquad (3.2b)$$

The average heating rate, $S_1$, is 22.5 kW derived from measurements of heater current and voltage during the heatup runs. The system heat transfer conductance (loss conductance) $h_2A_2$ is not known, however, if $d\theta/dt$ is evaluated at low system temperature where $\theta$ is relatively small the loss term may have little effect as is evident from Eq. (3.2b). A value of $h_2A_2 = 70$ Btu/hr °F was tentatively selected.

Once the total system heat capacitance has been determined, the system metal capacitance can be obtained in the case of water only in the chimney from

$$MC = M_1C_1 + M_2C_2 \ , \qquad (3.3a)$$

and in the case of water and rock in the chimney from

$$MC = M_wC_1 + M_rC_r + M_2C_2 \ . \qquad (3.3b)$$

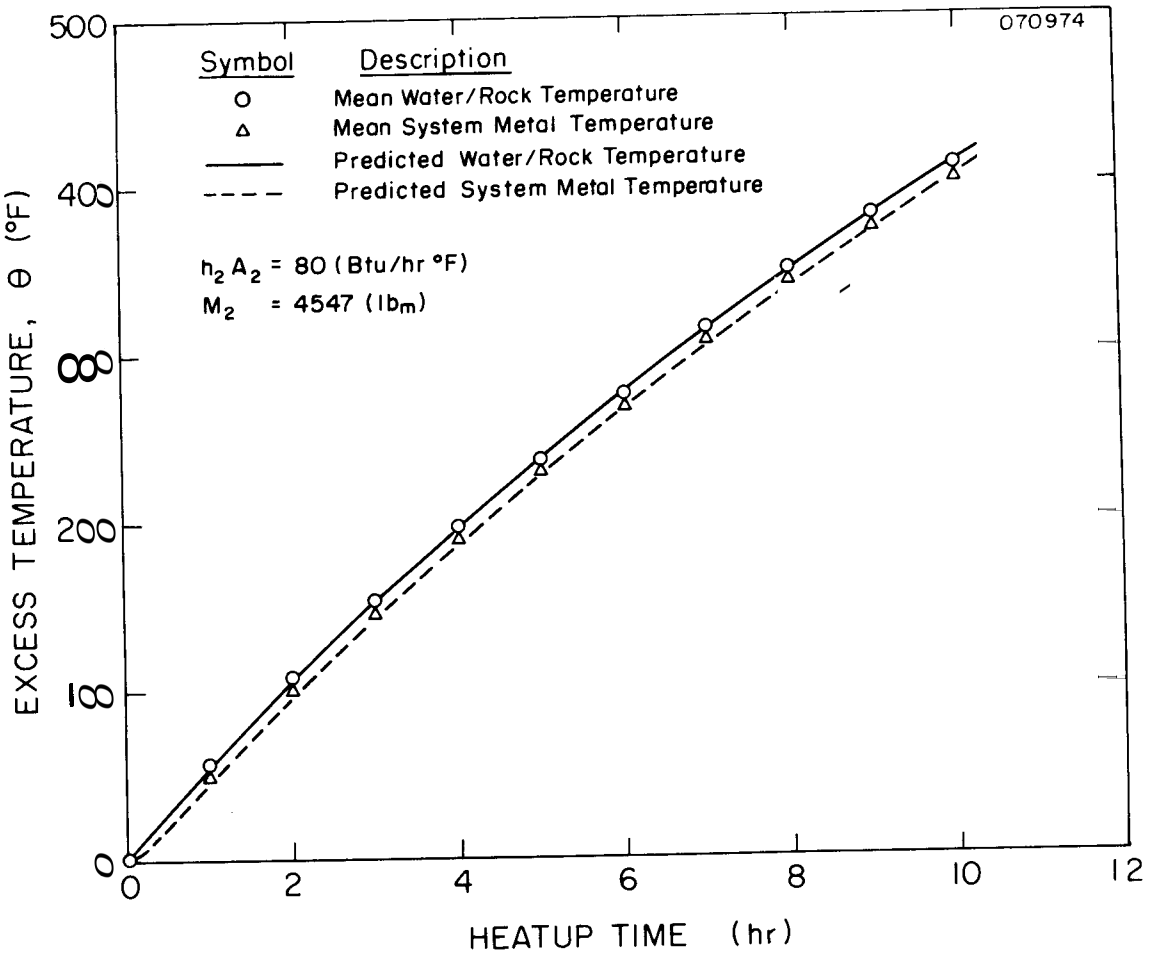


Figure 3.2 Typical heatup transient with water and rock in the chimney

Several numerical values are required in the above equations and the values used in this analysis along with reference to source are given in Table 3.3.

TABLE 3.3

Tat lation of Numerica_ Data
Used ir Evaluating System Metal Mass

| Quantity | Numerical Value | Source |
|---|---|---|
| $M_1 = \rho V$ = mass of water in system (no rock in system) | 1153 $lb_m$ | Density $\rho^*$ (Kreith, 1965) System volume computed |
| $C_1$ = specific heat of water | 1.0 Btu/$lb_m$ °F | (Kreith, 1965) |
| $M_w = \rho V$ = mass of water in system (rock in system) | 585 $lb_m$ | Density $\rho$ (Kreith, 1965) System volume computed |
| $M_r$ = mass of rock in chimney | 1640 $lb_m$ | Measured prior to loading |
| $C_r$ = specific heat of rock | 0.2 Btu/$lb_m$ °F | (Kreith, 1965) |
| $C_2$ = specific heat of steel | 0.117 Btu/$lb_m$ °F | (Goldsmith et al., 1961) |

* All quantities dependent on temperature were evaluated at T = 200°F.

Using mean $d\theta/dt$ data between 2 and 3 hours heating time in Eq. (3.2b), the numerical data in Table 3.3 and Eqs. (3.3), the data listed in Table 3.4 were obtained.

The mean value of the computed system metal mass as given in Table 3.4 is 4784 $lb_m$. The sensitivity of system metal mass as evaluated by this procedure to variation in the system loss conductance can be obtained by using different values of $h_2A_2$ in evaluating $M_2$. The results of this analysis are given in Table 3.5.

TABLE 3.4

Heatup Transient Data Evaluation

| Run ID No. | Chimney Loading | Mean Chimney Temp* (°F) | Mean Slope** dθ/dt (°F/hr) | Total System Heat Capacitance, *** MC (Btu/°F) | Computed System Metal Heat Capacitance, $M_2C_2$ (Btu/°F) | Computed System Metal Mass $M_2$ ($lb_m$) |
|---|---|---|---|---|---|---|
| 032274 | Water | 115 | 40 | 1730 | 577 | 4930 |
| 051574 | Water | 108 | 40 | 1740 | 587 | 5020 |
| 061074 | Water/Rock | 134 | 48 | 1415 | 510 | 4360 |
| 070974 | Water/Rock | 129 | 46 | 1480 | 575 | 4910 |
| 072274 | Water/Rock | 126 | 47 | 1455 | 550 | 4700 |

*Mean temperature between 2 and 3 hours of heating time — Mean = 4784 $lb_m$

**Mean slope between 2 and 3 hours of heating time — Standard Deviation = ± 252 $lb_m$

***For a heat loss conductance of 70 Btu/hr °F.

TABLE 3.5

Sensitivity of Computed System Metal Mass to Variation in System Loss Conductance

| System Heat Loss Conductance $h_2A_2$ (Btu/hr °F) | Computed System Mean Metal Mass, $M_2$ ($lb_m$) |
|---|---|
| 50 | 5273 |
| 70 | 4784 |
| 90 | 4310 |

Thus, a reduction of $h_2A_2$ from 70 to 50 Btu/hr °F (28 percent) results in an increase in computed $M_2$ of about 10 percent. Similarly, a 28 percent increase in $h_2A_2$ results in a decrease in the computed mass of almost 10 percent. This is not insignificant and in order to resolve the argument about what value of $h_2A_2$ is correct, the characteristic curvature or decrease in slope of the heatup temperature curves on Fig. 3.2 with increasing temperature level can be used along with the analytic solution of the two-mass model. For the case of simple heating from room temperature this solution becomes (see Appendix A)

$$\theta_1 = C_{13}\left(e^{m_1 t} - 1\right) - C_{14}\left(e^{m_2 t} - 1\right), \tag{3.4a}$$

$$\theta_2 = C_{25}\left(e^{m_1 t} - 1\right) - C_{26}\left(e^{m_2 t} - 1\right), \tag{3.4b}$$

where

$$C_{13} = \frac{\bar{S}_1(m_1+a_2+a_3)}{(m_1-m_2)m_1}, \quad C_{14} = \frac{\bar{S}_1(m_2+a_2+a_3)}{(m_1-m_2)m_2},$$

$$C_{25} = \frac{\bar{S}_1 a_2}{(m_1-m_2)m_1}, \quad C_{26} = \frac{\bar{S}_1 a_2}{(m_1-m_2)m_2}. \tag{3.5}$$

Using these equations and the input data presented in Table 3.6 below, the effect of using 50, 70, and 90 Btu/hr °F for $h_2A_2$ (corresponding values of $M_2$ from Table 3.5) was investigated.

TABLE *3.6*

Input Data for Heatup Transient Predictions

(Run ID No. *070974)*

| Case | $h_1A_1$ (Btu/hr °F) | $M_1C_1$ (Btu/ F) | $h_2A_2$ (Btu/hr F) | $M_2C_2$ (Btu/ °F) | $S_1$ (Btu/hr) |
|---|---|---|---|---|---|
| 1 | 5800* | *903* | *50* | *638* | *76,800* |
| 2 | *5800* | *903* | *70* | *579* | *76,800* |
| 3 | *5800* | *903* | 90 | 521 | *76,800* |

* The inside surface area in contact with water, $A_1$, was estimated to be 58 $ft^2$. The heat transfer coefficient, $h_1$, was determined to be 100 Btu/hr-$ft^2$ °F by adjusting model predictions to match experimentally determined water/metal mean temperature differences.

The predicted water temperature transients are shown in Fig. *3.3* with the corresponding measured water/rock temperature data. It appears that the most likely mean value of $h_2A_2$ is between *70* and *90* Btu/hr °F. The predicted transient with $h_2A_2$ = 80 Btu/hr °F and a corresponding value of $M_2$ = *4547* $lb_m$ are shown in Fig. 3.2 for run ID No. *070974.* The agreement of predictions with experiment is excellent.

In order to test further the prediction method and the $h_2A_2$ and $M_2$ values one of the early heatup transients with water only in the system was selected. The results are shown in Fig. *3.4.* The general agreement between experiment and predictions is very good except near the end of the transient. During the course of these experiments portions of the system insulation were removed and subsequently reinstalled. It is believed that degradation of insulation capability resulted. Additionally, room air-conditioning was installed and in use during the latter part of the test period when the calibration data were obtained. The effects of these items would result in higher loss conductance $h_2A_2$ for data obtained during the latter part of the test period and a corresponding increase in the mean value would result. Thus, a run made early would have a loss conductance lower than the mean for the complete test period and exhibit correspondingly less curvature towards the end of the transient.

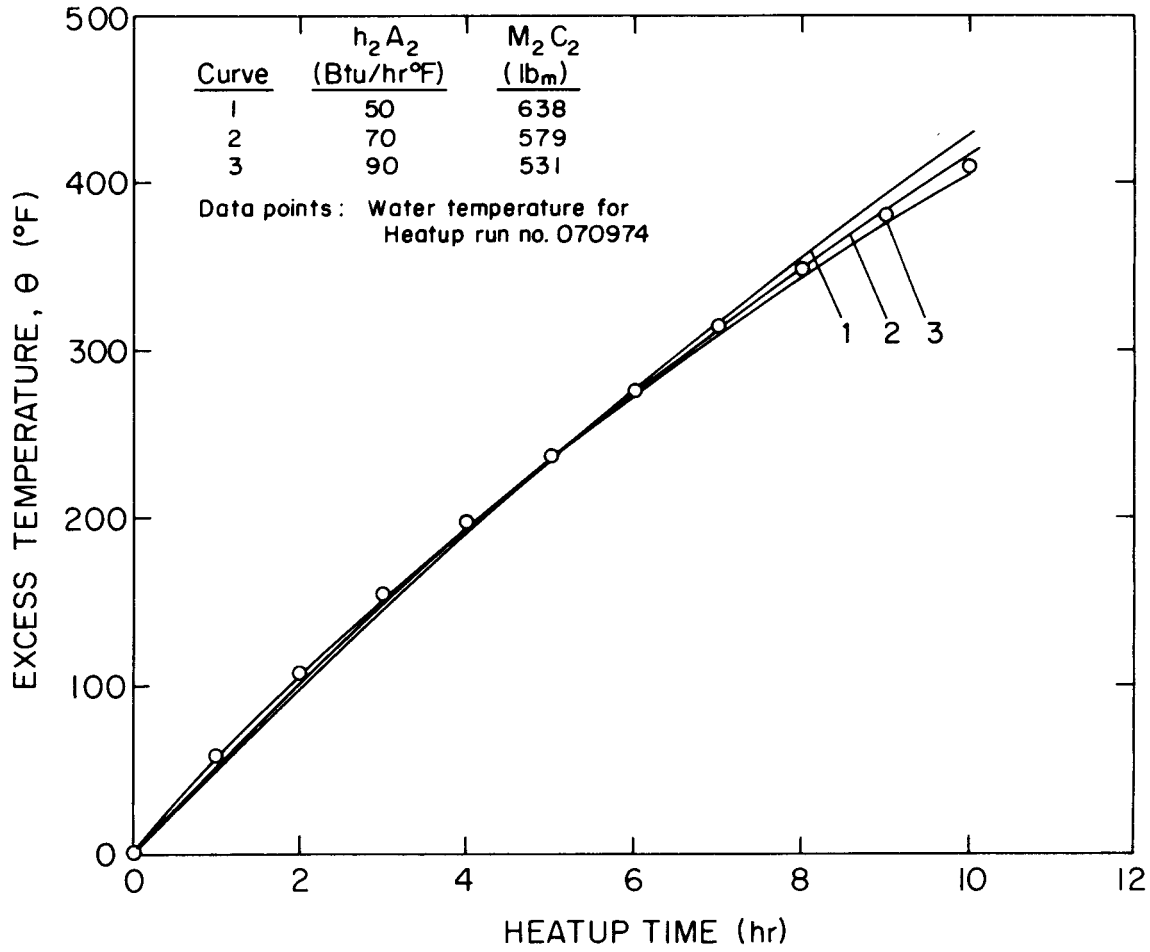


Figure 3 3 Predicted water temperature transients for different heat loss conductances

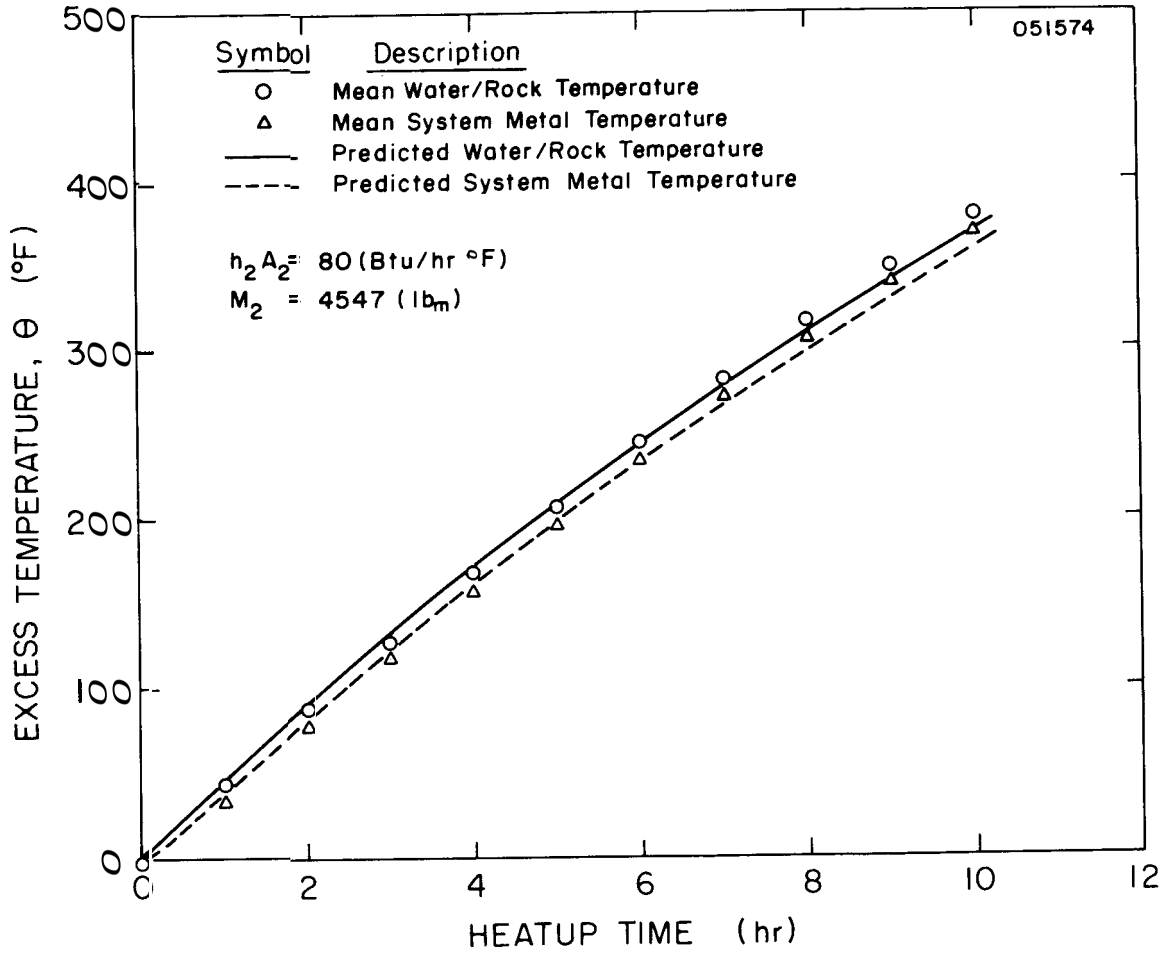


Figure 3.4 Heatup transient with water only in the system - comparison of experiment and prediction

To assess the uncertainty associated wit4 the computed mean value of the system mass ($M_2$ = 4547 $lb_m$) one can calculate the standard deviation associated with $M_2$. The standard deviation is $\pm$ 245 $lb_m$ which corresponds to approximately $\pm$ 5 percent, which will be adapted as the error sigma* for the effective system mass.

There may be two explanations for $M_2$ based on experiment being lower than the estimated value given in Table 3.2. The estimated value may be biased towards the high side, or not all mass involved is effective, i.e., does not "see" the full temperature change. There are several places where this is the case, e.g., the sight glasses, part of the chimney support structure, and accumulator 2 were all observed to remain at temperatures considerably lower than the mean due to poorer insulation and water circulation. Despite these observations there is no basis for changing the estimated mass fractions in Table 3.2. The corresponding adjusted system masses are given in the third column of Table 3.2.

It is difficult to estimate an error sigma for the mass fractions given in Table 3.2 and $\pm$ 5 percent has been assumed. Appropriate propagation** of the errors associated with system mass fraction and the chimney mass yields an estimated error sigma of about $\pm$ 7 percent for the effective chimney mass.

The mass fractions associated with the various sections of the chimney given in the second column of Table 3.1 were also retained as originally estimated. These mass fractions are used to determine the chimney section masses from total chimney mass as listed in the third column of Table 3.1.

### 3.1.3 Cooldown Transient Experiments

Several cooldown experiments without circulation were run with and without rock in the chimney to estimate the effective mean heat loss conductance for the chimney alone. In the previous section the loss

---

* Terms used to indicate uncertainties throughout this report are (1) standard deviation obtained from statistical analysis of data, and (2) estimated uncertainty based on best estimate. The term error sigma is used for the relative uncertainty (relative to mean values or e.g. scale reading).

** Combined error computed from $\sigma = (\sigma_1^2 + \sigma_2^2 + \ldots + \sigma_n^2)^{1/2}$.

conductance for the complete system was determined to be about 80 Btu/hr °F and the loss conductance for the chimney alone is somewhat lower.

A cooldown transient is shown in Fig. 3.5. The cooldown curve is fairly linear on semilog paper after an initial adjustment period. However, after about 20 hours of cooling, deviation from this linear behavior occurs, believed to be due primarily to non-linear heat transfer effects such as decreasing importance of radiation. The predicted cooldown transient from specified initial conditions without external heating is given by the general transient model solution from Eqs. (3.1a) and (3.1b) (see Appendix A) as:

$$\theta_1 = C_{11}e^{m_1 t} - C_{12}e^{m_2 t}, \tag{3.6a}$$

$$\theta_2 = C_{21}e^{m_1 t} - C_{22}e^{m_2 t}, \tag{3.6b}$$

where $C_{11}$ through $C_{22}$ are given by

$$C_{11} = \frac{\theta_{10}(m_1+a_2+a_3) + \theta_{20}a_1}{m_1 - m_2}, \quad C_{12} = \frac{\theta_{10}(m_2+a_2+a_3) + \theta_{20}a_1}{m_1 - m_2},$$

$$C_{21} = \frac{\theta_{20}(m_1+a_1) + \theta_{10}a_2}{m_1 - m_2}, \quad C_{22} = \frac{\theta_{20}(m_2+a_1) + \theta_{10}a_2}{m_1 - m_2}, \tag{3.7}$$

and the inverse time constants $m_1$ and $m_2$ are given by Eq. (A.10) in Appendix A. If realistic numbers are used to calculate $m_1$ and $m_2$, one finds that $|m_2| \gg |m_1|$. Moreover, $m_1$ and $m_2$ are negative. Thus, the last term in Eqs. (3.6a) and (3.6b) become relatively small after about one hour, and $\theta_1$ becomes approximately

$$\theta_1 \simeq C_{11}e^{m_1 t} \quad \text{for} \quad t \geq 1\,\text{hr}.$$

Taking the natural logarithm

$$\ln \theta_1 = \ln C_{11} + m_1 t,$$

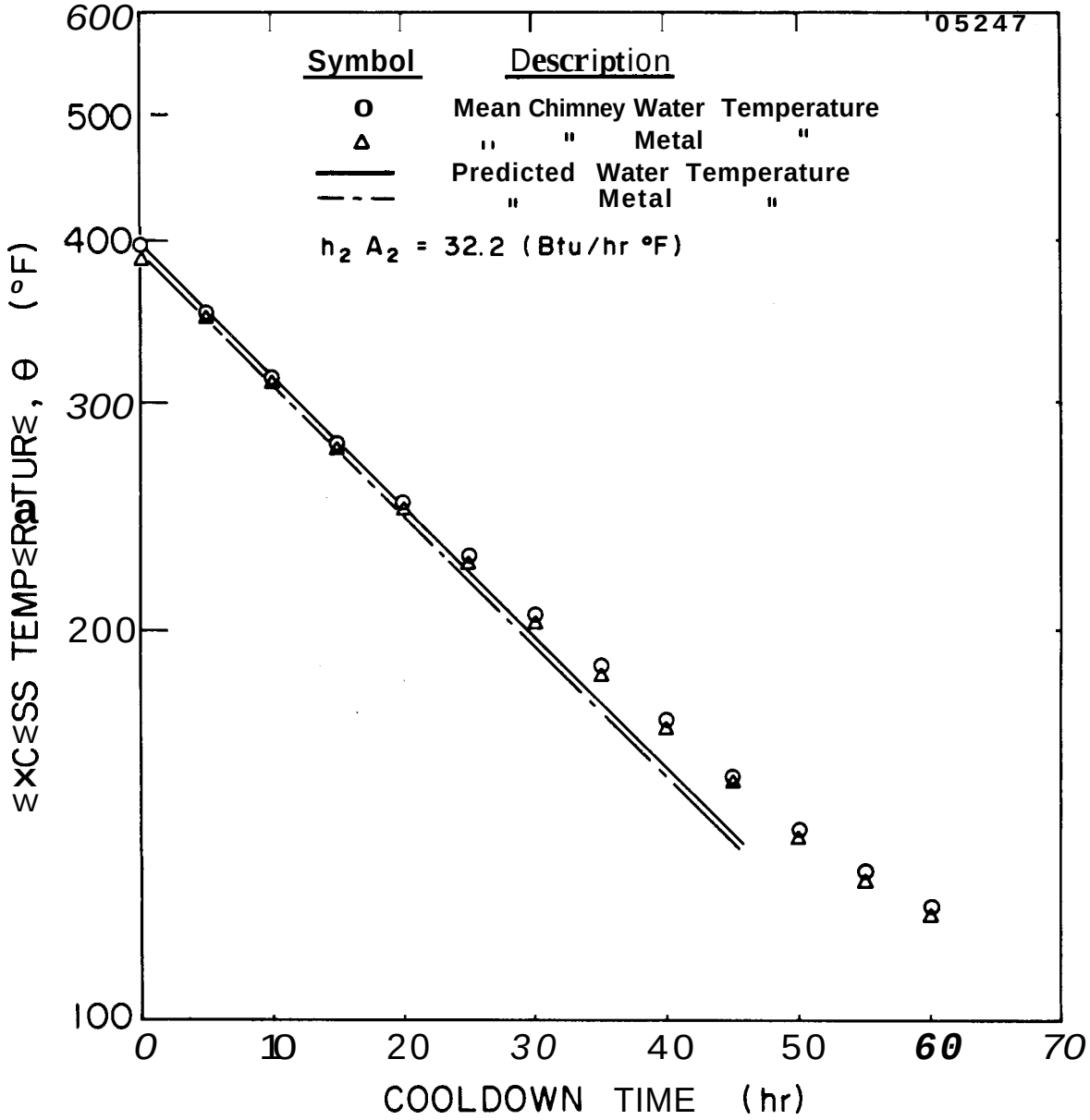


Figure 3.5 Typical chimney cooldown transient

and evaluation at two times $t_1$ and $t_2$ gives the slope

$$m_1 = \frac{(\ln \theta_1)_1 - (\ln \theta_1)_2}{t_1 - t_2} \quad . \tag{3.8}$$

Thus, from data that plot approximately as a straight line on semilog paper, the dominant inverse time constant, $m_1$, can be determined from the slope between two points in time. The mean slope was evaluated between time 0 and 20 hours where the cooldown curves are relatively linear. This region spans the temperature range of interest during production runs and it is therefore desired to predict heat losses in this region with the greatest accuracy.

The effective chimney heat transfer loss conductance, $h_2A_2$, can be derived from mean values of $m_1$. The expression for $m_1$ and $m_2$ (Eq. A.10) can be approximated using a binomial expansion of the square root term by the following expression:

$$m_1 \simeq \frac{a_1 a_2}{(a_1+a_2+a_3)} \quad .$$

Substituting for $a_1$, $a_2$, and $a_3$ using the relations (A.6),

$$h_2A_2 \simeq m_1(M_1C_1 + M_2C_2) \quad . \tag{3.9}$$

The experimentally determined values of $m_1$ and computed values of $h_2A_2$ using Eq. (3.9) and other pertinent information are summarized in Table 3.7. The heat capacitances in Eq. (3.9) were evaluated at a mean temperature of 400°F. The input data sources used are the same as those used for the heatup transient, listed in Table 3.3. Also, the derived value of $M_2$ given in the previous section was used here.

From Table 3.7 it can be seen that the mean time constants for the water runs are slightly higher than for the water/rock case. Although the effect is not pronounced, from a physical point of view this is to be expected due to the slighly lower (8.6 percent) total heat capacitance of the water/rock system as compared to the water system. The mean value of the computed heat loss conductance is 32.2 Btu/hr °F and the

TABLE 3.7

Summary of Data from Cooldown Experiments

| Run ID No. | Medium in Chimney | Initial Water Temp (°F) | Initial Metal Temp (°F) | Surrounding Temp, $T_\infty$ (°F) | Measured Mean Slope (1/hr) | Time Constant (hr) | Computed $h_2A_2$ (Btu/hr °F) |
|---|---|---|---|---|---|---|---|
| 032774 | Water | 500 | 486 | 78 | -0.0215 | 46.5 | 29.4 |
| 052174 | Water | 485 | 473 | 75* | -0.0250 | 40.0 | 34.2 |
| 052474 | Water | 473 | 462 | 75* | -0.0235 | 42.6 | 32.1 |
| 080924 | Water/rock | 474 | 463 | 80 | -0.0257 | 38.9 | 33.0 |

*Air-conditioning system in operation.

Mean = 32.2 Btu/hr °F

Standard Deviation = 1.2 Btu/hr °F

standard deviation is f1.2 Btu/hr °F, which corresponds to an error sigma of ± 3.6 percent.

A comparison of the magnitudes of the total system heat loss to the chimney model heat loss (80 vs 32.2 Btu/hr °F) shows that the chimney model heat loss is about 40 percent of the total system heat loss. This is as expected since the surface area of the chimney model is about one half of the total system surface area. Moreover, the insulation on the chimney is thicker than the mean for the system with correspondingly lower heat transfer coefficient for the chimney model.

The parameters calculated in these sections, the effective chimney mass and heat loss conductance and their estimated error sigmas are summarized in Table 3.8 for later reference.

TABLE 3.8

Tabulation of Chimney Parameters

| Parameter | Mean Value | Estimated Error Sigma (percent) |
|---|---|---|
| Effective chimney model mass ($M_2$) | 3428 $lb_m$ | 7 |
| Effective chimney model heat loss conductance ($h_2A_2$) | 32.2 Btu/hr °F | 3.6 |

# CHAPTER 4

# ROCK CHARACTERIZATION

To compare experiments with various types and sizes of rocks in the chimney model, some uniform description or measurement of the rock is needed. These measurements are useful when (1) the performances of the various rock types are to be compared, and (2) when the chimney performance results are to be utilized in estimating the performance of real systems. However, the characteristics of rocks in a real system are seldom known. Little information is available about rock statistical size distributions resulting from hydraulic fracturing, thermal fracturing, and chemical explosive fracturing. On the other hand, some data do exist for rubble chimnies resulting from contained underground nuclear explosions.

## 4.1 Rock Statistics

Characteristics of rocks that appear to be significant for the present study includes linear length dimensions, shape and roundness factors, volume, surface area, and surface roughness. Measurement of rock characteristics such as shape and roundness is difficult; several methods have been devised (Griffiths, 1967; Krumbein, 1941; Pettijohn, 1951). A large number of measurements is required for a single rock to define its characteristics accurately. However, for a large assembly of similar rocks a practical scheme is based on measurement of the three orthogonal axis of the rocks illustrated on the upper portion of Fig. 4.1. Corresponding to the shape factors obtained from these three measurements ( b/a and c/a ) the verbal classification scheme shown on the lower part of Fig. 4.1 has been utilized.

A measure of the roundness or a roundness factor, $\psi$ , (Griffiths, 1967), based on the three length dimensions is given by

$$\psi \triangleq (bc/a^2)^{1/3} . \qquad (4.1)$$

The equivalent diameter, d , of a rock is related to the volume determined from weight and density measurements by

$$\text{Equivalent diameter } d \triangleq (6V/\pi)^{1/3} . \qquad (4.2)$$

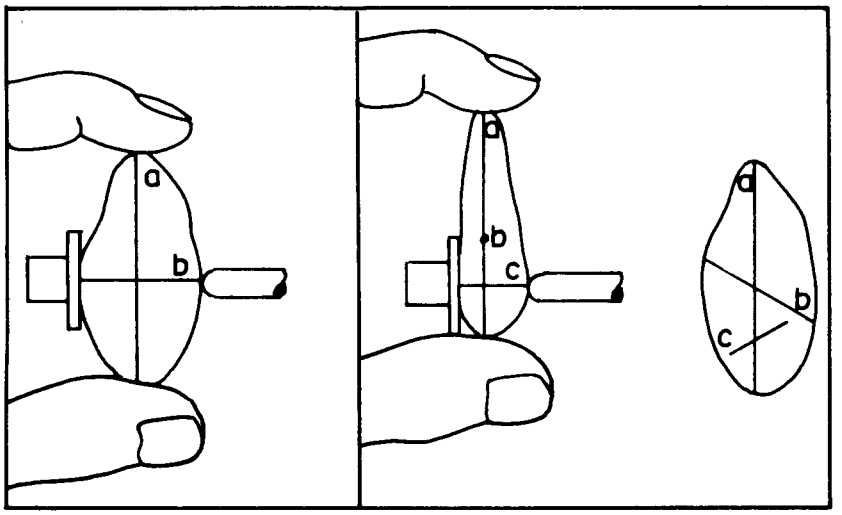


a = length
b = breadth
c = thickness

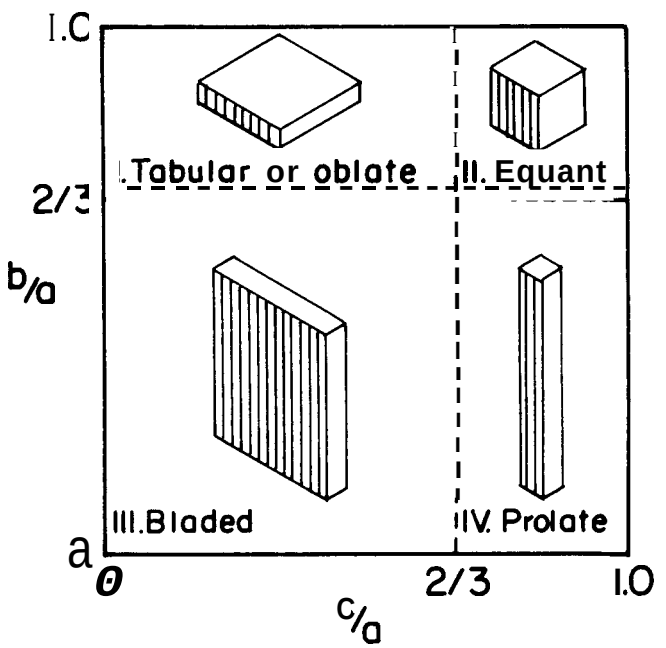


**Figure 4.1** Zingg classification system for rock shapes (from Krumbein, 1941; Prttijohn, 1951)

Another method of characterizing rock is sieving. However, sieving gives only an overall or mean measure of size, thus the method does not provide any specifics about shape and roundness.

### *4.2* Sampling Techniques

A major object of any statistical sampling procedure is to obtain a representative or random sample of the population for reliable statistical information. The sampling techniques considered for this study include:

1. The selection of a large sample (order of 10 percent of population) with no particular precautions taken to assure randomness of the sample.
2. Point counting, a method involving a relatively small sample but where particular emphasis is on assuring randomness of the sample.
3. The selection of several smaller samples from various locations in the rock pile, e.g., one shovel each from top, middle, bottom and side of rock pile.

The reason for considering all these methods is to attempt to find a method which will provide the maximum information with minimum effort, as it is important to find the most efficient method for use on future rock loads. To date the analysis of the data consisting of length dimension ( a , b , and c ) and mass measurements on individual rocks obtained using sampling procedure (1) has been completed and work is in progress on method (2).

### *4.3* Preliminary Results of Rock Statistical Analysis

The sample analyzed consisted of 1978 rocks (140 $lb_m$) and were selected from a population of 1100 $lb_m$ . This population was the rock left over after the chimney had been loaded with *1640* $lb_m$ from the original population of about 2700 $lb_m$. The rock type was granite which had been crushed and passed through a 1.5 inch mesh. The sample and the chimney rock were cleaned with water while located in a No. 8 sieve (1/4 inch mesh) to remove smaller particles that would be a danger to system components such as the circulation pump. Each rock was measured to determine dimensions a , b , and c and its weight. From these measurements the

following quantities were computed for each rock:

$$\text{Breadth/length ratio} \triangleq b/a \,, \tag{4.3}$$

$$\text{Thickness/length ratio} \triangleq c/a \,, \tag{4.4}$$

Roundness factor (Eq. 4.1))

Equivalent diameter (Eq. (4.2))

$$\text{Surface area} \quad A \triangleq \pi d^2 * \tag{4.5}$$

The rock volume, V , used in Eq. (4.2), was computed using the mean density of the chimney rock load which was determined to be $\rho = 2.79\ g/cm^3$ (see page 53 for further discussion of this measurement). For each of the original measurements and the quantities derived from them, Eqs. (4.1) through (4.5) the cumulative distribution functions and the probability density functions were computed. For computation and in plotting of the results, the range of each quantity was divided into 10 equal intervals. The resulting cumulative distribution and probability density functions are shown in Figs. 4.2 through 4.10. **Also,** included in these figures are the statistical parameters computed using the formulas listed below:

$$\text{Mean} \qquad \bar{X} \triangleq \frac{1}{n} \sum_{i-1}^{n} X_i \,, \tag{4.6a}$$

$$\text{Variance} \qquad s^2 \triangleq \frac{1}{n-1} \sum_{i=1}^{n} (X_i - \bar{X})^2 \,, \tag{4.6b}$$

$$\text{Standard deviation} \qquad \sigma = (s2)1/2 \,, \tag{4.6c}$$

$$\text{Skewness} \qquad Sk = \frac{1}{2\sigma^3 n} \sum_{i=1}^{n} (X_i - \bar{X})^3 \,, \tag{4.6d}$$

$$\text{Peakedness} \qquad k = \frac{1}{a^4 n} \sum_{i=1}^{n} (X_i - \bar{X})^4 \,. \tag{4.6e}$$

* This is the simplest (and least accurate) method for obtaining surface area. It is recognized that a more thorough approach is desirable.

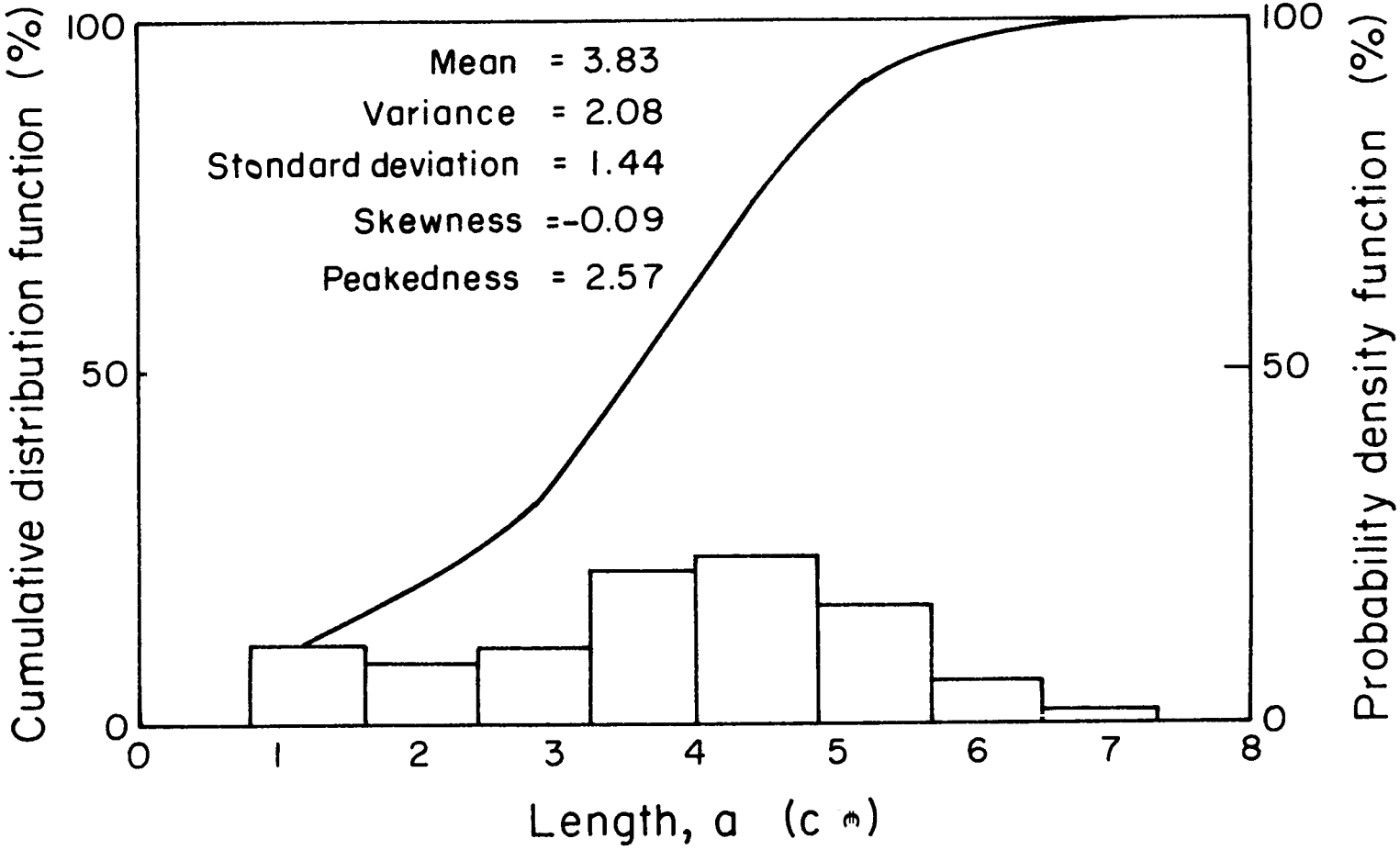


Figure 4.2 Cumulative distribution and probability density functions for rock length dimension

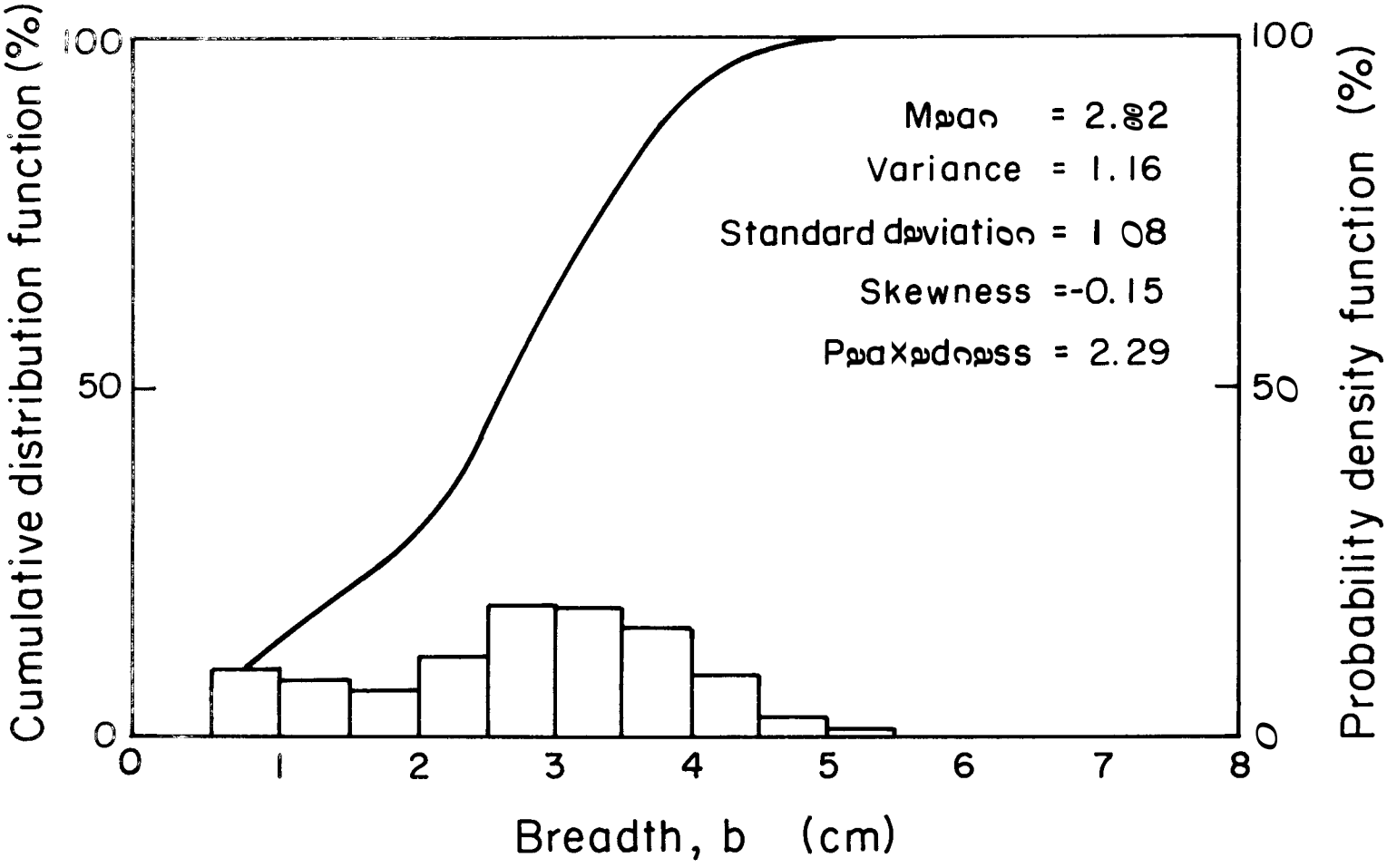


Figure 4.3 Cumulative distribution and probability density functions for rock breadth dimension

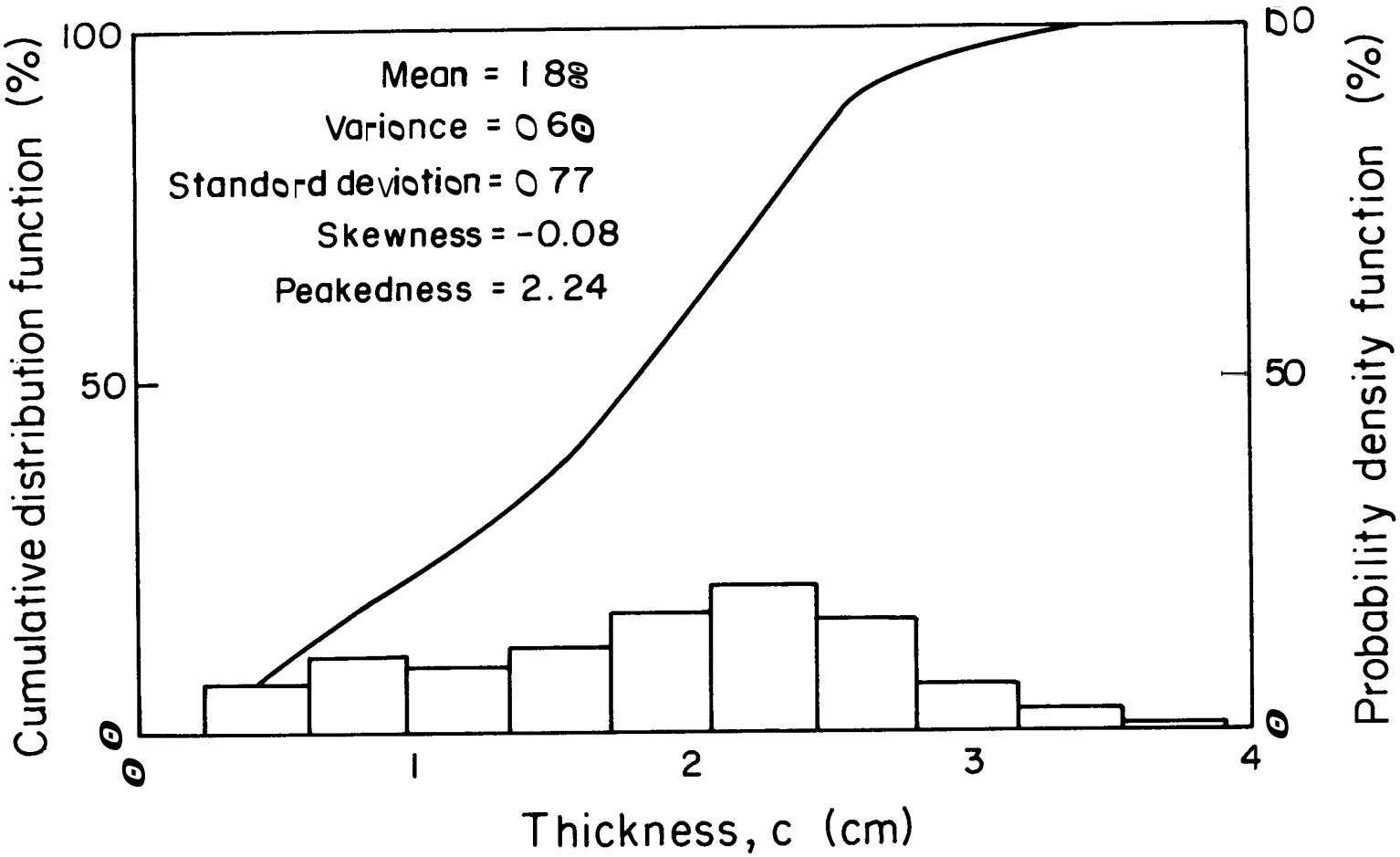


Figure 4.4 Cumulative distribution and probability density functions for rock thickness dimension

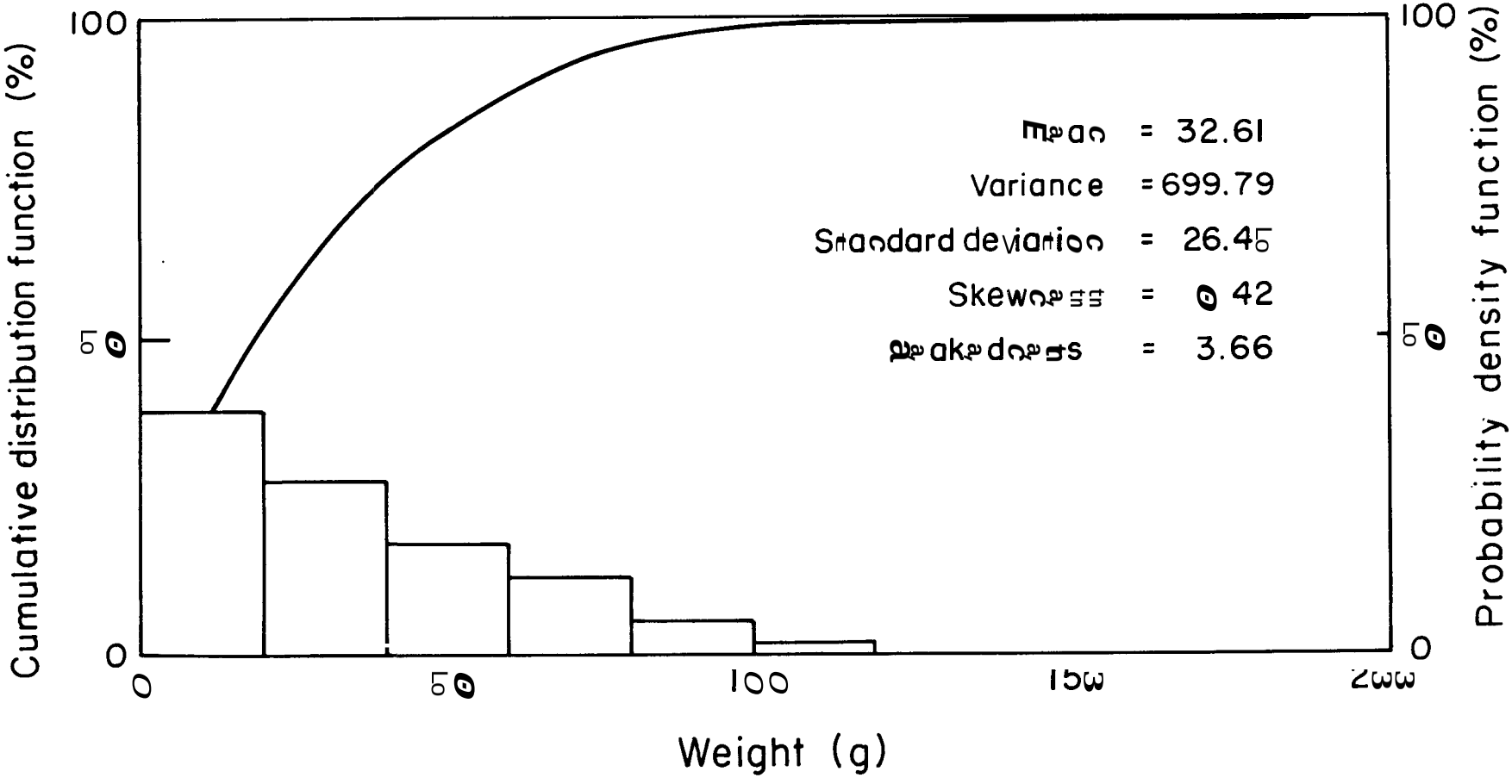


Figure 4.5 Cumulative distribution and probability density functions for rock weight

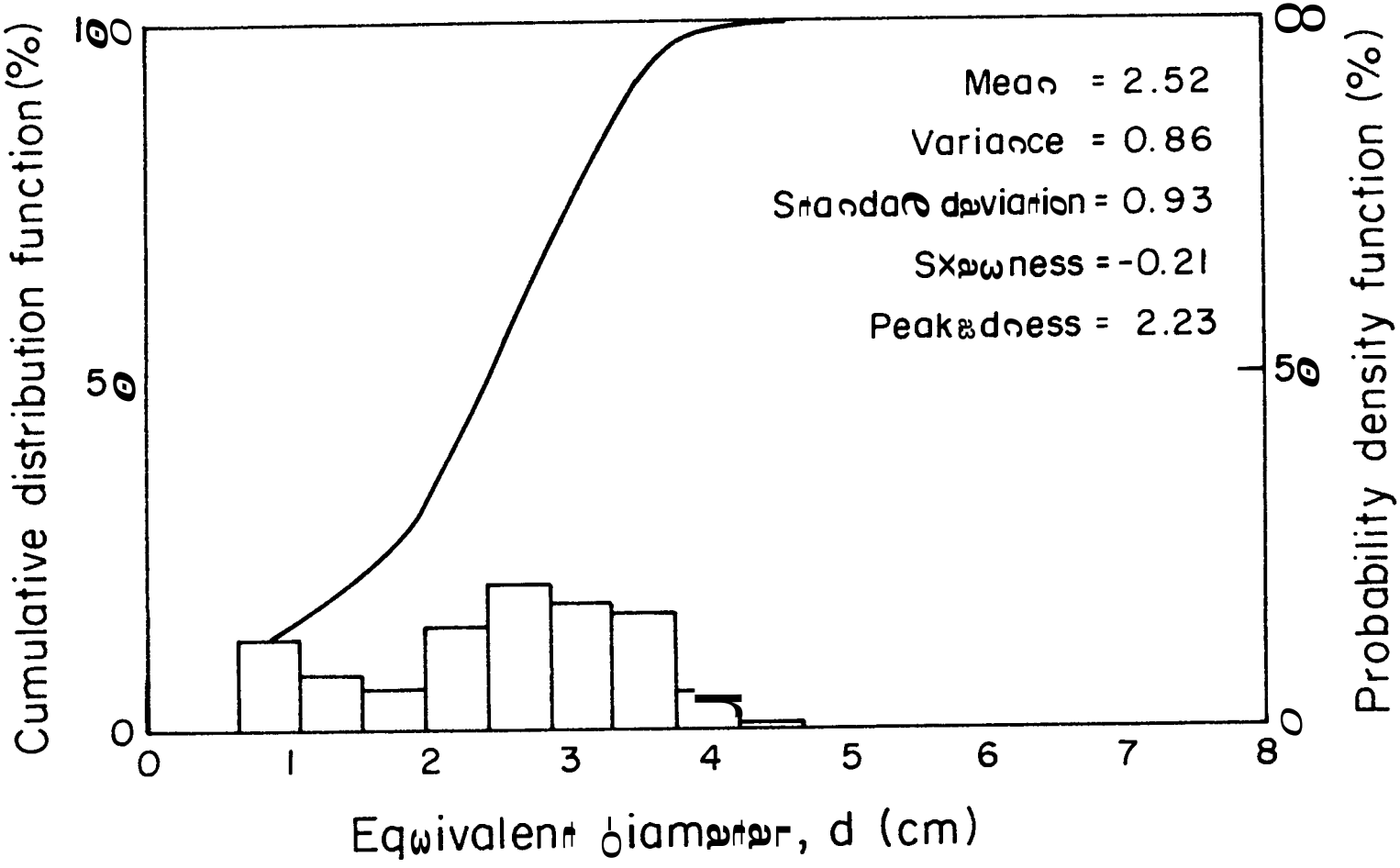


Figure 4.6 Cumulative distribution and probability density functions for rock equivalent diameter

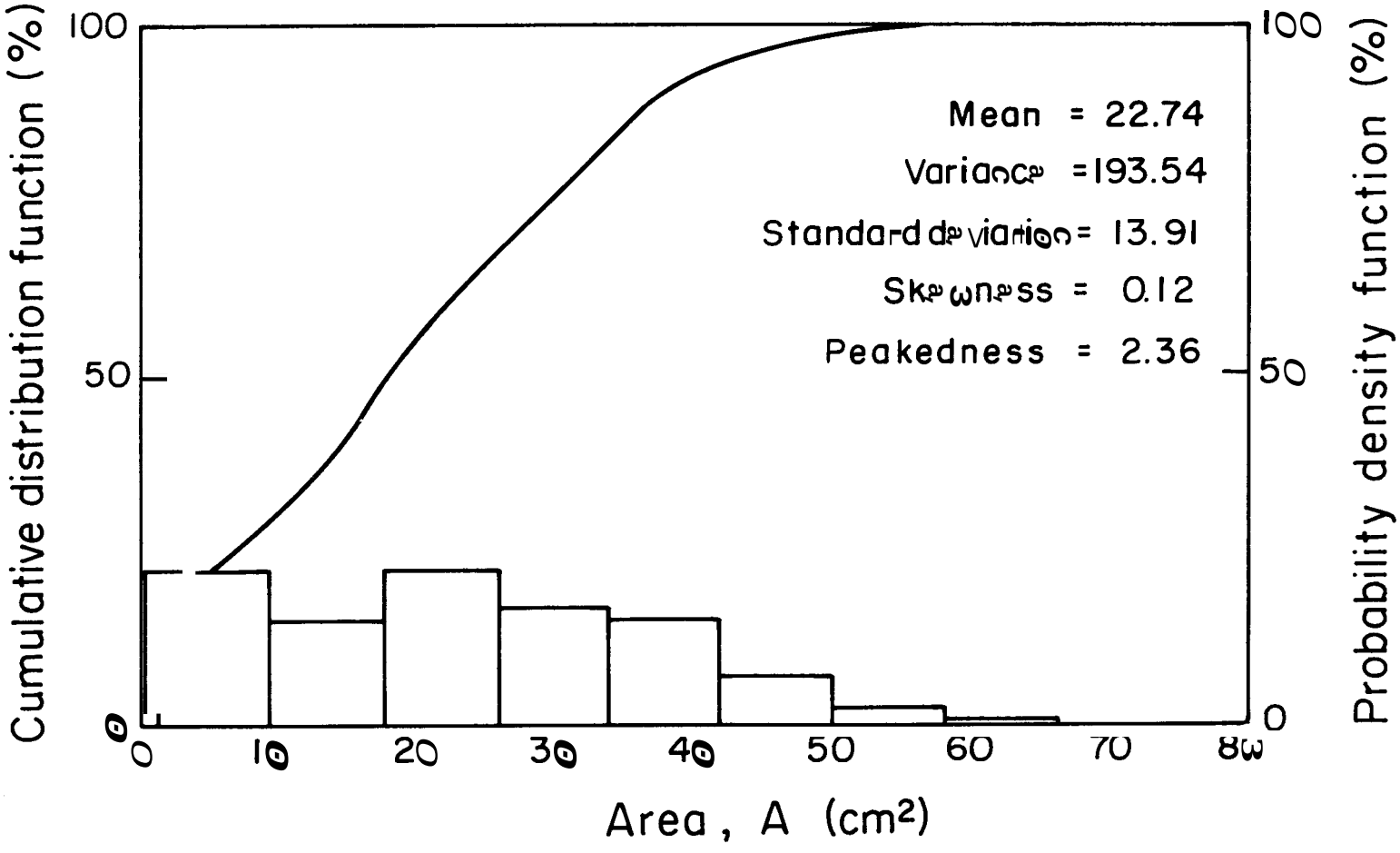


Figure 4.7 Cumulative distribution and probability density functions for rock area

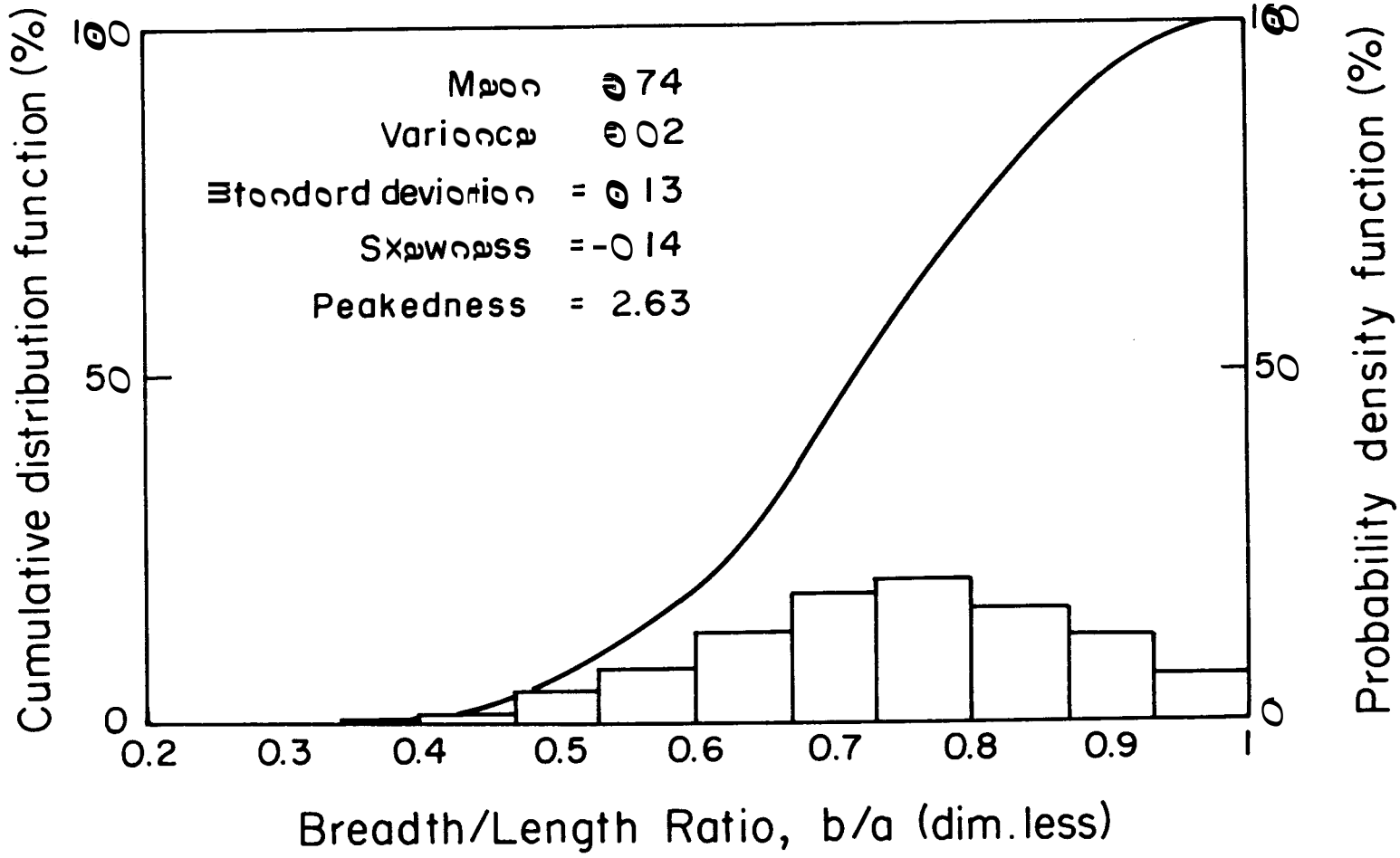


Figure 4.8 Cumulative distribution and probability density functions for breadth/length ratio

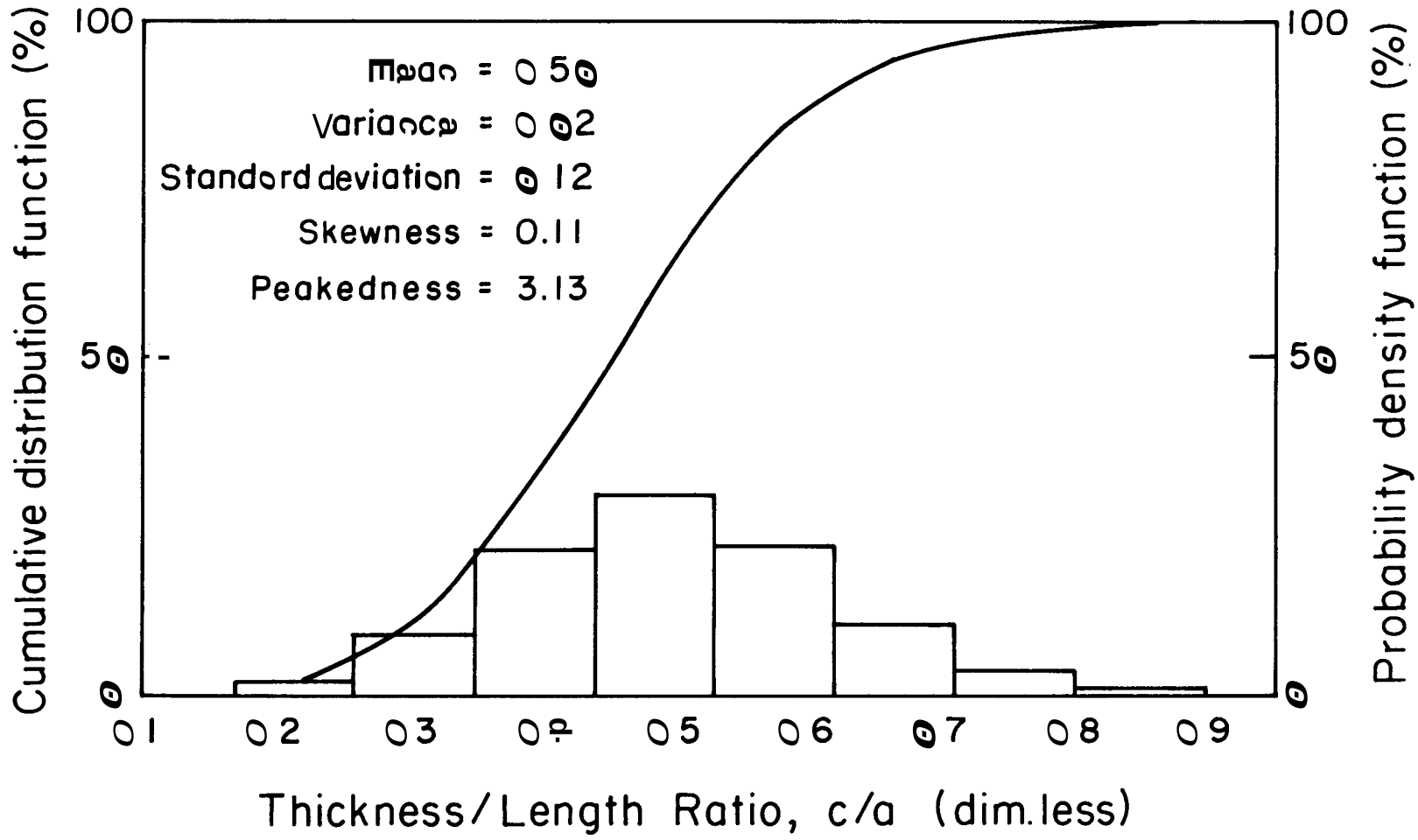


Figure 4.9 Cumulative distribution and probability density functions for thickness/length ratio

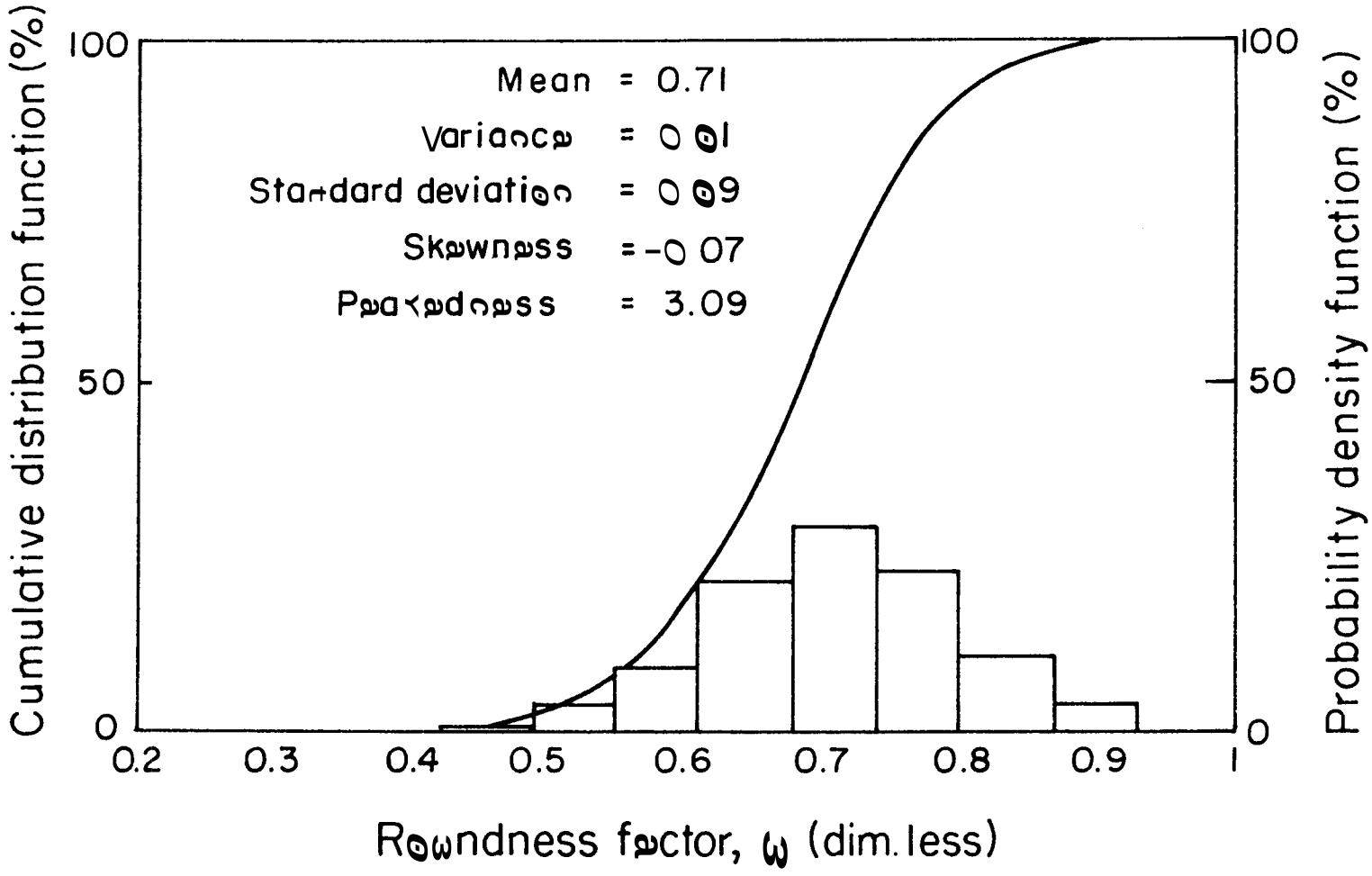


Figure 4.10 Cumulative distribution and probability density functions for roundness factor

The units of $\bar{X}$ and $\sigma$ are the same as for $X_i$ . The units of $s^2$ are the units of $X_i$ squared. The last two parameters, Sk and k are dimensionless.

The probability density functions of Figs. 4.2 through 4.4 for a , b , and c , show that the distributions of these quantities are not normal on the low side but they are fairly normal on the high side. It is apparent that there is a higher probability of encountering rocks with very small individual dimensions than very large. The probability density distribution for weight (Fig. 4.5) indicates that a rock with one relatively small dimension has the two other measurements of the same order. Additionally, a rock with one dimension near the mean has two other measurements which are substantially different from the mean. This may be one explanation for the pronounced skewness or the weight probability density function. The probability functions of the derived dimensionless quantities in Figs. 4.8 through 4.10 show a remarkable degree of normalcy, particularly the roundness factor. The statistical parameters obtained for the first sample are used as representative of the first rock load.

The mean values of the dimensionless ratios b/a and c/a yield one point in Fig. 4.11. According to the Zingg classification system on Fig. 4.1, the present rock sample is classified as tabular (or oblate) in shape ( b/a = .74, c/a = .50 ).

## 4.4 Determination of Rock Matrix Parameters

The "bulk parameters" of the rock after loading into the chimney are also of importance for the interpretation of the experimental results. The term "bulk parameters" refers to such parameters as total rock mass, mean density, volume of void, surface area/volume ratio, porosity, and permeability for the chimney load. The volume of rock with associated void space is referred to as the rock matrix. The rock matrix extends from the flow distribution baffle at the bottom to the flange face at the top of the chimney (see Fig. 2.10). Thus, there are spaces in the chimney and in the inlet/outlet piping where there are no rocks. Considerations is needed for the definition of the porosity of the rock load. On the one hand, one could use the ratio of the total chimney void between isolation valves not occupied by rock to the total

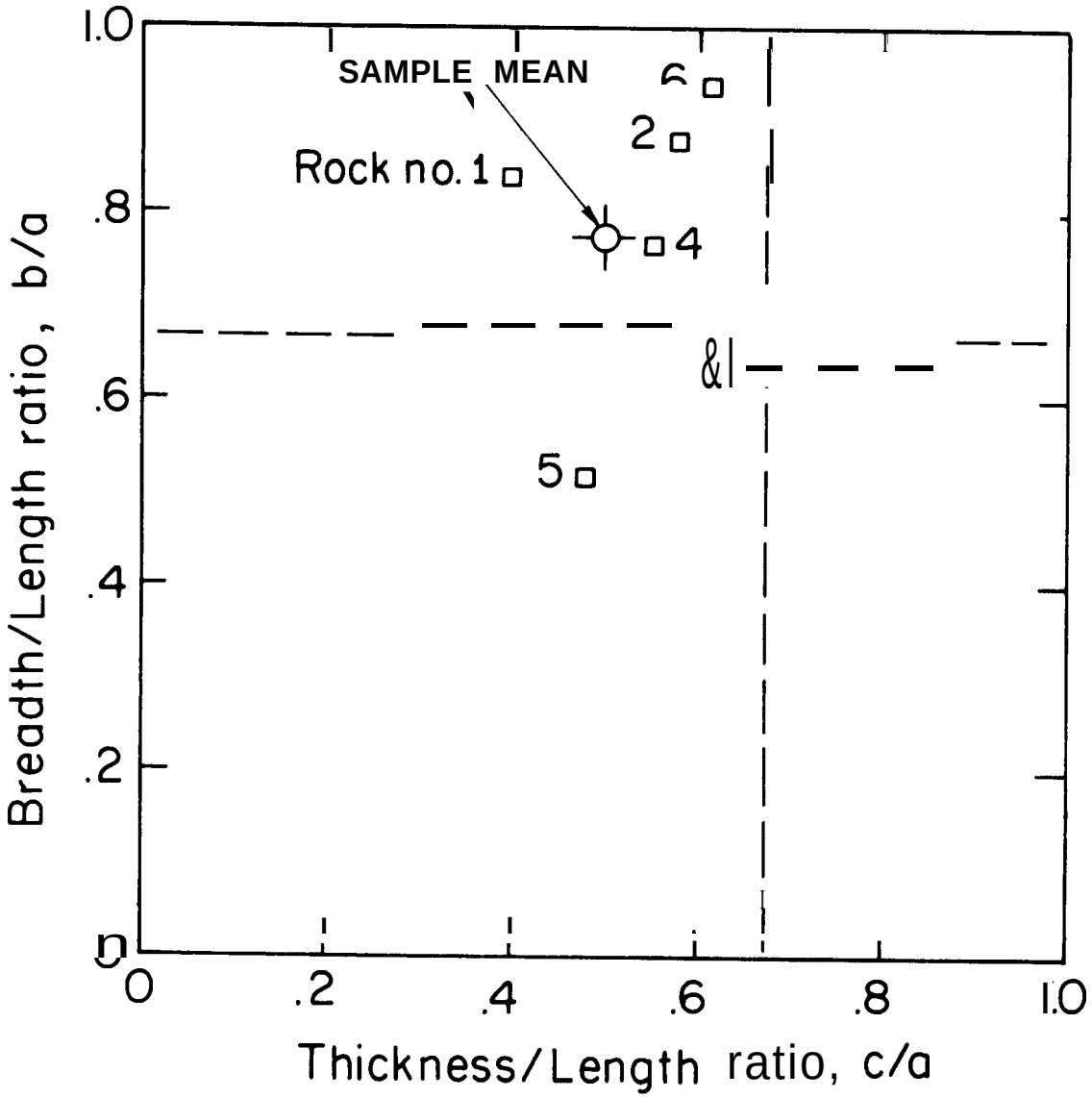


Figure *4.11* Classification of rocks using breadth/length and thickness/length ratios as coordinates

chimney void between isolation valves with no rock in chimney. Another definition for the porosity deemed more appropriate is to use the rock matrix porosity defined as follows

$$\varphi \triangleq \frac{\text{Volume of void in rock matrix}}{\text{Volume of rock matrix}} \qquad (4.7)$$

The following procedure was used to obtain the bulk parameters for the first load:

**(1)** The volume of the space between the flow distribution baffle and the inlet isolation valve was determined by filling it with water * at room temperature and weighting the quantity of water after draining.

(2) Rocks were put on a No. 8 sieve and thoroughly hosed off to remove sand, dust, and small rock particles.

**(3)** Each batch of rock was weighted and emptied into the chimney. The total rock weight was determined from the sum of the batch weights,.

*(4)* After loading of rock, step **(1)** was repeated, but this time the water was filled to the top flange face (top of rock matrix) and then drained. The difference between volumes determined from step *(4)* and **(1)** is the rock matrix void.

(5) Equation *(4.7)* was then used to compute the rock matrix porosity. This porosity should be referred to as the drainage porosity for the rock matrix since a small amount of water was retained on the rock surfaces.

*(6)* The rock matrix mean density was then computed using volume of rock (rock matrix volume less void) and the measured rock mass.

The bulk rock matrix permeability has not been determined because it is considered to be infinitely large (no resistence to flow).

A chemical analysis of the rock has not been performed and determination of the rock intrinsic properties of porosity and permeability was not made. It is anticipated that both these intrinsic properties are very small and of little importance to these experiments. Density measurements on individual rocks have not been made since it is anticipated that the bulk density determined for the load is adequate.

A summary of data determined for the rock load characteristics is presented in Table *4.1.*

* A drain line at the low point of the inlet line was used for filling and draining operations (see Fig. 2.1).

TABLE 4.1

Summary of Data for the First Rock Load

| | | Source |
|---|---|---|
| Rock type | Granite, "1-1/2 inch" | -- |
| Chemical analysis | Not determined | -- |
| Mass of rock in chimney | 1640 $lb_m$ | Weighing |
| Overall volume of rock matrix | 16.57 $ft^3$ | Computed |
| Volume of rock matrix void | 7.25 $ft^3$ | Weighing |
| Drainage porosity of rock matrix | 43.7 percent | Computed |
| Intrinsic rock porosity | Not determined(- 0) | -- |
| Rock matrix permeability | Infinite | -- |
| Mean bulk density | 99 $lb_m/ft^3$ | Measurement* |
| Intrinsic permeability | Not determined(- 0) | -- |
| Mean length (a) of rocks | 3.83 cm | Measurement |
| Mean breadth (b) of rocks | 2.82 cm | Measurement |
| Mean thickness (c) of rocks | 1.88 cm | Measurement |
| Mean weight of rocks | 32.61 g | Measurement |
| Mean equivalent diameter (d) | 2.52 cm | Measurement |
| Mean surface area of rocks | 22.74 $cm^3$ | Computed |
| Mean breadth/length ratio (b/a) | 0.74 (dimensionless) | Computed |
| Mean thickness/length ratio (c/a) | 0.50 (dimensionless) | Computed |
| Mean roundness factor ($\psi$) | 0.71 (dimensionless) | Computed |
| Mean solid density of rock | 2.79 $g/cm^3$ | Measurement |
| Specific heat capacity | 0.2 $Btu/lb_m$ °F | (Kreith, 1965) |
| Thermal conductivity | 0.54 Btu/hr-ft °F | (Kreith, 1965) |
| Thermal diffusivity | 0.019 $ft^2/hr$ | (Kreith, 1965) |
| Surface area conditions | Not defined | -- |
| Surface area per unit volume | 18.6 $ft^2/ft^3$ | Computed |

* Based on statistical analysis of measurements from first sample.

## 4.5 Description of Instrumented Rocks

Several "instrumented" rocks were positioned at various locations in the rock matrix to measure the temperature behavior of a rock during fluid production testing (see Fig. 2.10). The instrumentation consisted of 1/16 inch thermocouples inserted in 1/8 inch diameter holes drilled in selected rocks and cemented in place using a high temperature porcelain type cement. Data on the six instrumented rocks are tabulated in Table 4.2. The last column in the table shows the thermocouple number

TABLE 4.2

Data on Instrumented Rocks

| Rock ID No. | Length, a, (cm) | Breadth, b, (cm) | Thickness, c, (cm) | Equivalent diameter, d, (cm) | Ratio (b/a) | Ratio (c/a) | Roundness parameter ($\psi$) | Weight (g) | Depth of Drill (cm) | Thermocouple Number* |
|---|---|---|---|---|---|---|---|---|---|---|
| 1 | 6.4 | 5.1 | 2.5 | 4.0 | .80 | .40 | .68 | 93.6 | 1.9 | 202 |
| 2 | 4.3 | 4.1 | 2.8 | 3.8 | .98 | .58 | .79 | 77.6 | 1.9 | 204 |
| 3 | 5.3 | 3.6 | 3.3 | 3.9 | .69 | .62 | .74 | 86.3 | 2.2 | 210 |
| 4 | 5.6 | 4.1 | 3.0 | 3.9 | .97 | .55 | .74 | 89.1 | 2.2 | 211 |
| 5 | 6.4 | 3.3 | 3.0 | 4.1 | .95 | .48 | .63 | 98.3 | 2.0 | 215 |
| 6 | 4.2 | 3.9 | 2.5 | 3.6 | .99 | .61 | .83 | 65.6 | 1.3 | 217 |

*Refer to Fig. 2.10.

embedded in each rock. The location of each rock in the rock matrix can be inferred from this information and from Fig. *2.10.* A photograph of some of the instrumented rocks is shown in Fig. *4.12.* The dimensionless ratios b/a and c/a for each of these rocks are plotted in Fig. *4.11.* A comparison of the mean quantities for the six instrumented rocks and for the larger sample are made in Table *4.3.* It is apparent from this comparison that the average shape of the instrumented rocks are similar to the mean shape for the rock matrix while the mean weight is almost a factor of three larger. The instrumented rocks will therefore have somewhat larger thermal capacitance and smaller surface area/volume ratio than the mean rock in the first rock load and will tend to cool at a slower rate when located in an environment of decreasing temperature.

TABLE *4.3*

Comparison of Selected Mean Quantities for the Six Instrumented Rocks

| | b/a | c/a | $\psi$ | Weight (g) | Equivalent diameter (cm) |
|---|---|---|---|---|---|
| Mean of the six instrumented rocks | *.75* | *.54* | .73 | *85.2* | *3.88* |
| Mean of first large sample | *.75* | .50 | *.71* | *32.6* | *2.54* |

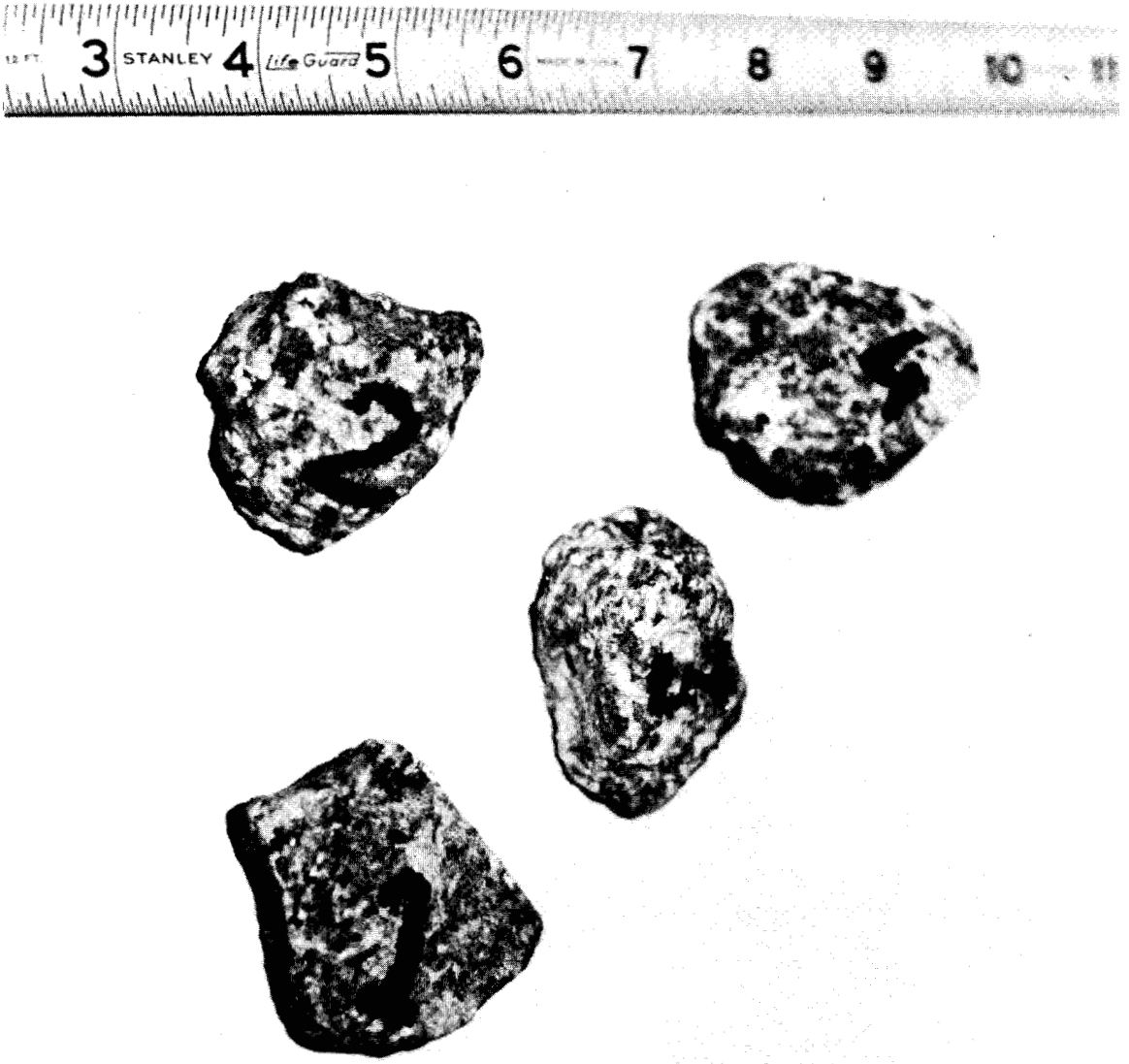


Figure 4.12 View of a few of the instrumented rocks

# CHAPTER 5

# TEST AND DATA ANALYSIS PROCEDURES

## 5.1 Test Procedure

Test procedures for fluid production runs consisted of the following steps:

1. The system was filled with tap water until desired water levels were established. Argon gas was added to accumulators 1 and 2 to establish system pressure of 100-200 psig. Chemicals for corrosion control were added at the beginning of the water fill. During the early phase of the test program hydrazin ($H_2NNH_2$) was used; later sodium sulfite ($Na_2SO_3$) was preferred.
2. The circulation pump and the electric circulation heater were turned on and heatup initiated. Heatup to initial fluid production conditions of about 490°F from room temperature was accomplished in about ten hours. When the desired temperature was reached (adjusted by the heater thermostat setpoint) the heater would trip. Pump circulation was maintained to establish temperature equilibrium of the chimney water/rock/metal system. After a few minutes the system had cooled enough so that the thermostat would switch the heater back on again and this cycling was repeated for about one half hour. All recording equipment was in operation during the heatup procedure.
3. The circulation pump was turned off and the chimney was isolated by closing the isolation valves on the inlet and outlet lines (see Fig. 2.1). Prior to initiating fluid production, the cooling water for the condenser was turned on and the initial weight (tare) of the fluid production tank and the gage pressure were recorded. Fluid production was initiated by opening the pressure control valve (see Figs. 2.1 and 2.9) until the desired initial production rate was established. Manual logging of chimney gage pressure, weight of fluid production tank, and chimney liquid level were made initially at frequent intervals. At later times in the production cycle less frequent logging was

required. Automatic recordings were made of the temperature data, chimney pressure, and condenser flow rate using multi-point chart recorders. In the cases of external heating being applied by the chimney tape heaters, current and voltage were also logged.

4. The two fluid production modes tested were (i) constant Pressure Control Valve (PCV) setting, and (ii) constant production flow rate. In the first mode the PCV setting was left unchanged during the production run while in the second mode the PCV setting was adjusted (based on plots of cumulative fluid production vs time) to maintain an approximate constant fluid production rate.
5. Fluid production was continued until a low pressure condition had been reached. The nominal objective was to produce to about 50 psig. Often, however, it was decided to discontinue at a higher pressure to initiate another run the same day. As a final step the data from the recorder charts were tabulated in convenient form for computer processing.

## 5.2 Data Reduction Procedure

### 5.2.1 Specific External Heat Transfer Parameter

The term "specific external heat transfer parameter" is used to describe the total amount of energy transferred as heat to the water/rock system contained inside the chimney, per pound of water originally in the system. The term is defined as

$$q_m \triangleq Q_m/(M_w)_o \ , \qquad (5.1)$$

where

$q_m$ = specific external heat transfer parameter (Btu/$lb_m$) ,

$Q_m$ = total external heat transfer (Btu) , and

$(M_w)_o$ = total amount of water in chimney at start of production ( t = 0 ) ($lb_m$) .

An expression for the quantity $Q_m$ has been derived from energy considerations in Appendix B and is*

$$Q_m = \int_0^{t_f} S_2 dt + M_2 \int_{\theta_{2f}}^{820} d(C_2\theta_2) - h_2A_2 \int_0^{t_f} \theta_2 dt \ , \qquad (5.2)$$

where the symbols are described in the Nomenclature.

Also, it is of interest to obtain an equation for $Q_m$ on a rate basis. An approximate expression for the mean value of this quantity in the finite time interval $t = t_1$ to $t = t_2$ is derived in Appendix B and is

$$(\bar{\dot{Q}}_m) \simeq \bar{S}_2 - M_2 \frac{(C_2\theta_2)_2 - (C_2\theta_2)_1}{t_2 - t_1} - h_2A_2\bar{\theta}_2 \ . \qquad (5.3)$$

The numerical values for $M_2$ and $h_2A_2$ given in Table **3.8** are used in Eqs. (5.2) and (5.3). In evaluating the chimney metal temperature the weighting factors presented in Table **3.1** are used as described in Chapter **3.**

5.2.2 Chimney Exit Enthalpy

It is anticipated that when the flash front has receded into the rock matrix the steam exiting from the chimney will be either slightly superheated steam or slightly wet steam. While the steam is passing from the top of the rock matrix to the PCV (see Fig. **2.9)** the steam will be degraded due to line heat losses to the surroundings. The steam exit condition at the PCV can be evaluated by an energy balance on the condenser. The derivations are presented in Appendix B. The major assumptions involved are that there are no heat losses from the condenser and no energy storage effects. The equation for the steam enthalpy at the PCV is given by

$$i_e = i_{H,out} + \frac{\dot{m}_c}{\dot{m}_p} \bar{C} \ (T_{c,out} - T_{c,in}) \ . \qquad (5.4)$$

* The integration in the second integral in Eq. (5.2) can be carried out directly to yield $M_2(C_2\theta_{20} - C_2\theta_{2f})$ .

The terms on the right are known from temperature and flow rate measurements. Since the adiabatic throttling in the PCV is a constant enthalpy process, $i_e$ is also the steam enthalpy just upstream of the PCV. If the steam is wet, the steam quality is computed from

$$X_e = \frac{i_e - i_f}{i_{fg}} \quad , \tag{5.4}$$

where the steam properties are evaluated at the chimney pressure (for negligible pressure drop in line upstream of the PCV).

5.2.3 Chimney Flash Front Location

The sight glass installed on the chimney to observe the effective flash front position during fluid production tests is rather poorly insulated and therefore the water contained in the glass is at considerably lower temperature than the water in the chimney. This introduces a density error in the observations which needs to be corrected. A formula for this correction is derived in Appendix B and is in dimensionless form

$$\frac{\ell}{h} = \left(1 - \frac{v_L}{v_{SG}}\right)\frac{H}{h} + \frac{v_L}{v_{SG}}\frac{\ell'}{h} \quad , \tag{5.6}$$

where

$\frac{\ell}{h}$ = corrected flash front position expressed as a fraction of rock matrix height (dimensionless) ,

$\frac{\ell'}{h}$ = observed or indicated flash front position (dimensionless) ,

$v_L$ = mean specific volume of liquid water in the chimney ($ft^3/lb_m$) ,

$v_{SG}$ = mean specific volume of liquid water in the sight glass ($ft^3/lb_m$) .

5.2.4 Void/Steam Quality Relationships

During fluid production testing the two phase mixture contained inside the chimney will pass through a series of states on the T-s diagram.* To determine the production path and particularly the end state,

* T-s diagram refers to temperature-entropy diagram.

two independent state variables are required. One state variable readily available is the chimney pressure. A second state variable that can be determined is the steam quality. The steam quality is defined by (see the Nomenclature for explanation of symbols):

$$X \triangleq \frac{M_g}{Mg + M_f} = \frac{M_g}{M_w} = 1 - \frac{M_f}{M_w} . \qquad (5.7)$$

Another quantity of interest is the void fraction defined by

$$\alpha \triangleq \frac{V_g}{V_g + V_f} = \frac{V_g}{V} = 1 - \frac{V_f}{V} . \qquad (5.8)$$

An expression for the void fraction, $\alpha$, in terms of the flash front position ( $\ell/h$ ) is derived in Appendix B and is given by

$$\alpha = (V_d + V_{sc} + V_c \varphi \frac{\ell}{h})/V , \qquad (5.9)$$

where the total volume occupied by steam and water between the chimney isolation valves is

$$V = V_d + V_{sc} + V_c \varphi + V_i . \qquad (5.10)$$

Thus, when $\ell/h$ is available, e.g. from observations (see previous section), the void fraction can be computed.

A relationship between the void fraction and the steam quality in terms of the void fraction $\alpha$ and the mass fraction is (derived in Appendix B)

$$X = 1 - \frac{v_o}{v_L M_w^*} (1 - \alpha) , \qquad (5.11)$$

where

$v_o \triangleq V/(M_w)_o$ = initial specific volume ( t = 0 ) ($ft^3/lb_m$) ,

$v_L$ = mean specific volume of liquids (saturated or slightly subcooled) ($ft^3/lb_m$) ,

$M_w^* \triangleq M_w/(M_w)_o$ = mass fraction remaining in system at time = t (dimensionless).

The mass fraction $M_w^*$ can be computed at any time $t$ from fluid production and fluid injection data, which with values of $\alpha$ and specific volumes will yield the steam quality by Eq. (5.11). This may be a useful procedure in determining the production path. One problem, however, with respect to the computation of $\alpha$ using observed $\ell/h$ values is that the sight glass does not extend to the very top of the rock matrix so that observations can start only after $\ell/h$ values of $-0.2$ have been reached. It would therefore be useful to have an analytic expression for $\ell/h$ in terms of $M_w^*$ which agrees with observations in the visible range that can be used for extrapolations to the invisible ranges (near top and near bottom of rock matrix). Such an expression has been derived in Appendix B for the case of saturated steam and liquid phases, and is

$$\ell/h = \left[\left(\frac{\dot{d}}{V_c\varphi} + \frac{\dot{s}c}{V_c\varphi}\right)\frac{1}{v_g} + \left(1 + \frac{\dot{i}}{V_c\varphi}\right)\frac{1}{v_f} - \frac{M^*}{V_c\varphi/(M_w)_o}\right] \qquad (5.12)$$

## 5.3 Fluid Production Model

The value of experimental results are greatly enhanced if a mathematical model of the physical phenomenon involved can be developed and validated. If this model can predict the observed behavior of the System with particular sets of relevant parameters, prediction of the behavior of similar systems with different sets of parameters can be made within the limitations of the model. A mathematical model describing the pressure decline as a function of time in terms of chimney parameters for given fluid production and fluid recharge histories is given. Testing of the model using experimental data obtained with the chimney model is in progress. Although no results are available at this time, it is useful to present the essence of the model for the purpose of illustrating where some of the non-dimensional variables proposed and used in the presentation of the experimental data originated.

A number of idealizations are inherent in the model and the important ones are listed below:

1. Both the steam and liquid phases within the chimney are saturated.

2. The temperature is that of saturated steam at the given pressure (uniform temperature throughout the chimney).
3. The rock is in thermal equilibrium with the surrounding two phase mixture.

Using the principles of conservation of mass and energy on a control volume enclosing the water/rock system inside the chimney, the following equation for the pressure decline can be derived:

$$\frac{dP}{dt} = \frac{\dot{Q}_m + \left(i_i + v_f \frac{e_{fg}}{v_{fg}} - e_f\right)\dot{m}_i - \left(i_p + v_f \frac{e_{fg}}{v_{fg}} - e_f\right)\dot{m}_p}{\left[(e_f)' + \frac{V\varphi}{M_w}\left(\frac{e_{fg}}{v_{fg}}\right)' + \frac{M_r}{M_w}(e_r)' - \left(v_f \frac{e_{fg}}{v_{fg}}\right)'\right] M_w} , \qquad (5.13)$$

where $(\,)'$ indicates differentiation with respect to pressure and other symbols are explained in the Nomenclature. Equation (5.13) can be made non-dimensional to a certain extent by introducing the following quantities:

$P_o$ = chimney pressure at start of fluid production ( $t = 0$ ) (psia),

$P^* \triangleq P/P_o$ = non-dimensional chimney pressure (dimensionless) ,

$M_w$ = mass of water in chimney (liquid and steam) at time $t$ ($lb_m$) ,

$(M_w)_o$ = mass of water at $t = 0$ ($lb_m$) ,

$M_w^* \triangleq M_w/(M_w)_o$ = mass fraction remaining in chimney (dimensionless) ,

$\dot{m}_P$ = steam production flow rate ($lb_m/hr$) ,

$(\bar{\dot{m}}_p)$ = mean steam production rate for complete pressure depletion period ($lb_m/hr$) ,

$\dot{m}_P^* \triangleq \dot{m}_P/(\bar{\dot{m}}_P)$ = steam production rate parameter (dimensionless) ,

$m_i$ = fluid injection or recharge flow rate ($lb_m/hr$)

$\dot{m}_i^* \triangleq \dot{m}_i/(\bar{\dot{m}}_P)$ = fluid injection rate parameter (dimensionless)

$t$ = production time (hr)

$t^* \triangleq t(\bar{\dot{m}}_p)/(M_w)_o$ = non-dimensional production time parameter (dimensionless).

With this notation, Eq. (5.13) becomes

$$\frac{dP^*}{dt^*} = \frac{\dot{Q}_m/(\bar{\dot{m}}_p) + \left(i_i + v_f \frac{e_{fg}}{v_{fg}} - e_f\right)\dot{m}_i^* - \left(i_p + v_f \frac{e_{fg}}{v_{fg}} - e_f\right)\dot{m}_p^*}{\left[(e_f)' + \frac{1}{M_w^*}\frac{V\varphi}{(M_w)_o}\left(\frac{e_{fg}}{v_{fg}}\right)' + \frac{1}{M_w^*}\frac{M_r}{(M_w)_o}(e_r)' - \left(v_f \frac{e_{fg}}{v_{fg}}\right)'\right] M_w^* P_o} \quad .(5.14)$$

This form should make numerical calculations easier. Those non-dimensional parameters such as $t^*$, $M_w^*$, and $P^*$ are used extensively for presentation of the experimental results.

Some understanding of the pressure behavior of the reservoir can be obtained immediately by considering Eq. *(5.14):*

1. External heat transfer to the water/rock system, represented by $\dot{Q}_m/(\bar{\dot{m}}_p)$, results in slower rate of pressure decline ($dP^*/dt^*$ less negative).
2. Recharge of water, represented by $\dot{m}_i^*$, results in slower rate of pressure decline when the recharge water enthalpy is high enough, otherwise recharge may result in faster rate of pressure decline ($i_i$ relative to $e_f$ effect).
3. Fluid production, represented by $\dot{m}_p^*$, increases rate of pressure decline when the enthalpy of produced fluids is great enough, otherwise production may result in decreased rate of pressure decline ($i_p$ relative to $e_f$ effect).

# CHAPTER 6

# EXPERIMENTAL RESULTS

A total of nine fluid production runs have been made with the chimney model system. The test conditions are presented in Table 6.1. The first three tests (Runs 1 through 3) were with water only in the chimney and the remaining tests (Runs 4 through 9) were with water and rock. It is noted that Run 5 was for particularly low initial pressure and temperature conditions. This was caused by the circulation pump seal which started leaking during heatup requiring the circulation pump to be shut down. The run, however, is useful for evaluation of the effect of low initial pressure/temperature conditions on fluid production. The last run made was with recharge of cool water.

## 6.1 Specific External Heat Transfer Parameter

Since the procedure given in Section 5.2.1 involves considerable numerical evaluation results are available only for Runs 3 and 7. From these values estimates of the specific external heat transfer parameters for the remaining runs were obtained by extrapolation.

A convenient representation of the various energy quantities involved are given in Fig. 6.1 for Run 3. The curves represent the various terms in Eq. (5.3) computed from the experimental temperature data and system parameters evaluated previously. In this case there was no external heating. Thus the first integral on the right in Eq. (5.2) is zero. The second integral is equal to area cdefc less the very small area abca . The third integral is equal to area bfhgb . The total external heat transfer to the water/rock system, $Q_m$ , according to Eq. (5.2) is the area represented by the hatched area on Fig. 6.1.

The corresponding "energy" diagram for Run 7 is shown in Fig. 6.2. Heating was applied in this case and the total energy addition corresponding to the first integral in Eq. (5.2) is equal to area abcda . Numerical integration of the two integrals by the trapezoidal rule yielded the numerical values presented in Table 6.2.

The minus sign for the numerical values of $q_m$ indicates that energy has been removed from the water during the production and a plus sign indicates energy addition.

TABLE 6.1

Characteristics of Fluid Production Runs in the Chimney Model

| Run | Production Run ID No. | Chimney Loading | Initial Pressure (psia) | Final Pressure (psia) | Initial Temp.[2] (°F) | Final Temp.[3] (°F) | Production Mode | Re-charge | External Heating |
|---|---|---|---|---|---|---|---|---|---|
| 1 | 040274 | Water | 730 | 136 | 499 | 351 | Constant PCV Setting[4] | No | No |
| 2 | 041774 | " | 737 | 62 | 500 | 295 | " | " | " |
| 3 | 052974 | " | 796 | 40 | 498 | 264 | " | " | " |
| 4 | 072474 | Water/ Rock[1] | 604 | 32 | 477 | 255 | " | " | " |
| 5 | 072574 | " | 255 | 16 | 386 | 217 | Constant Production Rate[5] | | |
| 6 | 072974 | " | 659 | 23 | 486 | 236 | " | " | " |
| 7 | 080174 | " | 647 | 99 | 484 | 327 | " | " | Yes |
| 8 | 080274 | " | 647 | 57 | 486 | 290 | Constant PCV Setting | " | " |
| 9 | 080874 | " | 647 | 28 | 485 | 246 | Constant Production Rate | Yes | " |

[1] The characteristics of the rock loading are summarized in Table 4.1

[2] Temperature at chimney exit (subcooled conditions initially)

[3] Temperature at chimney exit (saturated steam at chimney pressure)

[4] Constant pressure control valve (PCV) setting means that steam exit valve is set at a particular opening throughout the experiment

[5] Constant production rate is maintained by adjusting the PCV as the pressure declines to obtain approximately constant production rate.

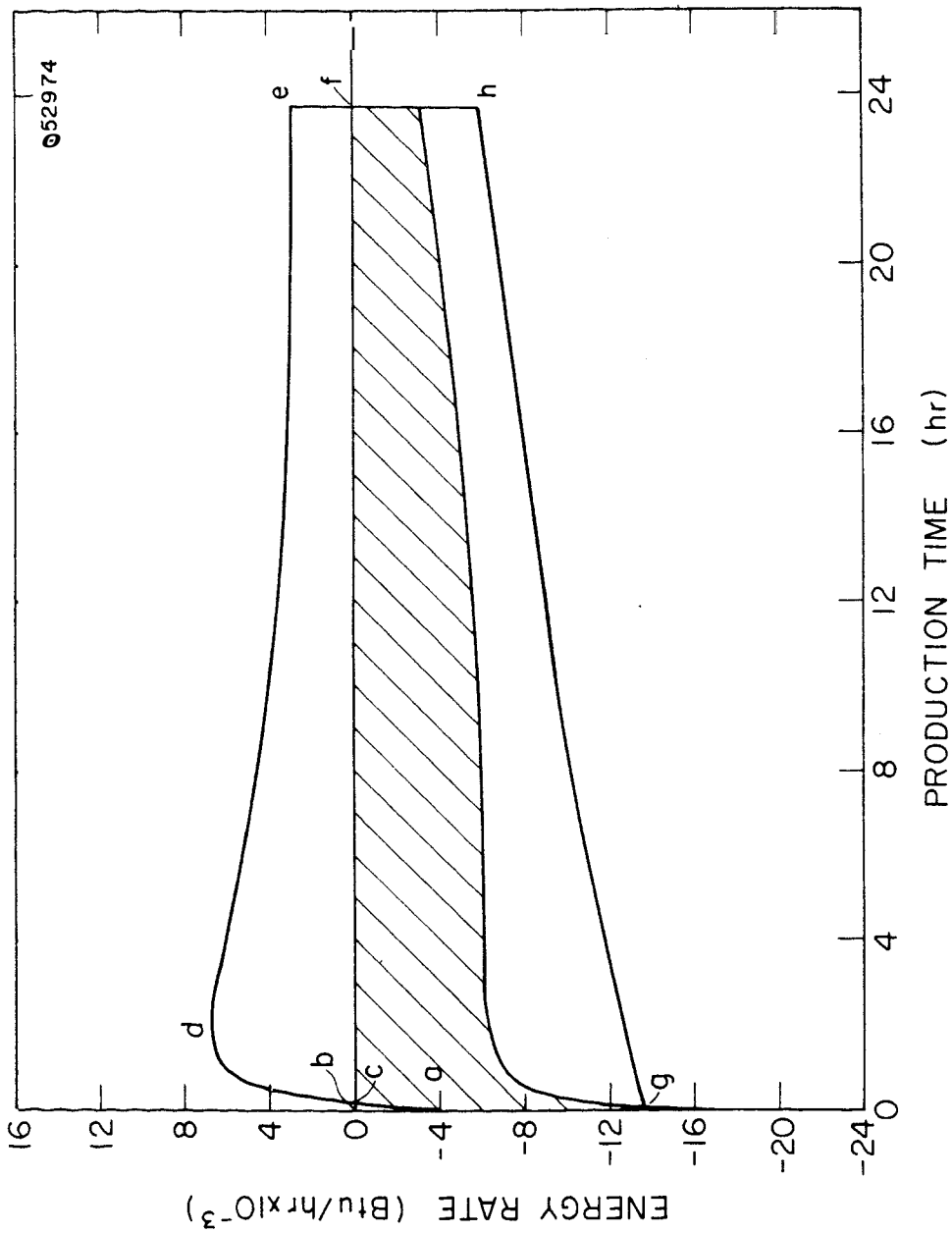


Figure 6.1 Diagram of energy quantities in the external heat transfer parameter for Run 3

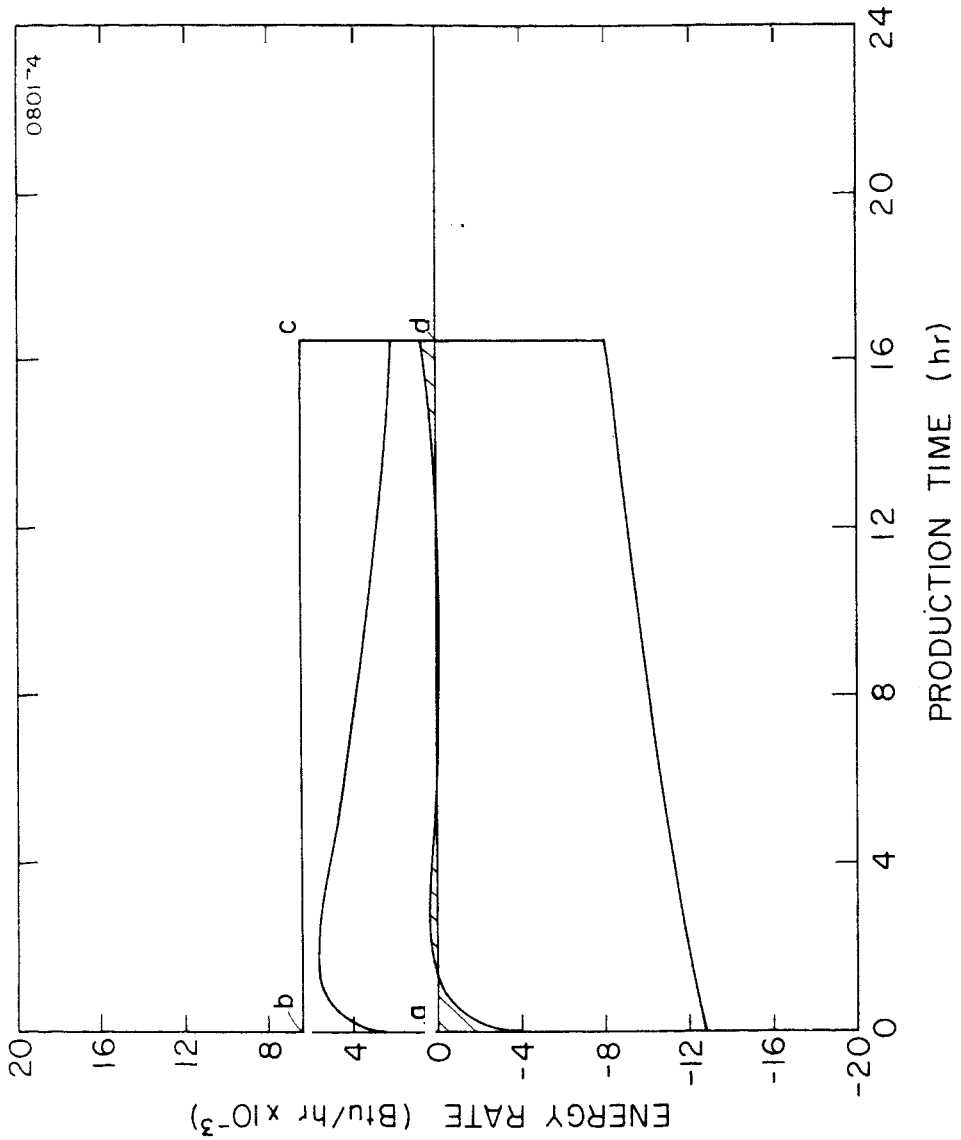


Figure 6.2 Diagram of energy quantities in the external heat transfer parameter for Run 7

TABLE 6.2

Numerical Data for Specific Heat Transfer Parameter Evaluation

| Run | $\int_0^{t_f} S_2 dt$ (Btu) | $M_2(C_2\theta_{20}-C_2\theta_{2f})$ (Btu) | $\int_0^{t_f} h_2 A_2 \theta_2 dt$ (Btu) | $Q_m$ (Btu) | Initial Mass $(M_w)_o$ ($lb_m$) | $q_m = Q_m/(M_w)_o$ (Btu/$lb_m$) |
|---|---|---|---|---|---|---|
| 3 | 0 | 109,200 | 220,400 | -111,200 | 865.7 | -129 |
| 7 | 105,800 | 70,300 | 176,000 | -100 | 416.8 | -1 |

## 6.2 Fluid Production and Recharge Characteristics

The cumulative fluid production vs production time for the runs of Table 6.1 are shown in Fig. 6.3. The two numbers at the endpoint of each curve are the total fluid production and the production time for a particular run. The table in Fig. 6.3 shows the production mode (either constant PCV setting or constant production rate) and the specific external heat transfer parameter, $q_m$, for each run.

The initial steam production rates were set by the operator. For the runs in which it was attempted to keep the production rate constant Runs 5, 6, 7, and 9) the operator also established to some extent the shapes of later portions for these curves.

The last run (Number 9) involved recharge of cool water. All other runs of Table 6.1 had no recharge. The recharge was accomplished with the injection pump. The recharge rate was determined by flow calibration of the pump at a particular setting prior to the test.

The recharge rate and cumulative recharge for Run 9 are shown in Fig. 6.4. It is noted that the recharge rate is low initially when the chimney pressure is highest. Increasing recharge rates resulted as the chimney pressure was reduced by fluid production.

## 6.3 Pressure Depletion

On initiation of the production cycle the liquid at the chimney exit was generally slightly subcooled, i.e., its temperature was lower than that corresponding to saturation temperature for the given system pressure. Figure 6.5 for Run 3 (water only) and Fig. 6.6 for Run 4 (water/rock in chimney) show the saturation and measured temperatures

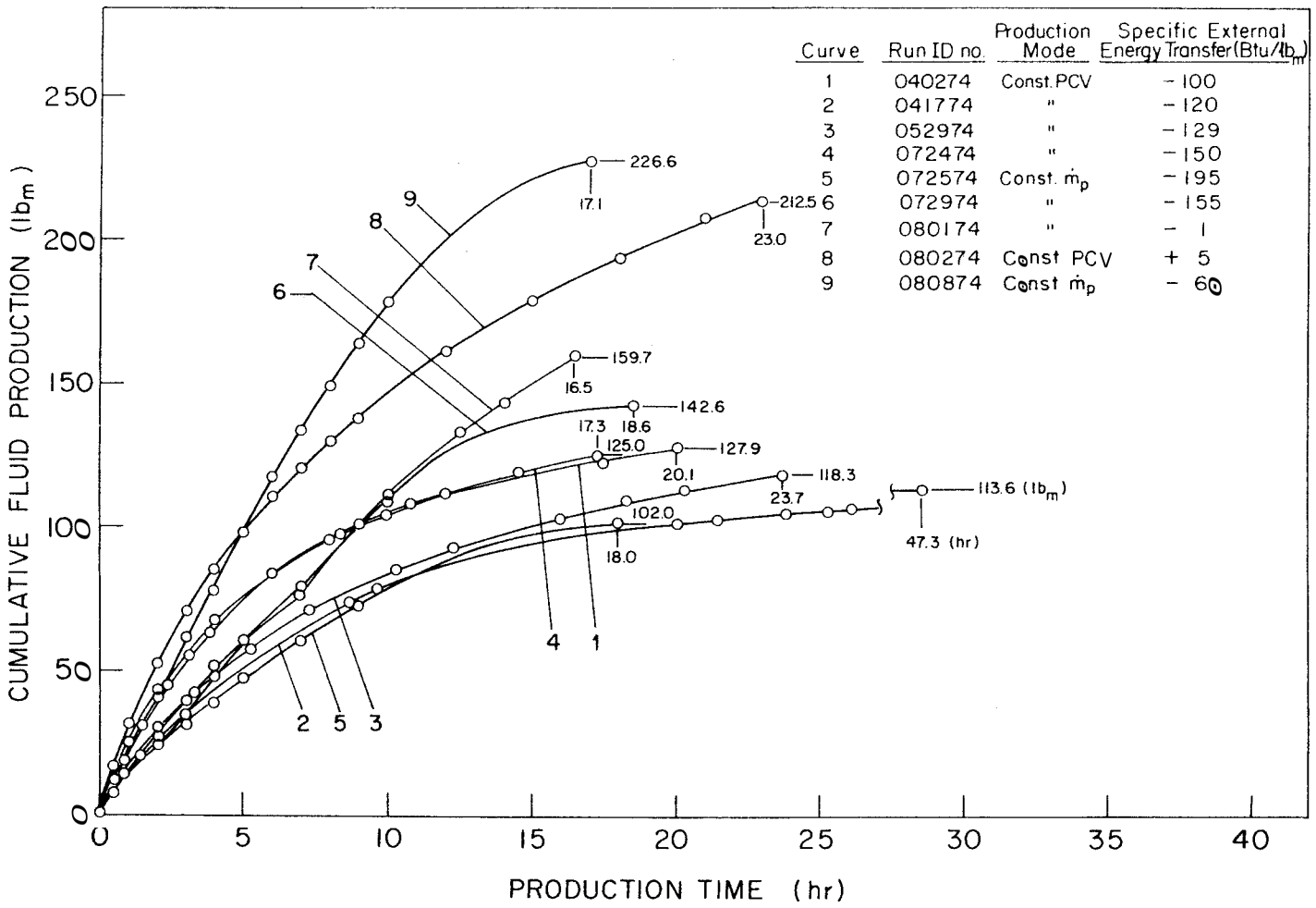


Figure 6.3 Cumulative fluid productions for first test series

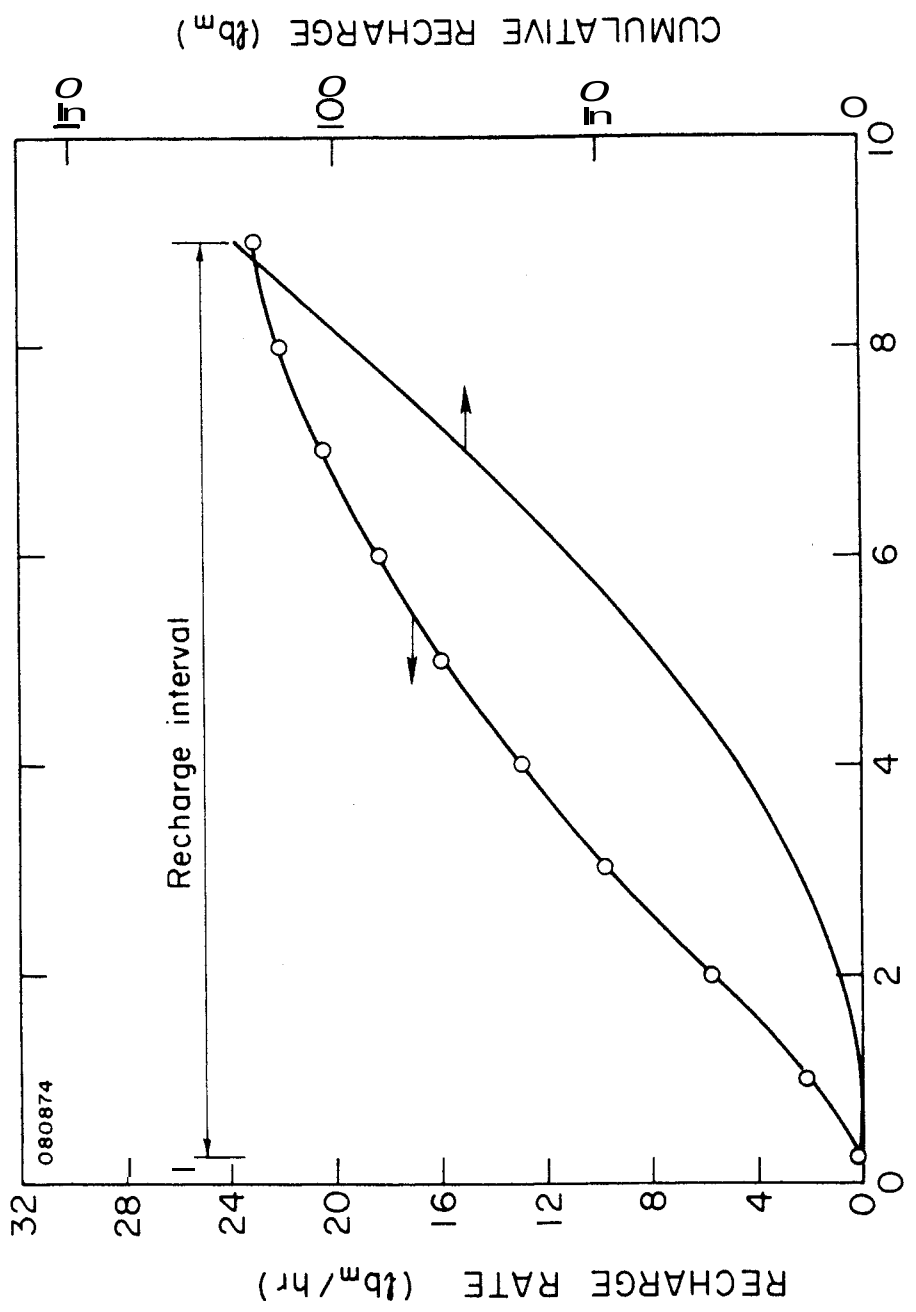


Figure 6.4 Cumulative recharge and recharge rate for Run 9

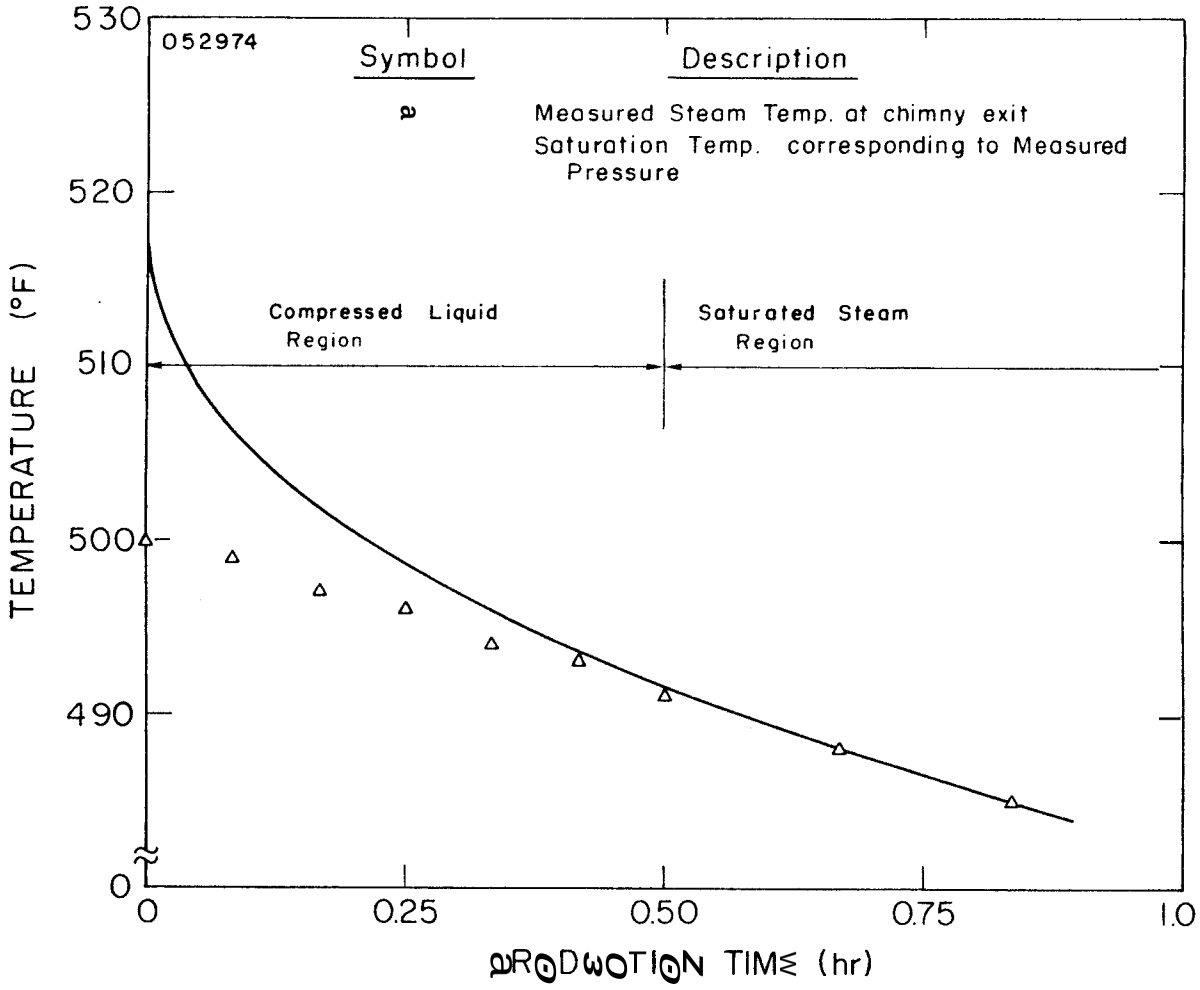


Figure 6.5 Illustration of compressed liquid region during early phase of production cycle for Run 3

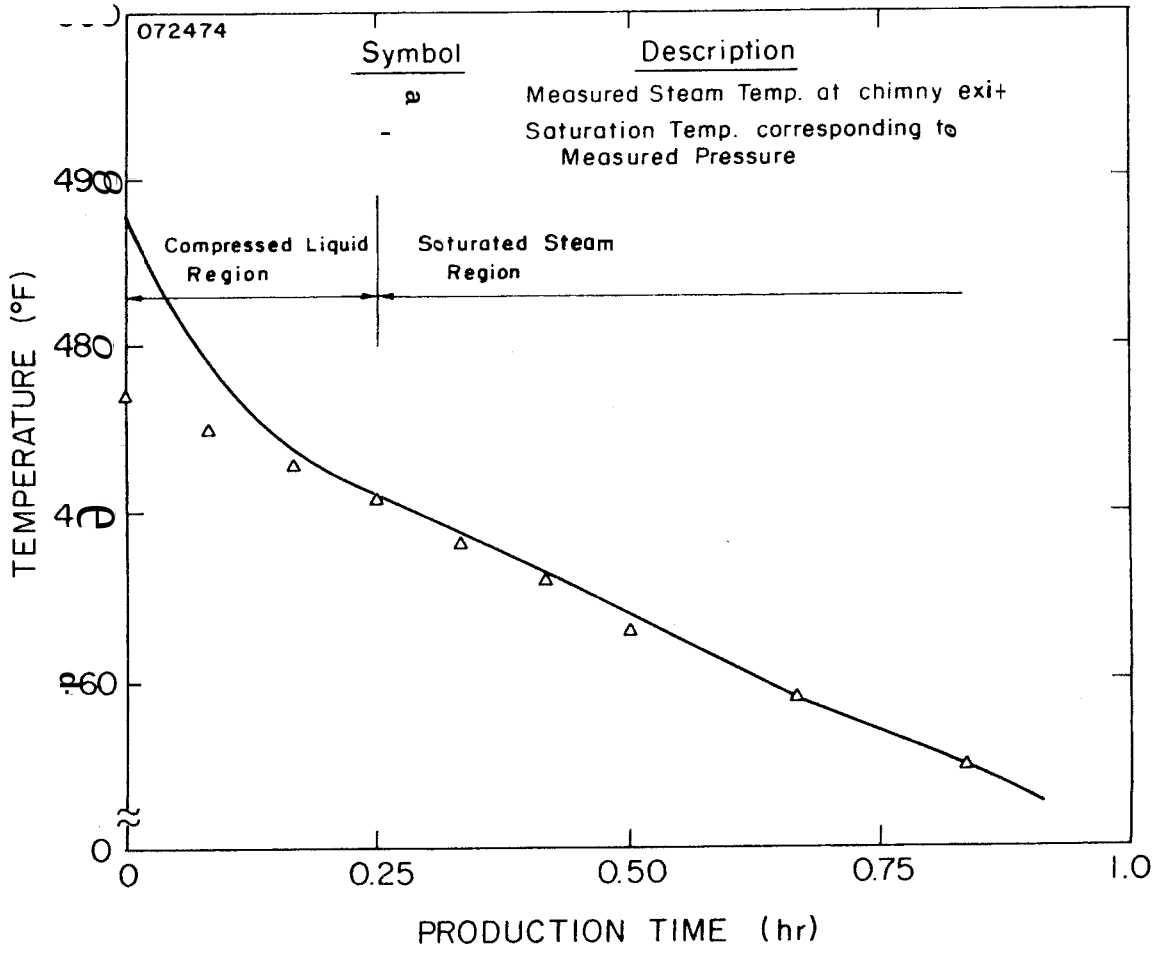


Figure 6.6 Illustration of compressed liquid region during early phase of production cycle for Run 4

as a function of production time. The measured water temperatures at the chimney exit are also plotted for the early phase of the fluid production period.

The complete chimney pressure depletion histories for all runs are shown in Fig. 6.7. The pressures along the ordinate are normalized to the initial chimney pressures (see Table 6.1). The production time is the non-dimensional time variable, $t^*$, defined in Section 5.3. It is observed that the use of these coordinates tends to introduce a wide range of data. The use of standard pressure and time variables would have resulted in a rather narrow range of data. Figure 6.7 shows some specific characteristics:

1. Runs with water only (1, 2, and 3) tend to deplete in pressure faster than the water/rock runs (4 through 9) when plotted in these non-dimensional coordinates. The one exception was Run 1 which tended to overlap the water/rock runs, 4 and 5. Run 1 was produced more rapidly (larger PCV opening) than Runs 2 and 3. This resulted in a comparatively smaller energy loss from the water/rock as indicated by the magnitudes of the specific external heat transfer parameter in the table in Fig. 6.7.
2. Run 5 had the lowest initial pressure (see Table 6.1) and the pressure depletion was below all other water/rock runs. This run also had a relatively high specific external heat transfer parameter.
3. The water/rock runs with external heating (Runs 7, 8, and 9) are considerably higher than all other runs. The supply of electrical energy by the heater tapes produced the low magnitudes of the specific external heat transfer parameters as indicated in the table. The use of non-dimensional coordinates also tended to "stretch" the curves for the heated runs to the right.

## 6.3 Fraction Produced

The fluids produced divided by the total amount of fluids originally in the system is of significance in geothermal resource evaluations. The fraction is often referred to as fraction produced.

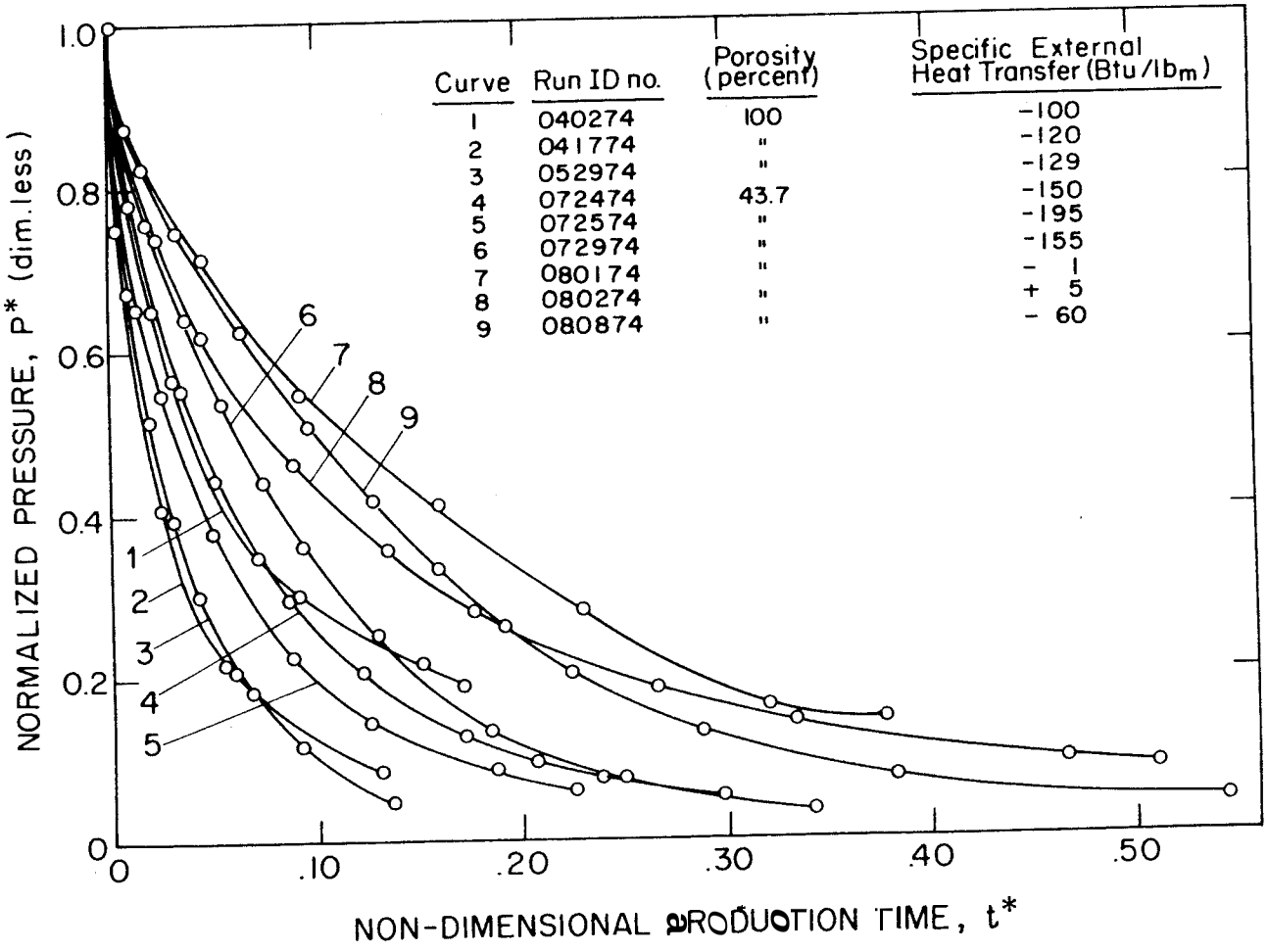


Figure 6.7 Pressure depletion histories for all runs of the first test series

In Fig. 6.8 the normalized chimney pressure vs fraction produced is given for all runs. Several characteristics are noted in this figure:

1. The water/rock runs have higher fractions produced than the water runs except for Run 5 which is among the water runs for most of the pressure range but higher fraction produced is achieved in the low pressure range. Since Runs 1 through 3 had porosity of 100 percent and Runs 4 through 9 had porosity 43.7 percent these results may indicate that systems with low porosities have higher fractions produced. When energy is extracted from the rock the observed behavior is expected from energy considerations.
2. The effect of initial pressure on the fraction produced can be seen by considering Run 5 in relation to Runs 4, and 6 through 9, which all were at relatively higher initial pressures (see Table 6.1). It also appears that the higher the initial pressure the higher the fraction produced.
3. It is observed from Fig. 6.8 that final fractions produced ranged between 13 and 15 percent for the water runs. The corresponding range for the unheated water/rock runs (Runs 4 through 6) was 22 to 34 percent. This represents roughly a factor of two which is what one would expect when a large fraction of energy contained in the rocks are extracted, since the heat capacity of the chimney rock is of the same order as that of a corresponding volume of water. Therefore, one can conclude that a large fraction of the energy stored in the chimney rock was released to the water during production.
4. Fractions produced of more than 50 percent was achieved when heating was applied at rates large enough to make the specific external heat transfer parameter zero or slightly positive (natural environment). Fractions produced of more than 50 percent therefore might be expected for natural systems with otherwise similar system parameters and at similar conditions (same energy extraction efficiency from the rock).
5. There appears to be a distinct difference between the curvatures for the water and water/rock runs. Whereas, the water runs are characterized by fairly constant slopes, the water/rock runs exhibit decreasing slope magnitude with decreasing pressure level.

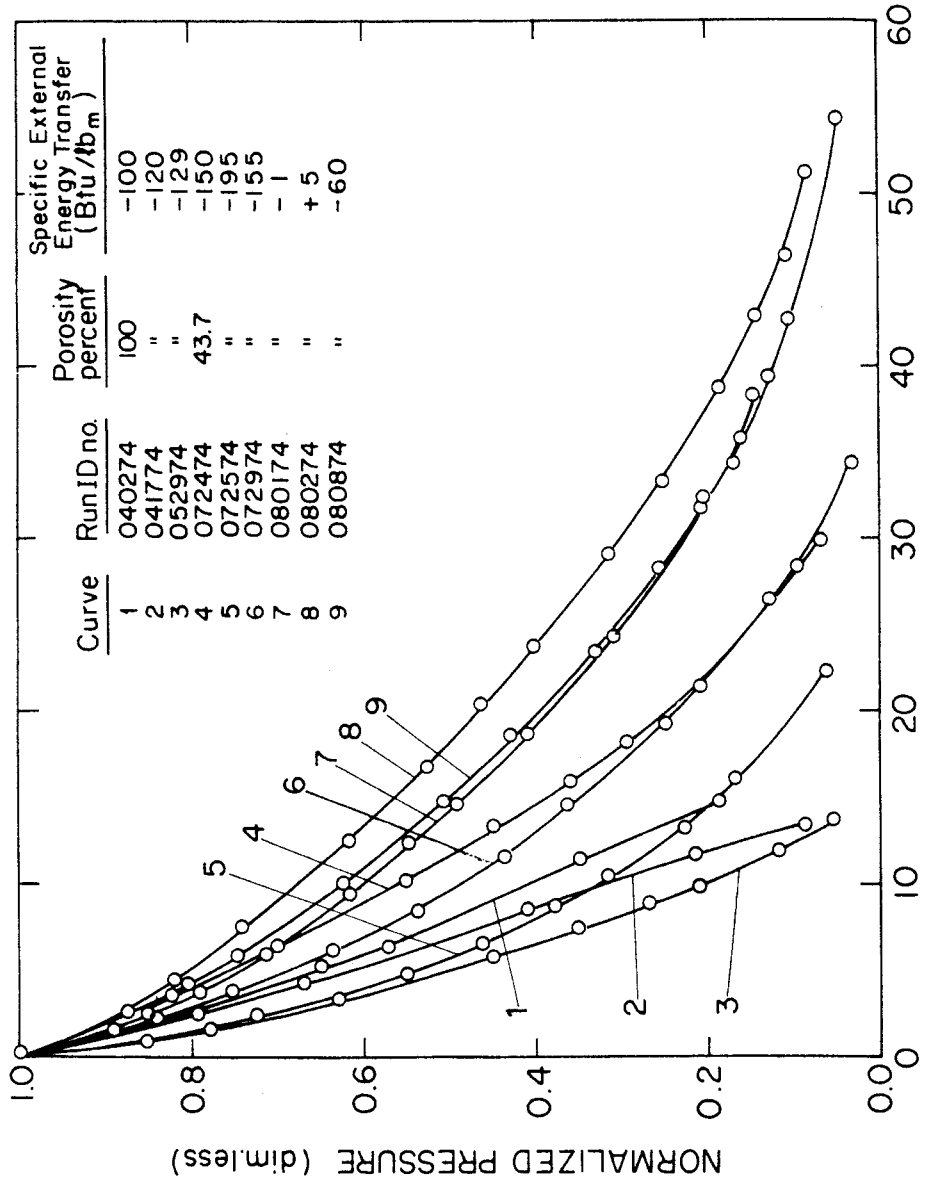


Figure 6.8 Fraction produced for water and water/rock systems

Comparison of Figs. 6.7 and 6.8 indicate some similarities. For example, a high level curve on Fig. 6.8 (which indicates that the ability to produce is high) has a high level counterpart on Fig. 6.7 even though there is not a one to one correspondence. It appears therefore that the relative position of a curve on Fig. 6.7 indicates what ability the system has to produce fluids.

Injection or recharge of essentially cool water did not increase the fraction produced for Run 9. However, such an increase is expected in general as long as the injection takes place at the bottom and the cooler fluid remains in the lower section of the chimney, i.e., does not mix with water at the surface (flash front). In this case, however, the apparent abnormality is believed to be caused mostly by the difference in specific external heat transfer parameters.

## 6.5 Flash Front Position

The sight glass on the chimney was used to observe where the effective flash front position or liquid level was located. These observations are presented in Fig. 6.9 where the flash front position measured from top of rock matrix is plotted in non-dimensional form as a function of production time for Run 4. Also given is the corrected flash front position based on Eq. (5.6) and the computed liquid level based on Eq. (5.12). The computed liquid level based on mass fraction from Eq. (5.12) is an average of 5 percent (of the chimney height) higher than the corrected observations.

## 6.6 Chimney Temperatures

The temperature measured at the chimney exit ( T/c 110 on Fig. 2.10) generally corresponded to the saturation temperature for the measured pressure. This temperature measurement was therefore used for the chimney system temperature. These temperatures are given as a function of non-dimensional production time in Fig. 6.10. The temperatures referenced to ambient temperature ( $T_\infty$ ) are normalized to $\theta_o = T_o - T_\infty$ which is the difference between the initial system temperature and the ambient temperature.

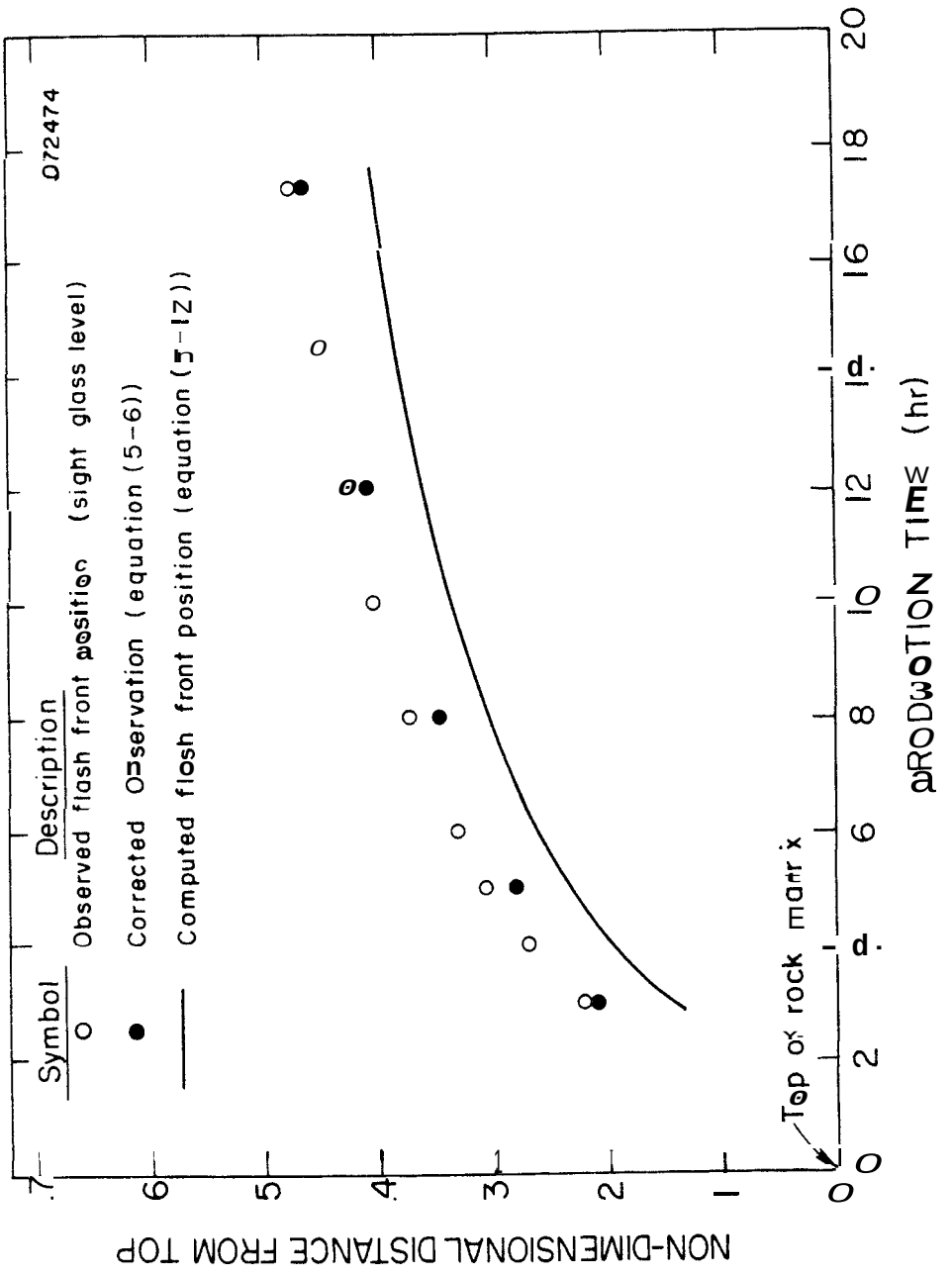


Figure 6.9 Flash front position during production Run 4

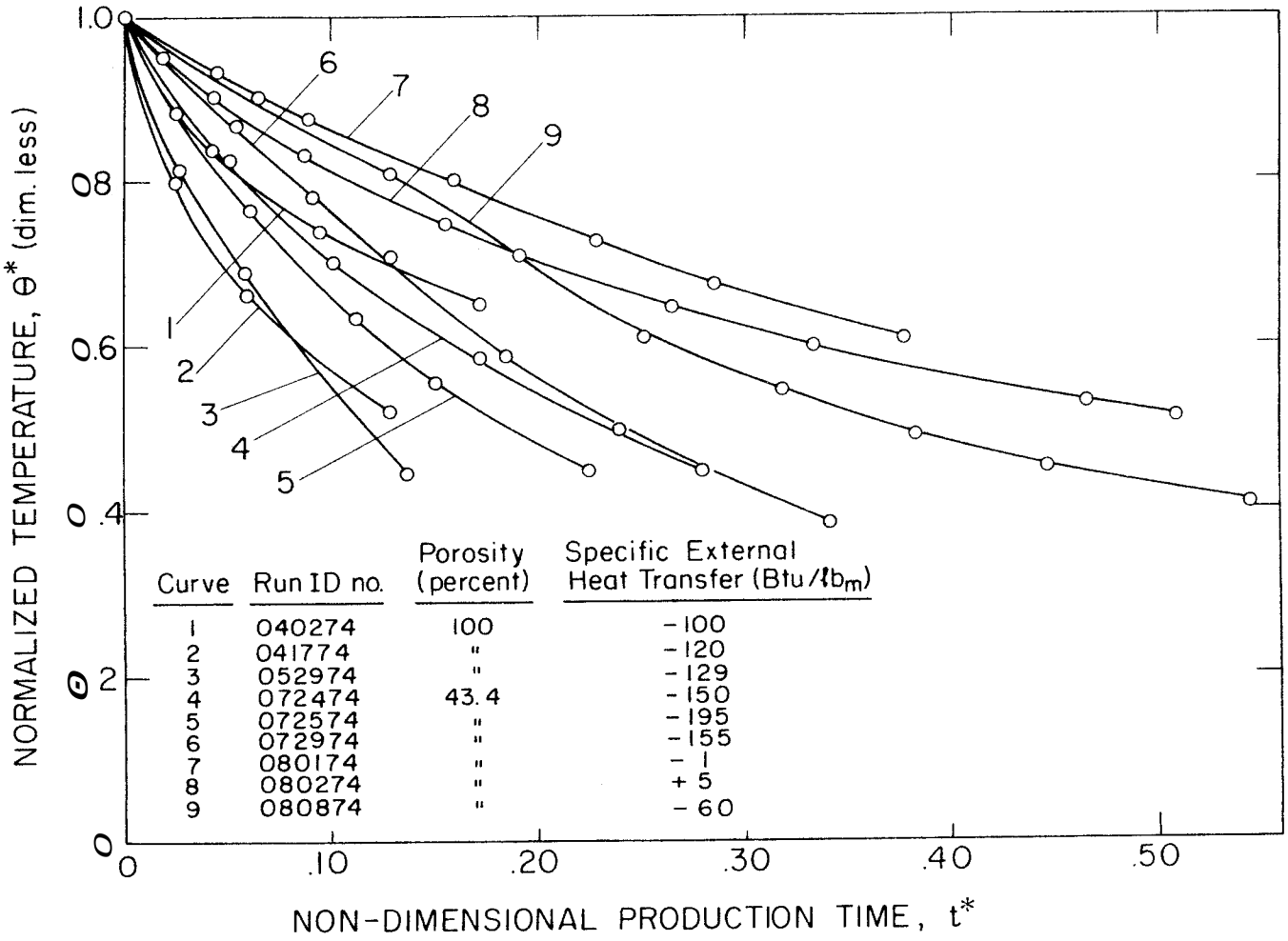


Figure 6.10 Chimney temperature histories for all runs of the first test series

Because of the vapor pressure/temperature relationship for saturated water the curves on Fig. 6.10 are expected to resemble the normalized pressure curves on Fig. 6.7 except for the very early part of the production period where the system is subcooled. A comparison of these two figures shows that the pressure and temperature curves for a particular run have the same relative locations on each figure.

### 6.6.1 Water/Rock Temperature Distribution

The locations of the thermocouples for the determination of chimney water and rock temperature distributions are shown in Fig. 2.10. Discussion of the "instrumented rocks" were given in Section *4.5*. From the temperature data provided by these thermocouples, the water/rock temperature distributions along the chimney center line* are shown on Figs. 6.11 through 6.16 for Runs 4 through 9. The water/rock temperature distributions are plotted at various values of the production time, t . Also, included are the measured chimney exit temperature which except for early production times is the saturation temperature corresponding to the chimney pressure. Additionally, the uncorrected observations of the water level or flash front positions are included (corrected values on Fig. 6.11). These data also show several characteristics:

1. It appears that the initial temperature distribution in the chimney is uniform to a very high degree. Temperature measurements along the walls of the chimney also showed similar behavior. This indicates that there is temperature equilibrium between the water and rock media at the start of the experiment.
2. During fluid production the water/rock temperature distribution appears to remain uniform and approximately equal to the saturation temperature in regions below the water level, i.e., there is temperature equilibrium between the instrumented rocks and the surrounding water. It is very likely that the instrumented rock temperatures are representative of the whole rock matrix submerged in water in view of the large mean mass of the individual instrumented rocks compared to that of the mean for the rock matrix (almost a factor of 3 to 1, see Chapter *4)*. Thus,

---

* An exception was the thermocouples next to the rock matric top which were located 5 inches off center (7 inches from the wall).

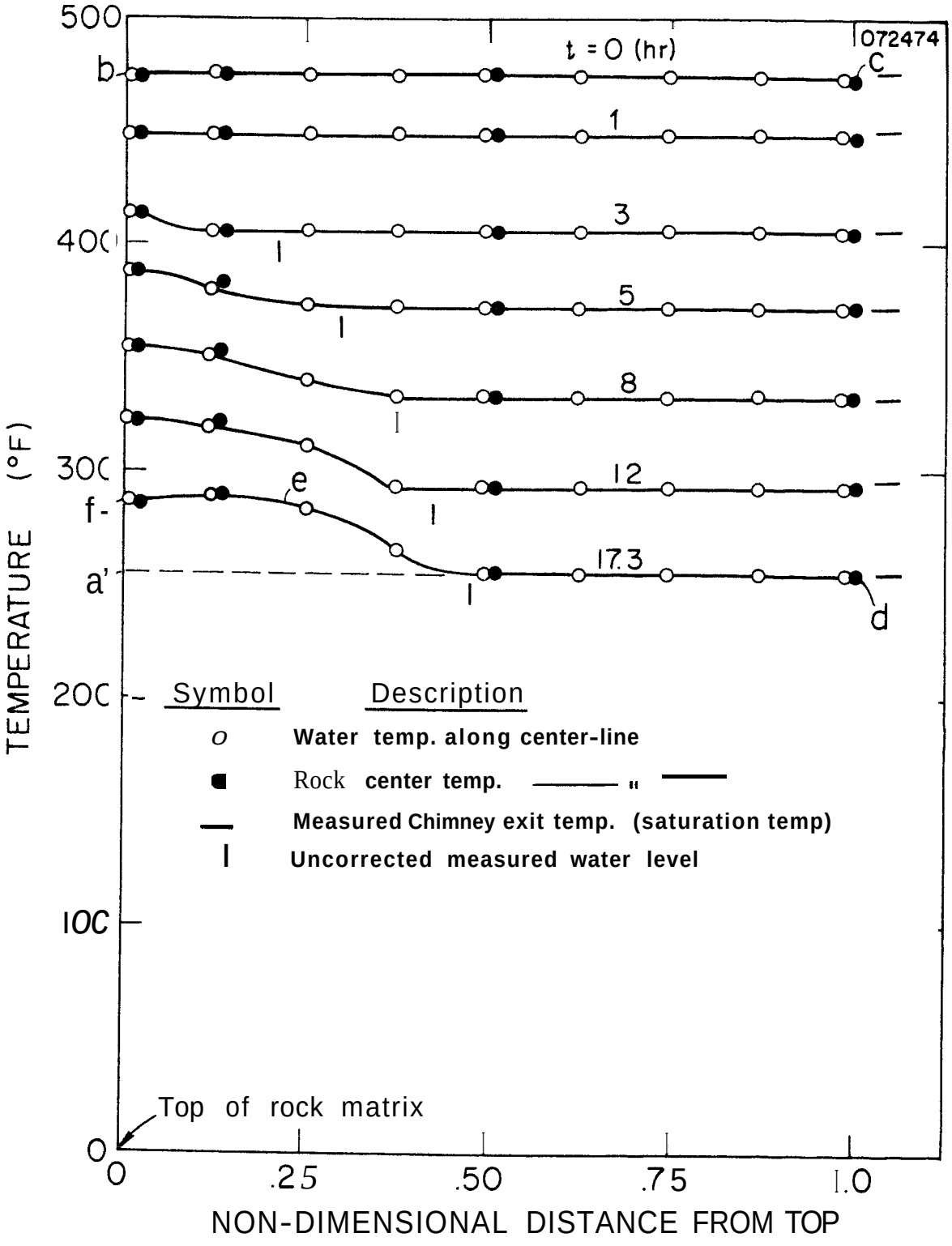


**Figure 6.11** Centerline water/rock temperature history for Run 4

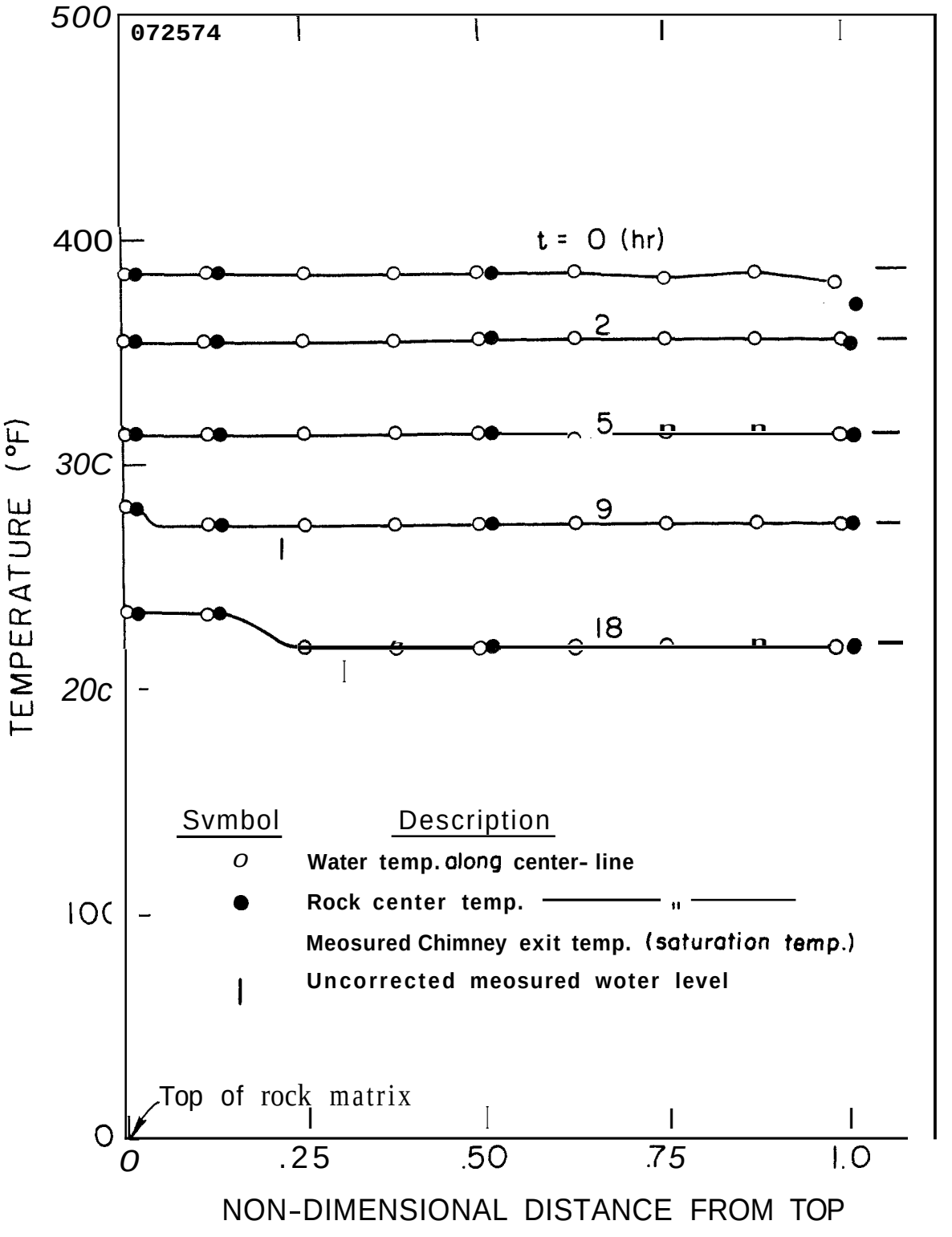


Figure 6.12 Centerline water/rock temperature history for Run 5

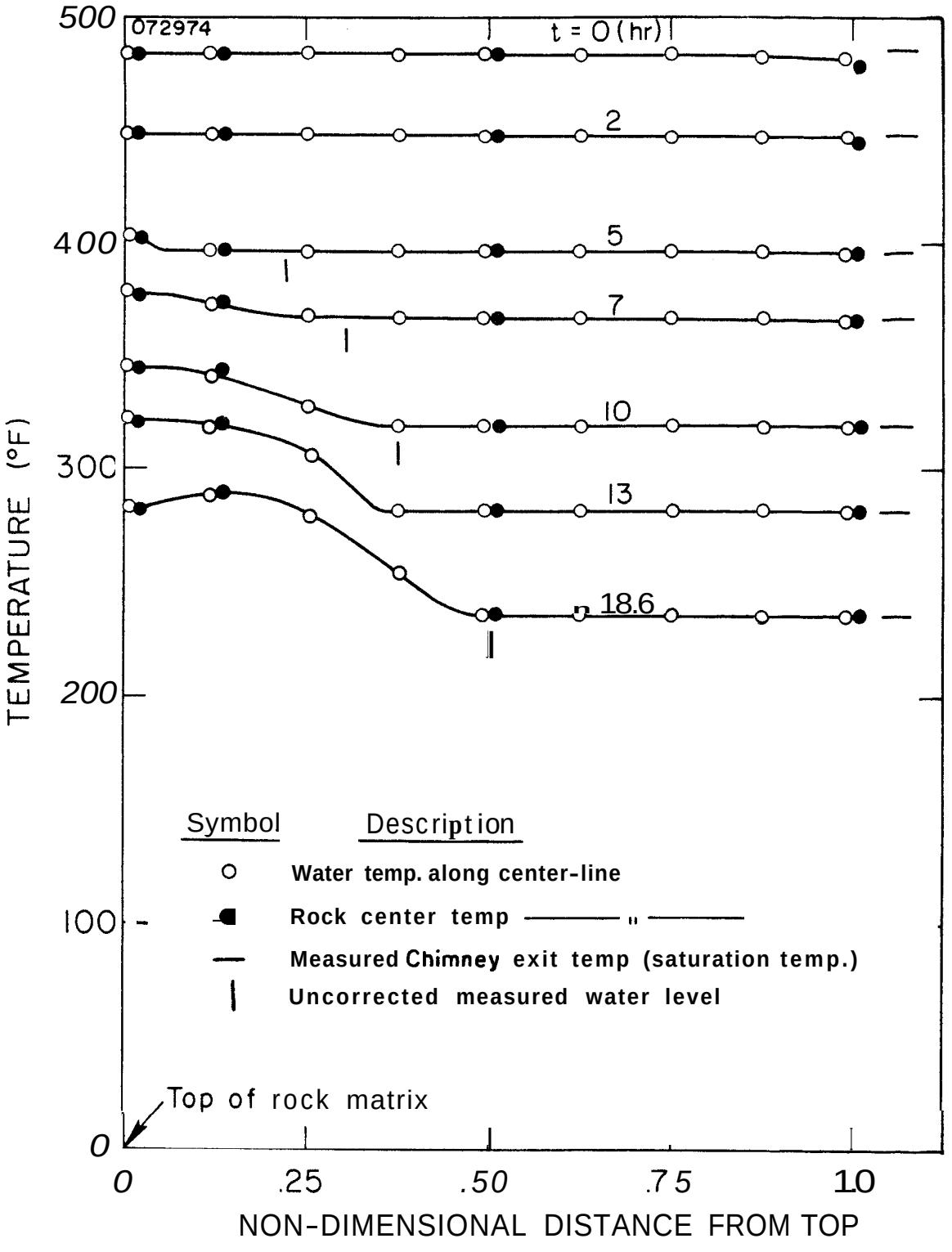


Figure 6.13 Centerline water/rock temperature history for Run 6

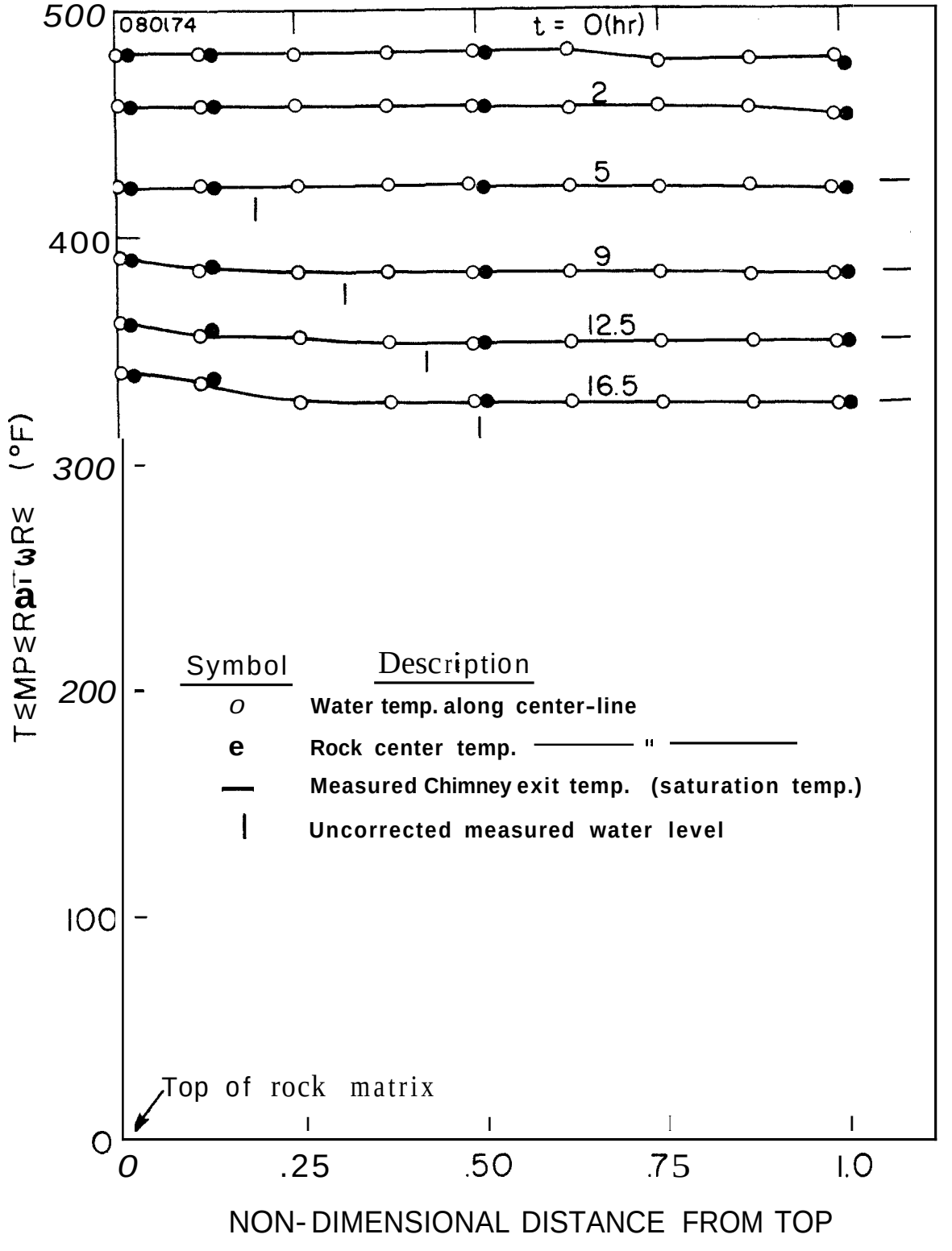


Figure 6.14 Centerline water/rock temperature history for Run 7

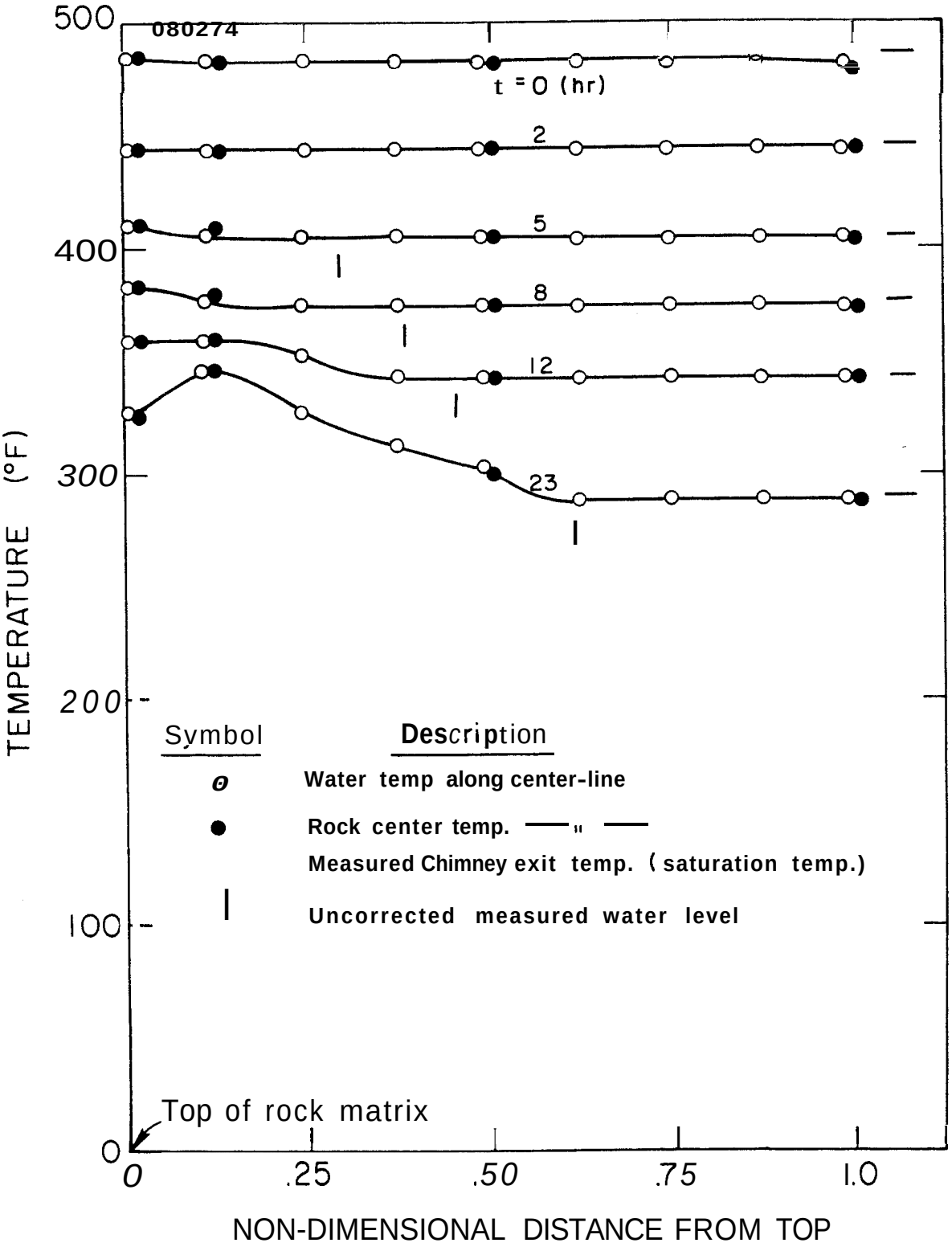


**Figure 6.15** Centerline water/rock temperature history for Run 8

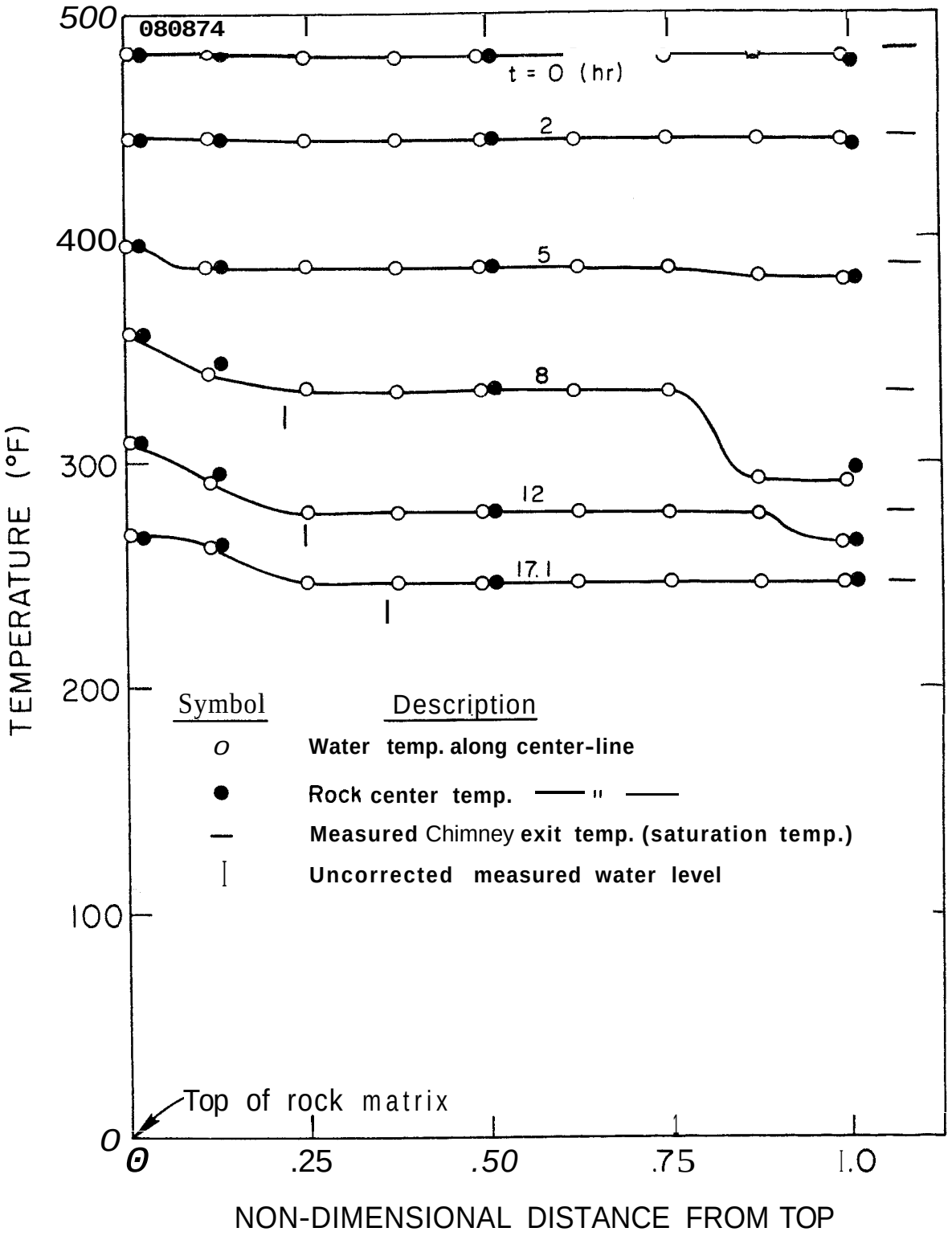


**Figure 6.16 Centerline water/rock temperature history for Run 9**

if the large rocks are in equilibrium with the surrounding water the smaller rocks should also be in equilibrium.

3. It is observed from Figs. 6.11 through 6.16 that when the flash frontreceeds into the chimney, the steam along the chimney centerline above the flash front generally becomes superheated. The degree of superheat generally increases with distance above the flash front for large production times. Exceptions are the behavior exhibited by 'Runs *4*, 6, and 8 which have maximum degrees of superheat at points below the top of the rock matrix.
4. During the fluid production process the rock temperatures are reduced indicating release of stored thermal energy in the rocks to the surrounding water. It is noted that the largest rock energy release was obtained when the flash front was located nearest the top of the rock matrix.
5. It is noted from Fig. 6.16 that the cool water recharged at the lower end of the rock matrix remains in the lower section of the rock matrix due to its higher density. The hotter water, due to its lower density, is located between the flash front and the cooler region and evaporation of this water determines the system pressure.

### 6.6.2 Rock Energy Extraction Efficiency

The degree to which energy is extracted from chimney rock, called the rock energy extraction efficiency, $\eta$, is defined by the fraction of energy actually extracted from chimney rock to maximum possible energy extraction between the process temperature limits. The energy extraction efficiency is given by

$$\eta \triangleq \frac{M_r \bar{C}_r (T_o - T_f')}{M_r \bar{C}_r (T_o - T_f)} \simeq \frac{T_o - T_f'}{T_o - T_f} , \qquad (6.1)$$

where

$T_o$ = initial equilibrium temperature of water/rock (°F) ,

$T_f$ = final temperature (saturation temperature corresponding to termination pressure) (°F) ,

$T_f'$ = final temperature of rock at end of production period (°F) .

The most difficult quantity to determine is the mean temperature of the rock, $T'_f$ . The measured rock temperature distributions are used in this case because these measurements are believed to be respresentative of the mean rock matrix temperature distribution.

From Fig. *6.11* the energy extracted from rocks is proportional to the area fbcdef while the maximum energy extraction possible for the process is proportional to the area abcda. The energy extraction efficiency, $\eta$ , was calculated for Runs *4* through 9 and the results are summarized in Table *6.3* below. It is observed from the table that the estimated $\eta$'s range between *92* and *98* percent.

| Run | Run ID No. | $T_o$ (°F) | $T_f$ (°F) | $T'_f$ (°F) | Computed Chimney Rock Energy Extraction Efficiency, $\eta$ , (dimensionless) |
|---|---|---|---|---|---|
| *4* | *072474* | *477* | *255* | *267* | *.95* |
| *5* | *072574* | *386* | **217** | *221* | *.97* |
| *6* | *072974* | *486* | *236* | *254* | *.93* |
| *7* | *080174* | *484* | *327* | *330* | *.98* |
| *8* | *080274* | *486* | *290* | *306* | *.92* |
| *9* | *080874* | *485* | 246 | *251* | *.98* |

*6.6.3* Chimney Exit Steam Quality

In Section 5.2.3 the term chimney exit steam quality was referred to as the steam quality at the PCV. When the steam reaches this position it has been degraded somewhat due to heat losses and condensation in the outlet line. Thus, the steam exiting the chimney has a somewhat higher steam quality and enthalpy than at the PCV. It is expected that the degree of degradation in steam quality will depend on the steam flow rate since the heat losses from the outlet line at a particular temperature level will not change with steam flow rate. A plot of data on steam quality at the PCV vs the steam flow rate (see Section 5.2.2) are presented in Fig. *6.17* for Run 4.

At early production times (highest production rate) the steam quality is about 90 percent at the PCV, indicating that the steam exiting

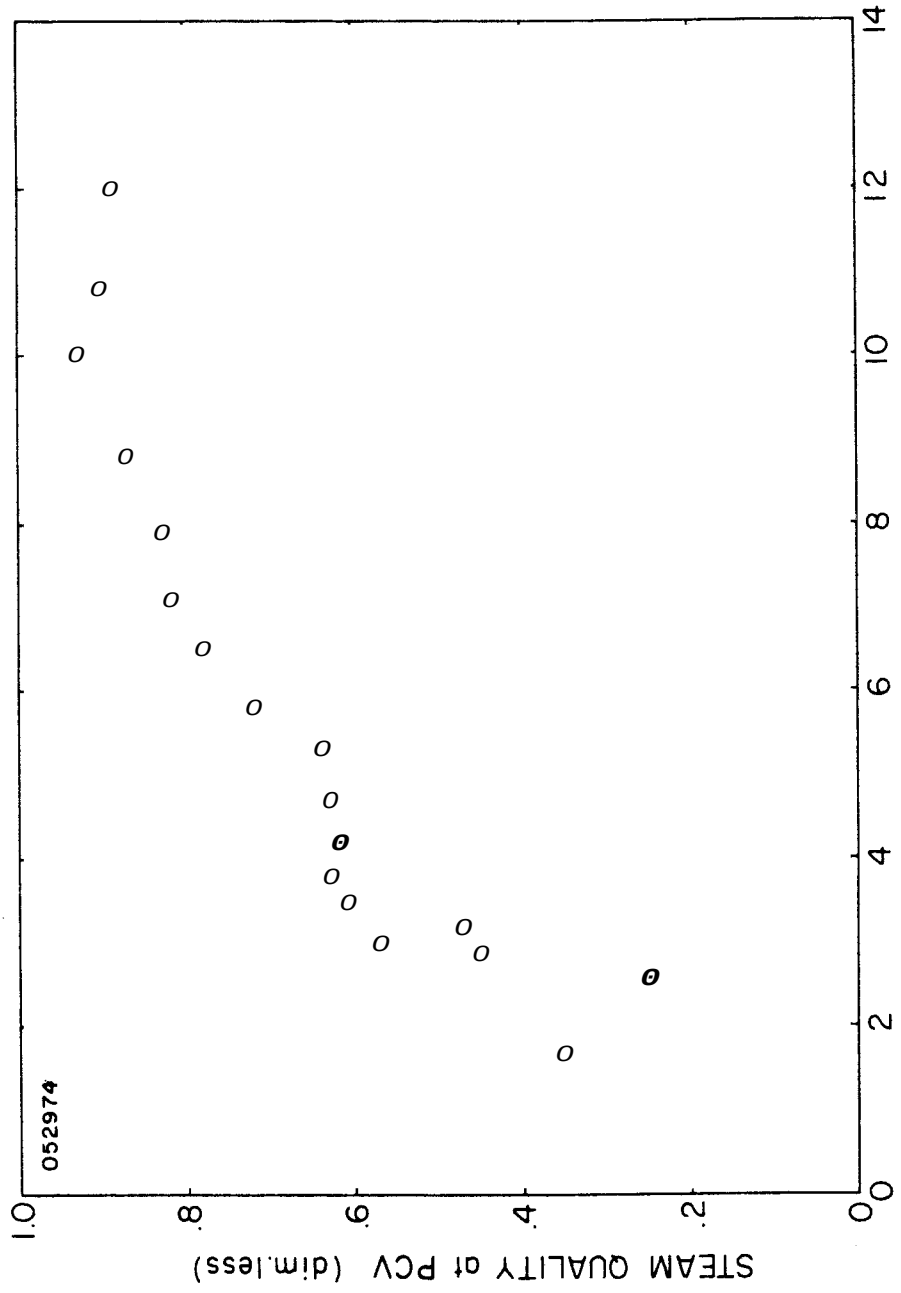


Figure 6.17 Effect of steam flow rate on steam quality at the pressure control valve

the rock matrix was near saturated, i.e., the steam quality was near 100 percent during early production times (except for very early production times when the system was subcooled). It is believed that this was the case for most of the production cycle although evidence of superheat was noted at the chimney exit thermocouple location for short periods of time. The thermocouple occasionally jumped from a reading corresponding to saturated conditions to a level 15 - 30°F higher but would then "de-superheat" rapidly.

## 6.7 Thermodynamic Path of Production Process

The water/steam mixture in the chimney passes through a series of thermodynamic states as fluids are produced and the chimney pressure declines. These series of states are denoted here as the thermodynamic path for the production process. In the subcooled region the path is determined by two independent state variables such as pressure and temperature which are available from measurements. In the more important saturated region, pressure and temperature are not independent so that only one state variable is known from measurements; either pressure or temperature can be used, An additional state variable, the steam quality can be obtained using the void/quality relationship presented in Section 5.2.4. The data necessary to compute the steam quality are the void fraction which can be obtained from observation of the flash front position. The void fraction and steam quality were computed using this procedure for Run 4 and the results are presented in Fig. 6.18. It is noted that the void fraction is closely associated with the liquid level parameter, $\ell/h$, shown in Fig. 6.9. At first when the pressure is relatively high and the specific volume of steam relatively low, the steam quality appears to rise sharply. As the pressure decreases and specific volume increases, there appears to be a temporary drop in the steam quality. Given values of temperature and steam quality the thermodynamic path for the production process can be sketched on the T-s diagram as indicated in Fig. 6.19. The area under the curve represents energy per $lb_m$ of fluids and is related to the net energy transfer to the water/steam mixture system.

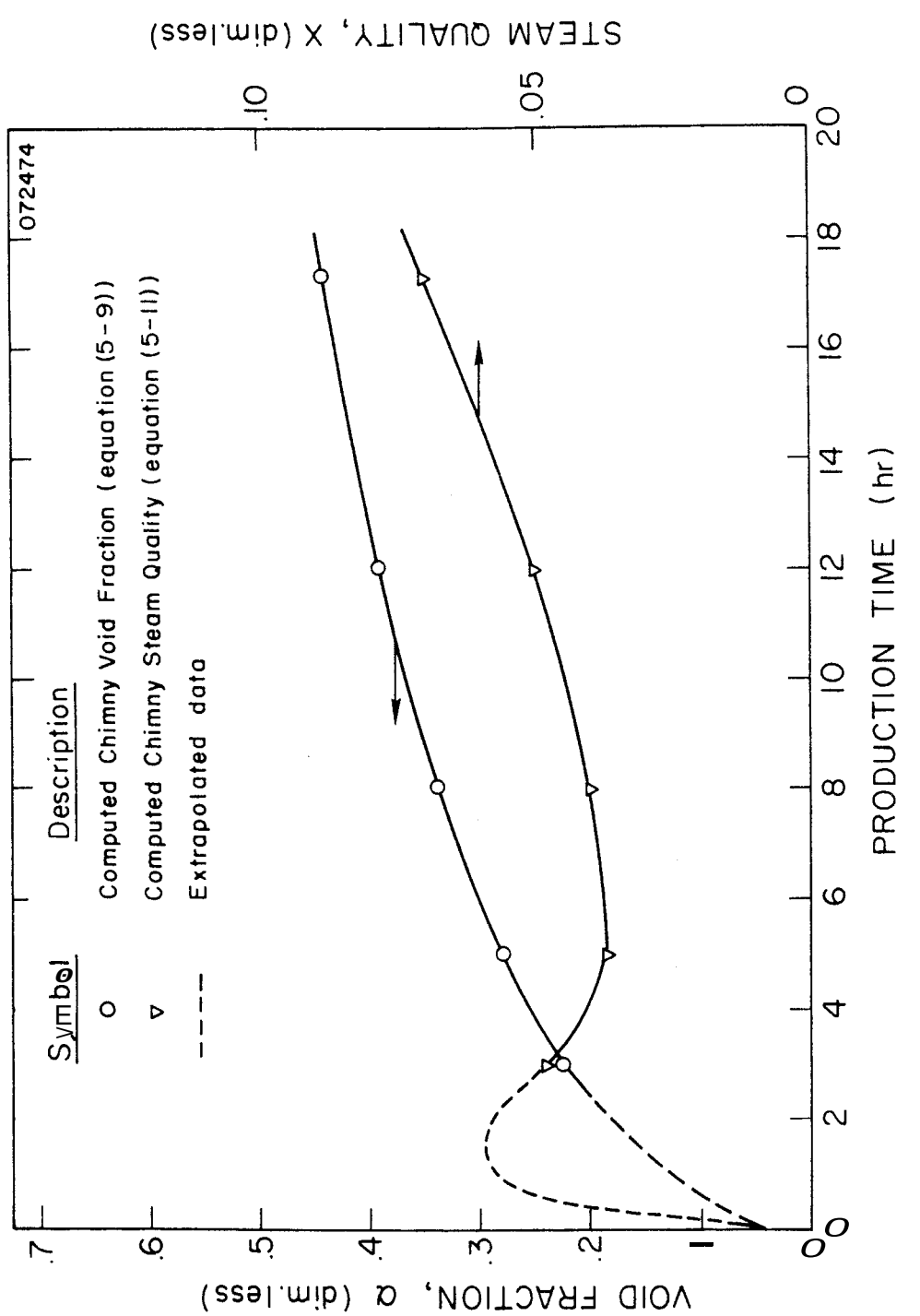


Figure 6.18 Void fraction and steam quality variation with production time for Run 4

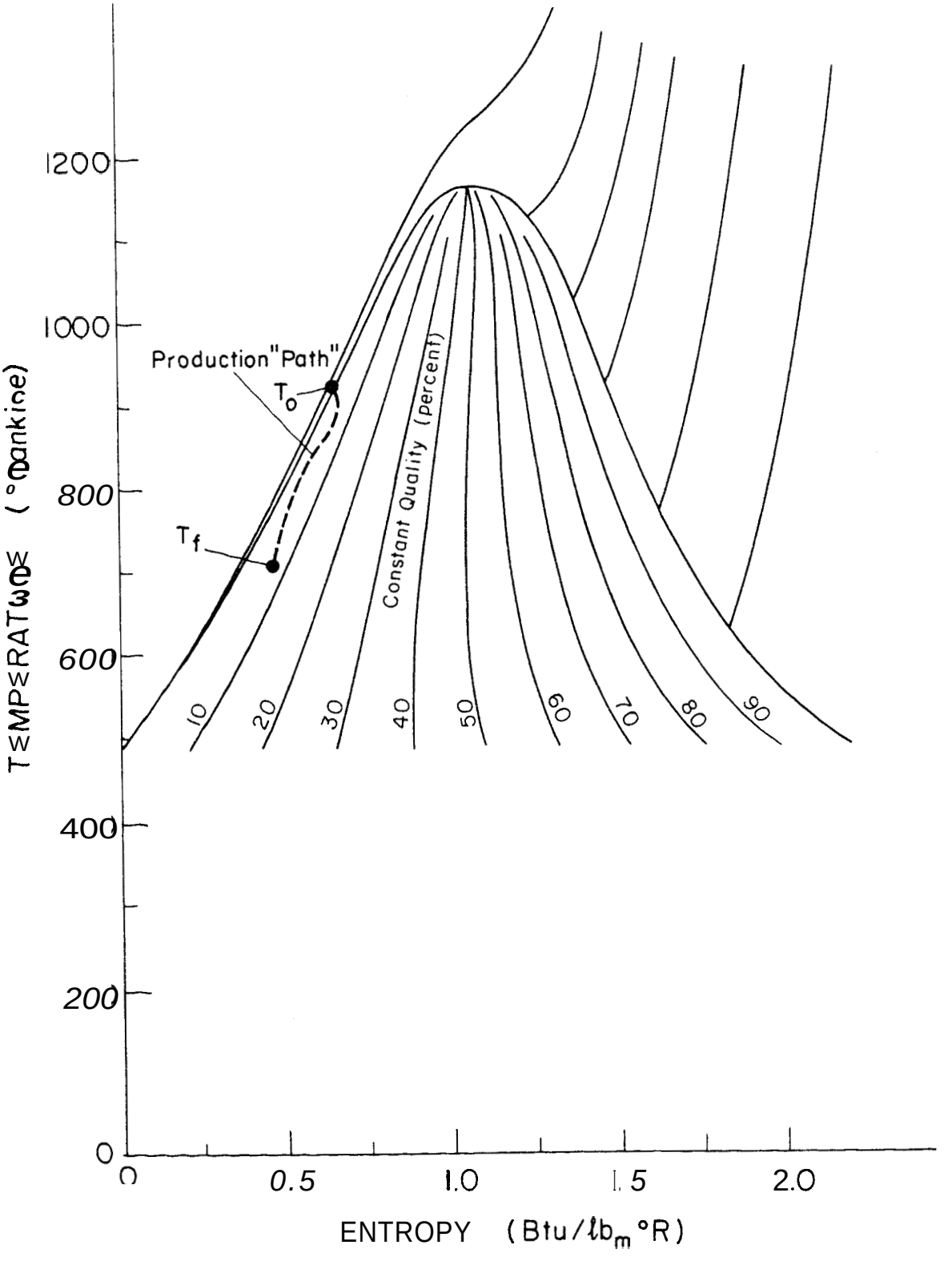


Figure 6.19 Temperature-entropy diagram showing thermodynamic production path for Run 4

# CHAPTER 7

# DISCUSSION

## 7.1 Results

The experimental results given in Chapter 6 are considered prilimi-nary because insufficient data have been obtained for firm conclusions to be drawn. Additionally, there has been insufficient time available for a complete data analysis. However, it is hoped that the data give a representative picture of the nature of the available experimental results. Moreover, it is believed that the preliminary results are useful for future test planning.

It is noted from the tables in Figs. 6.3, 6.7, and 6.8 that the specific external heat transfer parameter, $q_m$, is negative for Runs 1 through 6, when no electrical energy was added by the tape heaters on the chimney. Runs 7 and 8 were made with electrical power on two tapes and it is seen that $q_m$ is close to zero for both runs. Run 9 had only one heater tape on. To approximate conditions of a "natural" environment for the water/rock system under study $q_m$ should be slightly positive which can be achieved by supplying more electrical energyby the tape heaters. It would be convenient for comparison purposes to maintain $q_m$ constant for all future runs; however, this is very difficult to accomplish with manual control of tape heater power. Comparison of runs with different $q_m$ can be made indirectly by the use of the mathematical model for the fluid production process which is being developed.

The fluid production rate is determined by manual adjustment of the pressure control valve (PCV) but a skilled operator is required to obtain a desired fluid production characteristic. During these tests it was attempted to keep the production rate constant for some runs. From Fig. 6.3 it is apparent that fairly constant flow rates were achieved for these runs during most of the production period, but that the rates dropped off near the end. Due to difficulty in maintaining the desired fluid production characteristic (constant rate) for these runs, later runs should be made with constant PCV setting (constant flow area) since the operator then will have more time to attend other operator functions.

The rising recharge characteristic obtained for Run 9 is probably not representative for the different types of recharge from real reservoirs. It is expected that manual control of the injection pump can be used to provide preselected recharge characteristics for future runs.

The water became saturated as noted from Figs. 6.5 and 6.6 for Runs 3 and 4 at approximately 0.5 and 0.25 hour, respectively. The difference is reasonable, considering the chimney had about twice as much liquid in it in Run 3 compared to Run 4. With approximately equal initial production rates for both cases, the decompression times are expected to be about a factor of two different. It is also noted that the degrees of initial subcooling differs for the two cases. The combination of compressibility and degree of subcooling appears to account for the observed behavior.

When the pressure is lowered and boiling initiated in the rock matrix the temperature of the surrounding water is reduced. The rock/water temperature differences established result in heat transfer from the rocks to the water. The rate of heat transfer from the rocks will depend primarily on rock size/shape distributions and rate of cooldown of surrounding water. For the cooldown rates of these experiments (proportional to fluid production rates) the rock/water temperature differences were not measurable (about 1°F). Preliminary transient analysis of spherical rocks of diameter equal to the mean equivalent diameter for the rock load (about 1 inch) supports the experimental findings. The analysis showed that about four times as large cooldown rates are required to establish rock/water temperature differences of about 5°F. The time constant for a 1 inch spherical rock is about 0.10 hour depending on assumed surface heat transfer coefficient, while production transient lasted about 20 hours on the average. Since fluid production rates of the system is limited by the capacity of the condenser to about twice the rates of the present experiments, larger rocks are required to measure rock temperature transients.

The rock energy extraction efficiencies, $\eta$, that can be obtained depends mainly on the rock size/shape distributions and the rate of cooldown of surrounding water. Additionally, it is apparent from the experimental results that the location of the flash front has some influence on $\eta$

because rocks located above the flash front do not cool down as fast as rocks in water. Therefore, if high values of $\eta$ are desired provisions must be made to operate with the flash front near the top of the rock matrix.

The fraction produced for a system is largely determined by porosity, rock energy extraction efficiency, external heat transfer parameter, and initial and final pressures. When only water is present in a system (100 percent porosity) the energy available for flashing of water into steam is the thermal energy in the water. The higher the initial pressure the more energy available for flashing and the higher the fraction produced. From energy considerations one can also see that the lower the final pressure the higher the fraction produced.

When rock is present (porosity less than 100 percent) and the conditions are such that energy is extracted from the rock this energy is also available for flashing of water into steam and higher fraction produced will result. Heat transfer from the surrounding rock (host rock) or here from the chimney metal, given by the value of $q_m$, will (if $q_m$ is positive) have the same effect as heat transfer from the chimney rock.

Runs 1 through 6 had negative values of $q_m$ which indicates that energy was removed from the water. Higher fractions produced resulted for Runs 7 through 9 which had $q_m$ near zero or less negative than the first six runs. Only when all these factors are considered can the results of Fig. 6.8 be explained. Further evaluations of the results in conjunction with the analytic fluid production model are required later.

The usefulness of employing non-dimensional coordinates for the pressure depletion data can be demonstrated by an example. Suppose it were desired to estimate the production time necessary to reduce the chimney pressure to a particular value at a different mean production rate than the experimental but for otherwise similar conditions (same porosity, rock energy extraction, and external heat transfer parameter). For a given $P^*$ the $t^*$ value from Fig. 6.7 can be employed to compute the production time for the given new mean production rate. A similar procedure is useful for estimating pressure depletion times for real systems. Thus, results obtained with the laboratory model can be scaled employing $P^*$ and $t^*$ to obtain approximate results for real systems.

It was noted from Fig. 6.9 that the computed liquid level or flash front position was higher than the observed one by about 5 percent of rock matrix height. In deriving Eq. (5.12) used to compute the liquid level, it was assumed that the space above the liquid level including outlet line was occupied by saturated steam only. This is obviously not true because approximately 20 $lb_m$ of water (corresponding to 5 percent of liquid in chimney) has not been accounted for. The significance of this apparent anomaly is believed to be that liquids are present on metal and rock surfaces in the chimney above the liquid level as well as in the outlet line. The maximum amount of liquids that could be located in the outlet line is 7 $lb_m$ (completely filled line) and therefore a significant fraction of the "missing" 20 $lb_m$ liquids must be in the chimney. Also, since the surface area of the metal in the chimney is much less than that of the rock a significant amount of the 20 $lb_m$ liquids must be on the rock surfaces. If the 20 $lb_m$ of liquids were distributed evenly over the total rock surface above the liquid level, an average film thickness of about 0.017 inch would result. It is believed that this liquid "hangup" is accentuated for the annulus of rocks located near the chimney walls and near the top head.

It was noted from Figs. 6.11 through 6.16 that for large production times the steam above the flash front is superheated. The degree of superheat was often reduced when the steam was ascending towards the top of the rock matrix (see for example Fig. 6.15). One explanation for the observed behavior is that the ascending superheated steam is encountering liquids which originate from condensation of steam in the outlet line. The observed behavior of the thermocouple at the chimney exit ( T/c 110, Fig. 2.10), which often showed temperatures higher than saturation for periods of time during the production, also indicate that both liquids and superheated steam are present at the chimney exit. A preliminary estimate of heat losses in the outlet line indicates that about 6 $lb_m$ of steam are condensed per hour. Because of the piping arrangement about one half of the liquids will drain to the chimney and the other half to the PCV. Additional liquids may arise from condensation of steam on the chimney head and wall above the flash front. An analytic model for prediction of heat losses in the outlet line is being developed. The

conditions of the steam exiting the chimney can then be calculated using steam conditions at the PCV which is evaluated from a condenser heat balance.

Evaluation of the thermodynamic path from observed flash front position and system pressure data appears to be useful in obtaining an independent estimate of the external heat transfer parameter, $q_m$ , obtained by other means earlier. Further work is needed in this area.

## 7.2 Measurement Accuracy

During this initial phase of testing with the chimney model considerable experience with the experimental system has been gained with respect to (1) design and construction of the system hardware, (2) instrumentation of the system, (3) operation of the equipment, and (4) data reduction procedures. It is important now to take a closer look at areas of experimental uncertainty and determine where improvements can be made.

The chimney pressure gage and the pressure transmitter were calibrated simultaneously up to 500 psig using a dead weight tester (test range 0-500 psig) and both devices were found to be linear. Subsequently the pressure transmitter was calibrated against the gage to 800 psig and a slight deviation from linearity in the upper 10 percent of the scale was apparent. Which device was non-linear is not known, but since operation normally starts below the non-linear range, no correction was attempted. A comparison of data from the two measurements is shown i Pig. 7.1 for Run 3. The maximum discrepancy between the two measurements is about 10 psi. The saturation temperature corresponding to the pressure measured by the transmitter is shown in Fig. 7.2 (solid line) relative to the temperature measured at the chimney exit (T/c 110, Fig. 2.10). The maximum difference between the two measurements was 3°F. Checks of this type were made at periodic intervals during the testing to assure continuous calibration. No significant deviation from the original calibration was noted.

The thermocouples used for water and metal temperature measurements were calibrated relative to each other by turning the heater off and letting the circulation pump run. All thermocouple responses converged to one reading on the recorders which indicated that temperature equilibrium was achieved and that therelative errors between the thermocouples were about 2°F.

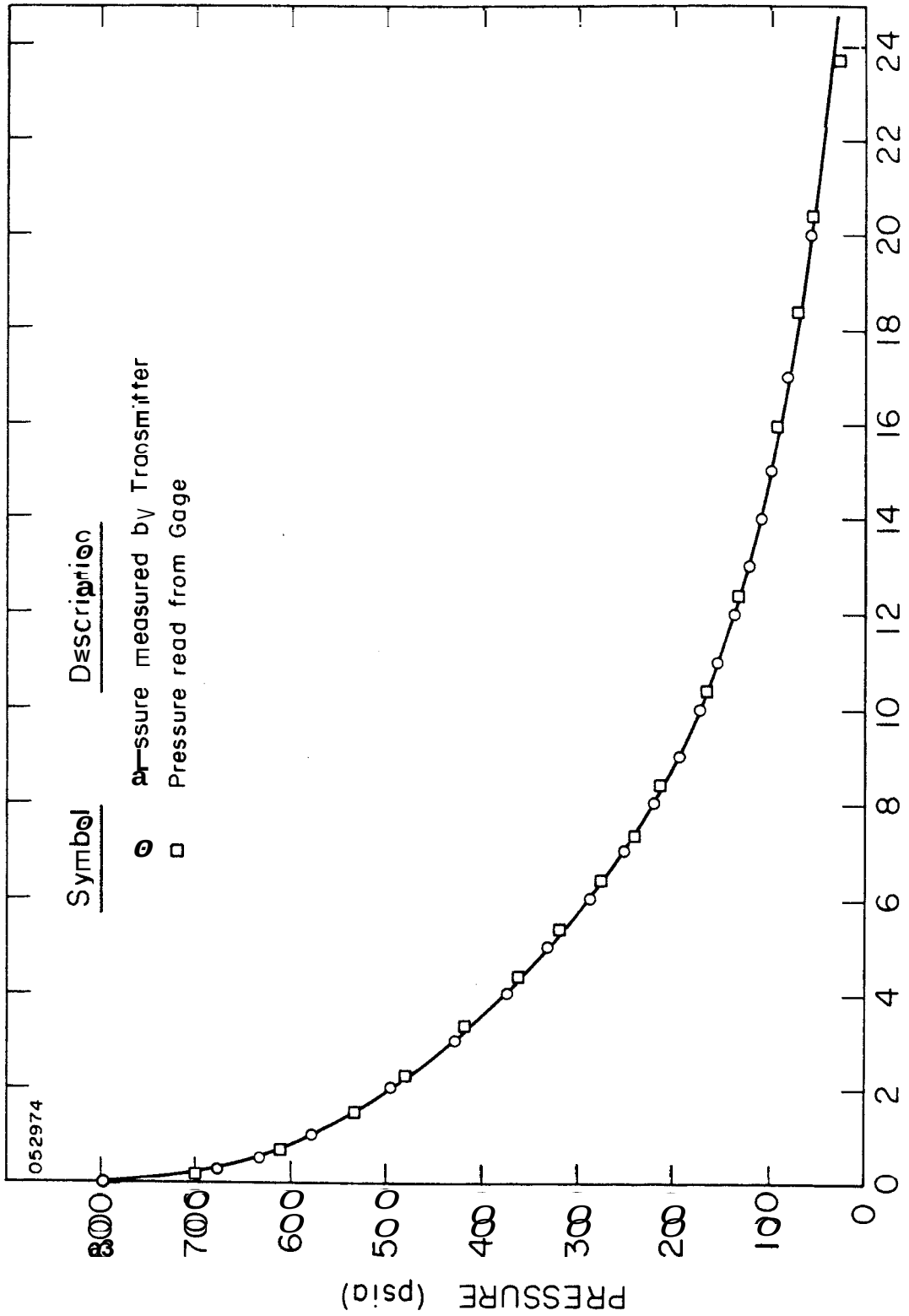


Figure 7.1 Comparison of independent chimney pressure measurements for Run 3

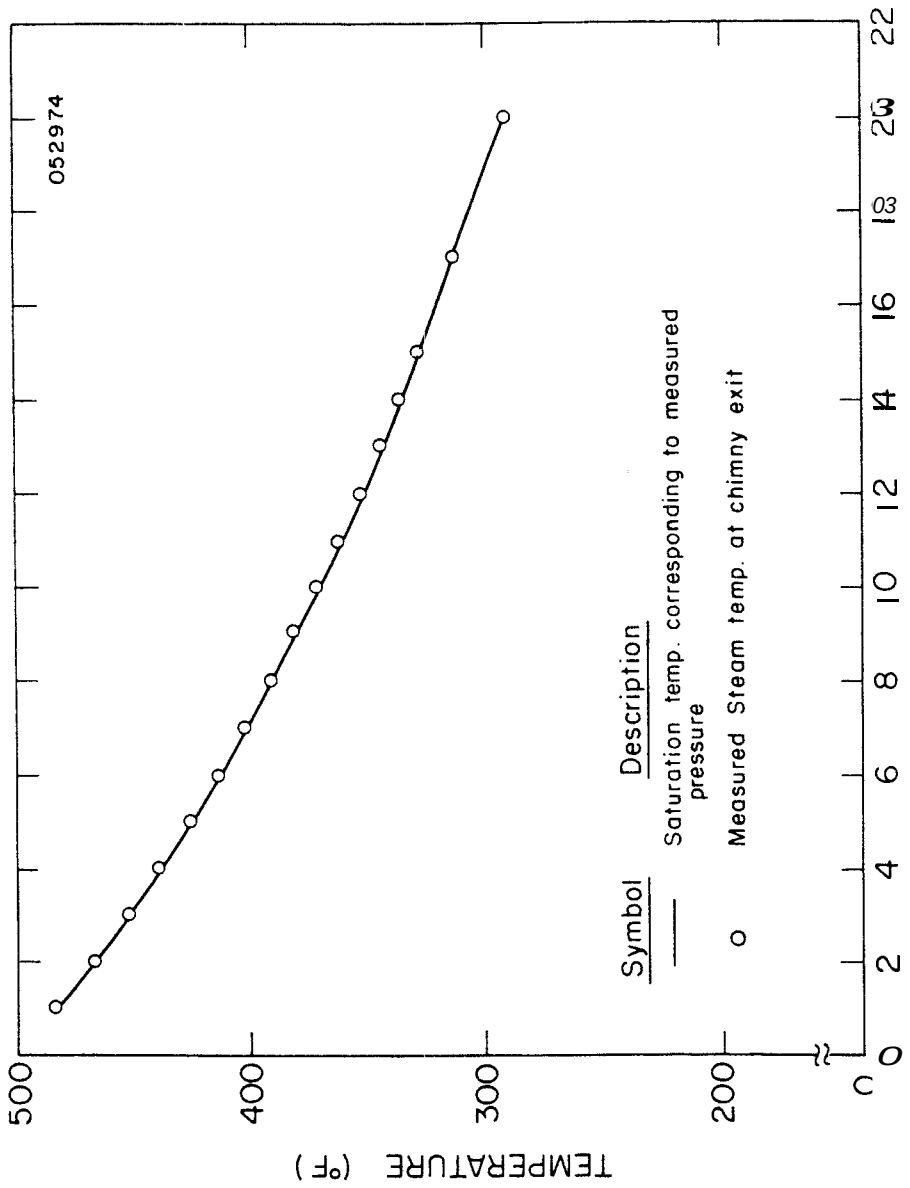


Figure 7.2 Comparison of measured chimney exit temperature to saturation temperature corresponding to measured pressure

Errors were also introduced in reading the data from the recorder charts on which the smallest subdivision (0.10 inch) represented 5°F. It was possible to interpolate between the lines and it is felt that the uncertainty introduced in the data reading process was ± 2°F. A summary of estimated uncertainties associated with the measurements made during the experiments are presented in Table 7.1. The second column gives the smallest subdivision of the indicator (recorder chart or gage). The estimated uncertainties are given in the third column. In making these estimates account was taken of (1) smallest subdivision, (2) reading of recorder charts, and (3) uncertainties associated with the primary sensors. The fourth column in Table 7.1 gives the estimated relative uncertainties or error sigmas at the low end of the scale where the relative uncertainty is greatest. The corresponding error sigmas at the high end of the scale are given in parentheses when there is a significant difference between the two.

TABLE: 7.1

Summary of Estimated Measurement Uncertainties

| Measurement | Smallest Sub-division | Estimated Un-certainties | Error Sigmas (percent)* |
|---|---|---|---|
| Pressure - gage | 10 psi | f 5 psi | ± 10 (± 1) |
| Pressure - transmitter | 8 psi | ± 5 psi | ± 10 (± 1) |
| Temperature - water/metal | 5°F | ± 2°F | ± 1 (± .5) |
| Temperature - condenser cooling water | 1°F | ± 1°F | ± 1.5 |
| Cumulative production - gravimetric measurement | 1 $lb_m$ | ± 2 $lb_m$ | ± 10 (± 1.3) |
| Flow rate - condenser cooling water (orifice) | 8 $lb_m$/hr | ± 20 $lb_m$/hr | ± 3 (± 2.5) |
| Heater tape - voltage | 5 volts | ± 2 volts | ± 0.5 |
| Heater tape resistance | 2 ohms | ± 1 ohm | ± 2 |
| Liquid level (flash front position) | 0.02 inch | ± 0.1 inch | ± 1 |

*Figures in parentheses indicate error sigmas at high end of scale.

It is apparent from Table 7.1 that relatively large error sigmas exist at the low end of the scale for the pressure measurements and the cumulative fluid production measurement. Improvements of the pressure measurement could easily be obtained by the installation of a low range pressure gage which could be switched in at low pressure. A similar arrangement could be used for the fluid measurement where a low range scale could be used during the early period of the production cycle.

The uncertainty associated with the total external heat transfer in comparison to the energy extraction from the rock is of particular importance in determining the usefulness of the present experimental system. Such a comparison is made in the following using numbers and the estimated error sigmas presented previously. The computation of the total external heat transfer was based on Eq. (5.2) which can be restated as follows:

$$Q_m = I_1 + I_2 - I_3 , \tag{7.1}$$

where the I's are the integrals and multipliers of each term in Eq. (5.2). The error sigma associated with $I_1$ is $\sigma_1$ and stems mainly from the measurement of the heater tape resistance (see Table 7.1). The error sigma associated with $I_2$ is $\sigma_2$ and since the error associated with the temperature measurement is small it can be assumed that the error is mainly associated with evaluation of the chimney mass $M_2$ (see Table 3.8). Similarly, the error sigma in $I_3$ is $\sigma_3$ which stems mainly from the error in the heat loss conductance $h_2A_2$. The error sigma for $Q_m$ is $\sigma_m$ and can be computed from the second-power equation (Kline and McClintock, 1953), which becomes with the present notation

$$\sigma_m = \left( \left( \frac{\partial Q_m}{\partial I_1} \frac{I_1\sigma_1}{Q_m} \right)^2 + \left( \frac{\partial Q_m}{\partial I_2} \frac{I_2\sigma_2}{Q_m} \right)^2 + \left( \frac{\partial Q_m}{\partial I_3} \frac{I_3\sigma_3}{Q_m} \right)^2 \right)^{1/2} , \tag{7.2a}$$

After evaluation of the derivatives using Eq. (7.1) the expression for $\sigma_m$ can be simplified to give

$$\sigma_m = \left[ (I_1\sigma_1)^2 + (I_2\sigma_2)^2 + (I_3\sigma_3)^2 \right]^{1/2} / Q_m . \tag{7.2b}$$

Using $\sigma_1 = \pm .02$ (from Table 7.1), $\sigma_2 = 10.07$, and $\sigma_3 = \pm 0.037$ (from Table 3.8) for the individual error sigmas and the numerical data for $Q_m$ and the I's in Table 6.2 one finds $\sigma_m$'s of $\pm 0.102$ and $\pm 84.3$ for Runs 3 and 7, respectively. The estimated uncertainties in $Q_m$ are given by $\sigma_m Q_m$ which become $\pm$ 11,300 Btu and $\pm$ 8,430 Btu, respectively.

It is useful to compare the estimated uncertainty in $Q_m$ to the energy extracted from the rock. For Run 7 the energy extracted from the rock was estimated to be 50,400 Btu. Thus, the uncertainty in $Q_m$ is about 17 percent of the rock energy extraction. Based on the previous evaluation it is clear that one cannot attempt to determine the magnitude of the energy extracted from two different rock types when the expected difference is less than about 17 percent unless representative rocks are instrumented. In that case the rock energy extraction efficiencies can be computed directly from measurements and one need not know $Q_m$ accurately.

# CHAPTER 8

# CONCLUSIONS AND RECOMMENDATIONS

## 8.1 Conclusions

1. Valuable experience has been gained in the design, construction, and operation of a laboratory size model of a stimulated geothermal reservoir at prototypical temperature and pressure conditions.
2. Analysis of the experimental data obtained to date shows that the behavior of most aspects associated with real stimulated geothermal reservoirs can be studied using the present laboratory model.
3. Experimental data for initial pressure and temperature conditions of up to 790 psia and 500 °F, respectively applicable mostly to fractured dry hot rock chimneys have been obtained. Corresponding to the more general stimulated reservoir conditions with recharge, only limited data have been obtained.
4. The wall effect or heat transfer from the vessel to the water/rock system can be accounted for using a combination of calibration experiments and analyses. The wall effect generally results in heat transfer away from the water/rock system. Addition of energy to the model by electrical heater tapes can be made to eliminate the wall effect.
5. The present experiments have demonstrated that energy can be extracted from hot rock by letting the flash front recede into the rock matrix. More that 90 percent of the thermal energy contained in the rocks between the temperature limits of these experiments was extracted during the fluid production. The percentage of energy that could be extracted from the rock matrix depended to some degree on the flash front position. Highest extractions were achieved with the flash front at the top of the rock matrix.
6. The fraction of fluids produced was roughly a factor of two higher for the water/rock system than for the water system due to energy extraction from the rock. Also, the fraction of

fluids that could be produced depended on the initial pressure and temperature of the system and on the system bulk porosity. The results of the experiments with the water/rock system suggest that approximately 35 percent of the original water in a system can be produced when the pressure is reduced from about 600 to 100 psia for similar conditions of rock energy extraction.

7. The experiments suggest that superheated steam is present in the region above the flash front. The degree of superheat is generally highest at some point between the flash front and the top of the rock matrix. Also, the experiments indicate that liquids on the rock and metal surfaces coexist with superheated steam in the region above the flash front.
8. In the case of no recharge the temperature of the water below the flash front remains at uniform temperature just below that corresponding to saturation during the entire production cycle. When limited recharge of cool water is used at the lower end of the chimney, the cooler recharge water remains in the lower section of the chimney below the hotter water at the flash front position. Recharge of larger quantities may alter this result.
9. The present laboratory model does not include: (a) realistic simulations of recharge mechanism from the surrounding aquifer and (b) realistic simulation of the two-phase phenomenon in the well-bore. Additionally, tests involving highly concentrated brines and liquids containing sand particles cannot be run using the present model. Another laboratory model designed specifically for such tests is required.

## 8.2 Recommendations

### 8.2.1 Hardware

The experience gained with the chimney model system during the initial phase has highlighted some areas of hardware improvements. Many of these areas have already been corrected or corrective action is in progress.

Difficulties have been experienced with the large diameter O-ring used for sealing of the quick-opening head. However, a new high durometer reading O-ring (Viton) has been acquired which performs well at slightly derated maximum conditions ($\sim$ 485°F instead of 500°F and $\sim$ 650 psig instead of 800 psig). If additional problems with the O-ring require further derating or corrective action, a plan for replacing the quick-opening head is being formulated.

Major problems were experienced with the circulation pump seal after 200-300 hours of operation. This item was responsible for considerable periods of down-time. New seals have been received. Adequate maintenance of the seal is expected to result in reduced down-time in the future.

The need for gravimetric measurements of the quantity of water injected became apparent during the initial test series. It is therefore recommended that a large head tank with sight glass be installed for direct observation of amount of fluids recharged. The cumulative fluids injected will be computed from the head tank water level.

Difficulties were experienced with control of the injection pump flow rate. The problem stems from the fact that operation in the lower 10 percent of the scale has been required. In this range inertia of the pump valves makes the pump flow rate sensitive to the magnitude of the back pressure (chimney pressure). The installation of a by-pass line on the injection or recharge pump is recommended to improve control over the recharge rate.

The present circulation heater control arrangement using an on/off thermostat performs well for heatup purposes but is inadequate when the circulation heater is used for preheating the recharge water. It is therefore recommended that a continuous power control system be installed. It is anticipated that the control system under consideration will allow recharge fluid temperature/time characteristics of linearly increasing, linearly decreasing, and constant recharge water temperature.

The condenser performed satisfactorily with the steam flow rates of these experiments ($\sim$ 10 $lb_m$/hr). At much higher pressure depletion and steam production rates, however, a cooling water flow rate of 2 gpm is inadequate. The cooling water flow rate can be increased to at least

5 gpm by increasing the orifice size. Further evaluation is recommended to determine if a condenser with higher rating needs to be acquired.

The need for an accurate low range pressure gage and an accurate low range scale for cumulative production measurement has become apparent. To improve measurement accuracies towards the low end of the scale, it is recommended that separate low range sensors be installed for the chimney pressure and fluid production measurements.

Installation of more tape heater capacity is required. It is recommended that moisture resistant tapes for high temperature service be acquired.

In general it is considered that the system performed well and it is believed that a majority of the originally planned tests for which the system was designed can be made with the present system. There are, however, certain kinds of problems that cannot be studied using the present system and these are: (1) scaling and corrosion problems associated with highly concentrated brines, (2) performance of rock loads containing sand such as friable sandstone, (3) two-phase flow in the well-bore, and (4) interaction between surrounding aquifer, rock chimney and delivery system (well-bore) which will control the chimney flash front position. Conceptual design of a new system in which these problems can be studied has been initiated. It is estimated that this system would cost $150,000 and the new system could be operational 24 months after start of final design phase. It is recommended that design efforts on such a system be intensified and construction initiated as soon as possible.

Due to the many problems experienced with the quick opening head and the mechanical seal in the circulation pump it is recommended that future systems not include these design features.

In instrumenting future rock loads efforts should be made to include instrumentation for closer study of the phenomenon of water coexisting with superheated steam in the region above the flash front.

Work on the mathematical model for the fluid production/pressure depletion process should be accelerated. A general mathematical model for parametric study of the transient behavior of individual rocks located in typical geothermal reservoir environments should be developed.

8.2.2 Test Priorities

The writing of this report has brought into focus areas of testing which should be given priorities in the near term test schedule. In general, it is felt that advantage should be taken of the test setup and rock loading as it existed during the most recent test period. Additional equipment installation is in progress which will make the system more flexible so that different types of tests can be performed. In the future efforts should be made to maintain the specific external heat transfer parameter, $q_m$, equal or slightly greater than zero for all runs, as this will make data interpretations and comparisons easier. More emphasis should be put on the completion of data reduction computer programs. Programming efforts on the mathematical model for the fluid production/pressure depletion process should be accelerated. Near term test objectives with the chimney model system should include the following:

1. Injection or recharge of cool and hot water while injection rate is maintained relative to the fluid production rate to achieve an approximateiy stationary flash front position. During the tests with hot water injection efforts will be directed towards maintaining constant and linearly decreasing injection water temperature.
2. The fluid production rate and corresponding pressure depletion history will be varied over a greater range than previously. It is believed that the relative magnitudes of pressure depletion rate and size of the rock will affect the energy extraction from the rock.
3. Cyclic recharge/fluid production will be attempted. During these tests hot water at constant temperature will be injected continuously. The fluid production is adjusted such that the flash front recedes into the rock matrix and when a certain level has been reached fluid production is stopped. The chimney is then recharged with hot water which increases pressure/temperature in the system. The cycle is then repeated.

The analytic modeling of the physical processes involved requires specific test data for model verification. It is expected that the data obtained to date together with the data expected in the near future may satisfy this requirement. Howe er, there is one parameter that is or' major importance which needs to be varied over a greater range, namely the rock matrix bulk porosity. Therefore, the selection of future rock loads should be made such that ower porosities can be achieved. In order to further investigate rock energy extraction a future rock load should have much larger size rocks. In instrumenting future rock loads emphasis should be placed on investigating the temperature distribution and liquid hangup phenomenon in the region above the flash front.

## APPENDIX A

## DERIVATIONS FOR TWO-MASS LUMPED PARAMETER TRANSIENT MODEL

The basis for the selection of the two-mass lumped parameter transient model shown on the upper portion of Fig. **3.1** was discussed in Chapter 3. The assumptions and idealizations inherent in the two-mass model are summarized below:

1. All water and the rock are at uniform or mean temperature, $T_1$.
2. All metal and insulation undergoing temperature changes are at mean temperature, $T_2$ .
3. The temperature of the surrounding is constant at $T_\infty$
4. Electric power is supplied as rectangular pulses.
5. Specific heats of the rock, water and chimney metal are constant.
6. The heat transfer conductances are constant.

The electrical analog of this system is shown on the lower portion of Fig. 3.1. The power sources, $S_1$ and $S_2$ , are applied as rectangular pulses by use of the unit step function

$$u(t - \tau) \begin{cases} = 0 & \text{for } t < \tau \\ = 1 & \text{for } t \geq \tau \end{cases} \qquad (A.1)$$

Thus, a constant power supply of $S_1$ applied between times $t = \tau_{11}$ and $t = \tau_{12}$ would appear as

$$S_1[u(t - \tau_{11}) - u(t - \tau_{12})] .$$

Derivation of Equations

The rate of creation of energy statement is in general form

$$\text{ROC } E = 0 = (\text{out}) - (\text{in}) + \frac{a}{at} (\text{storage}) . \qquad (A.2)$$

Applying this principle to each lumped mass there results the two equations:

$$m_d i_d + h_1 A_1 (T_1 - T_2) - S_1 [u(t - \tau_{11}) - u(t - \tau_{12})]$$

$$+ \frac{\partial}{\partial t} (M_w C_1 T_1 + M_r C_r T_1) = 0 , \qquad \text{(A. 3a)}$$

$$h_2 A_2 (T_2 - T_\infty) + h_1 A_1 (T_2 - T_1) - S_2 [u(t - \tau_{21}) - u(t - \tau_{22})]$$

$$+ \frac{\partial}{\partial t} (M_2 C_2 T_2) = 0 . \qquad \text{(A. 3b)}$$

The parameters in the first storage term have the following functional forms:

$$M_w = M_w(t) ,$$

$$M_r = \text{constant} ,$$

$$C_1 = C_1(T_1) = C_1[T_1(t)] ,$$

$$C_r = C_r(T_1) = C_r[T_1(t)] .$$

By differentiation of the first storage term using the chain rule there results:

$$\frac{\partial}{\partial t} (M_w C_1 T_1 + M_r C_r T_1) = M_w C_1 \frac{dT}{dt} + M_w T_1 \frac{\partial C_1}{\partial T_1} \frac{\partial T_1}{\partial t} + C_1 T_1 \frac{dM_w}{dt}$$

$$+ M_r C_r \frac{dT_1}{dt} + M_r C_r \frac{\partial C_r}{\partial T_1} \frac{\partial T_1}{\partial t} + C_r T_1 \frac{dM_r}{dt}$$

The changes in the specific heats of water and rock with temperature are not very significant and therefore the derivative of these terms can be neglected. Similarly, the derivative of $C_2$ with respect to temperature in Eq. (A.3b) can also be neglected. If $0\,^\circ F$ is taken as the basis for enthalpy of water and a mean specific heat is used the simplified energy equations become:

$$(M_w C_1 + M_r C_r) \frac{dT_1}{dt} + h_1 A_1 (T_1 - T_2) = S_1[u(t - \tau_{11}) - u(t - \tau_{12})] - \dot{m}_d C_1 T_1 - C_1 T_1 \frac{dM_w}{dt} , \quad (A.4a)$$

$$M_2 C_2 \frac{dT_2}{dt} + h_2 A_2 (T_2 - T_\infty) + h_1 A_1 (T_2 - T_1) = S_2[u(t - \tau_{21}) - u(t - \tau_{22})] . \quad (A.4b)$$

Applying the mass conservation principle to the water contained in the system we get in general

$$\text{ROC } M = 0 = (\text{out}) - (\text{in}) + \frac{a}{at} (\text{storage}) ,$$

or, in particular

$$\dot{m}_d + \frac{dM_w}{dt} = 0 .$$

Thus

$$\dot{m}_d = - \frac{dM_w}{dt} .$$

Using this in **Eq.** (A.4a) the two last terms cancel each other. New temperature variables are defined by

$$\theta_1 \triangleq T_1 - T_\infty , \quad \theta_2 \triangleq T_2 - T_\infty , \quad (A.5)$$

and coefficients are defined by

$$a_1 \triangleq \frac{h_1 A_1}{M_1 C_1} , \quad a_2 \triangleq \frac{h_1 A_1}{M_2 C_2} , \quad a_3 \triangleq \frac{h_2 A_2}{M_2 C_2} ,$$

$$\bar{S}_1 \triangleq \frac{S_1}{M_1 C_1} , \quad \bar{S}_2 \triangleq \frac{S_2}{M_2 C_2} . \quad (A.6)$$

Also, the differential operator D is defined by

$$D \triangleq \frac{d}{dt} .$$

The differential equations then become:

$$(D + a_1)\ \theta_1 - a_1\theta_2 = \bar{S}_1[u(t - \tau_{11}) - u(t - \tau_{12})] , \qquad (A.7a)$$

$$-a_2\theta_1 + (D + a_2 + a_3)\ \theta_2 = \bar{S}_2[u(t - \tau_{21}) - u(t - \tau_{22})] . \qquad (A.7b)$$

These equations are to be solved with the initial conditions

$$\theta_1(0) = \theta_{10} , \quad \theta_2(0) = \theta_{20} . \qquad (A.8)$$

Solution of Transient Problem

To solve the above equations analytically further assumptions have to be made with respect to the quantities $a_1$, $a_2$ and $a_3$. It is assumed that these are constants over the temperature range of interest The most severe variation in these quantities during a heatup transient is associated with the quantity $a_3 \triangleq h_2A_2/M_2C_2$. Here the effective heat transfer coefficient $h_2$ associated with heat losses to the surroundings may vary significantly over the temperatures experienced during heatup or cooldown transients particularly due to the radiation contribution. However, the convection contribution may also change significantly due to changes in the surroundings such as turning on the air-conditioning system, opening windows and doors, etc. In the evaluation of the solution, therefore, suitable mean values of $h_2$ have to be used.

With these additional assumptions the problem can be solved analytically by employing Laplace transforms to the equations. Taking the Laplace transform of Eq. (A.7a) and (A.7b), using (A.8) there results:

$$(s + a_1)\ \hat{\theta}_1 - a_1\hat{\theta}_2 = \theta_{10} + \frac{\bar{S}_1}{s} e^{-\tau_{11}} - \frac{\bar{S}_1}{s} e^{-\tau_{12}} ,$$

$$- a_2\hat{\theta}_1 + (s + a2 + a_3)\ \hat{\theta}_2 = \theta_{20} + \frac{\bar{S}_2}{s} e^{-\tau_{21}} - \frac{\bar{S}_2}{s} e^{-\tau_{22}} .$$

The characteristic equation is given by

$$A = \begin{vmatrix} s+a_1 & -a_1 \\ -a_2 & s+a_2+a_3 \end{vmatrix} = s^2 + (a_1 + a_2 + a_3)s + a_1a_3$$

$$= (s - m_1)(s - m_2) , \qquad (A.9)$$

where $m_1$ and $m_2$ are the roots of Eq. (A.9) given by

$$m_{1,2} = 1/2[-(a_1 + a_2 + a_3) \pm ((a_1 + a_2 + a_3)^2 - 4a_1a_3)^{1/2}] \qquad (A.10)$$

The solutions $\hat{\theta}_1$ and $\hat{\theta}_2$ in Laplace space becomes

$$\hat{\theta}_1 = \frac{1}{\Delta}\left[\left(\theta_{10} + \frac{\bar{S}_1}{s} e^{-\tau_{11}} - \frac{\bar{S}_1}{s} e^{-\tau_{12}}\right)(s + a_2 + a_3)\right.$$
$$\left. + \left(\theta_{20} + \frac{\bar{S}_2}{s} e^{-\tau_{21}} - \frac{\bar{S}_2}{s} e^{-\tau_{22}}\right) a_1\right], \qquad (A.11a)$$

$$\hat{\theta}_2 = \frac{1}{\Delta}\left[(s + a_1)\left(\theta_{20} + \frac{\bar{S}_2}{s} e^{-\tau_{21}} - \frac{\bar{S}_2}{s} e^{-\tau_{22}}\right)\right.$$
$$\left. + \left(\theta_{10} + \frac{\bar{S}_1}{s} e^{-\tau_{11}} - \frac{\bar{S}_1}{s} e^{-\tau_{12}}\right) a_2\right] . \qquad (A.11b)$$

In order to invert from Laplace space to real time space it is necessary to split these fractions into partial fractions and then invert each term. The algebra involved is lengthy and is not presented here. The final solutions appear as follows:

$$\theta_1 = C_{11} e^{m_1 t} - C_{12} e^{m_2 t}$$
$$+ C_{13}\left(e^{m_1(t-\tau_{11})} - 1\right) - C_{14}\left(e^{m_2(t-\tau_{11})} - 1\right)\Big] u(t - \tau_{11})$$

$$-\left[C_{13}\left(e^{m_1(t-\tau_{12})} - 1\right) - C_{14}\left(e^{m_2(t-\tau_{12})} - 1\right)\right] u(t - \tau_{12})$$

$$+\left[C_{15}\left(e^{m_1(t-\tau_{21})} - 1\right) - C_{16}\left(e^{m_2(t-\tau_{21})} - 1\right)\right] u(t - \tau_{21})$$

$$- C_{13}\left(e^{m_1(t-\tau_{22})} - 1\right) - C_{16}\left(e^{m_2(t-\tau_{22})} - 1\right)\Big] u(t - \tau_{22}), \quad \text{(A.12a)}$$

$$\theta_2 = C_{21} e^{m_1 t} - C_{22} e^{m_2 t}$$

$$+\left[C_{23}\left(e^{m_1(t-\tau_{21})} - 1\right) - C_{24}\left(e^{m_2(t-\tau_{21})} - 1\right)\right] u(t-\tau_{21})$$

$$-\left[C_{23}\left(e^{m_1(t-\tau_{22})} - 1\right) - C_{24}\left(e^{m_2(t-\tau_{22})} - 1\right)\right] u(t-\tau_{22})$$

$$+\left[C_{25}\left(e^{m_1(t-\tau_{11})} - 1\right) - C_{26}\left(e^{m_2(t-\tau_{11})} - 1\right)\right] u(t-\tau_{11})$$

$$-\left[C_{25}\left(e^{m_1(t-\tau_{12})} - 1\right) - C_{26}\left(e^{m_2(t-\tau_{12})} - 1\right)\right] u(t-\tau_{12}). \quad \text{(A.12b)}$$

The quantities $C_{ij}$ $(i = 1, 2, \quad j = 1..6)$ are given by the following expressions:

$$C_{11} = \frac{\theta_{10}(m_1 + a_2 + a_3) + \theta_{20} a_1}{m_1 - m_2}, \quad \text{(A.13a)}$$

$$C_{12} = \frac{\theta_{10}(m_2 + a_2 + a_3) + \theta_{20} a_1}{m_1 - m_2}, \quad \text{(A.13b)}$$

$$C_{13} = \frac{\bar{S}_1(m_1 + a_2 + a_3)}{(m_1 - m_2)\, m_1}, \quad \text{(A.13c)}$$

$$C_{14} = \frac{\bar{S}_1(m_2 + a_2 + a_3)}{(m_1 - m_2)\, m_2}, \quad \text{(A.13d)}$$

$$C_{15} = \frac{\bar{S}_2 a_1}{(m_1 - m_2)\, m_1} , \qquad \text{(A.13e)}$$

$$C_{16} = \frac{\bar{S}_2 a_1}{(m_1 - m_2)\, m_2} , \qquad \text{(A.13f)}$$

$$C_{21} = \frac{\theta_{20}(m_1 + a_1) +}{m_1 - m_2} , \qquad \text{(A.13g)}$$

$$C_{22} = \frac{\theta_{20}(m_2 + a_1) + \theta_{10} a_2}{m_1 - m_2} , \qquad \text{(A.13h)}$$

$$C_{23} = \frac{\bar{S}_2 (m_1 + a_2)}{(m_1 - m_2) m_1} , \qquad \text{(A.13i)}$$

$$C_{24} = \frac{\bar{S}_2 (m_2 + a_1)}{(m_1 - m_2) m_2} , \qquad \text{(A.13j)}$$

$$C_{25} = \frac{\bar{S}_1 a_2}{(m_1 - m_2) m_1} , \qquad \text{(A.13k)}$$

$$C_{26} = \frac{\bar{S}_1 a_2}{(m_1 - m_2) m_2} , \qquad \text{(A.13l)}$$

Specializations of the general solution given by **Eqs.** (A.12a) and (A.12b) are readily made, e.g. the special case of a heatup transient from room temperature becomes for

$$\theta_{10} = \theta_{20} = 0 ,$$

therefore

$$C_{11}, C_{12}, C_{21}, \text{ and } C_{22} = 0 .$$

Also,

$$\tau_{11} = 0 ,$$

and $\tau_{12}$, $\tau_{21}$, $\tau_{22}$ ar very large.

Thus the solution for $\theta_1$ and $\theta_2$ for a simple heatup transient are

$$\theta_1 = C_{13}\left(e^{m_1 t} - 1\right) - C_{14}\left(e^{m_2 t} - 1\right), \qquad \text{(A.14a)}$$

$$\theta_2 = C_{25}\left(e^{m_1 t} - 1\right) - C_{26}\left(e^{m_2 t} - 1\right). \qquad \text{(A.14b)}$$

Another special case is the cooldown transient from given initial conditions, $\theta_{10}$ and $\theta_{20}$. In this case we have no power sources so $\tau_{11}$, $\tau_{12}$, $\tau_{21}$, and $\tau_{22}$ are all large and the solutions are:

$$\theta_1 = C_{11} e^{m_1 t} - C_{12} e^{m_2 t}, \qquad \text{(A.15a)}$$

$$\theta_2 = C_{21} e^{m_1 t} - C_{22} e^{m_2 t} \qquad \text{(A.15b)}$$

Some examples of the use of Eqs. (A.14a) and (A.14b) were given previously (Kruger and Ramey, 1974). It was also pointed out that to predict the transients appropriate mean values of the heat transfer conductances and system heat capacitances are required. The initial experiments with the chimney model were directed at obtaining these quantities.

Derivations for the One-Mass Transient Model

The results from the heatup transient experiments showed that the slopes of the temperature curves for the water and metal were nearly the same throughout the transient except during the very early stages of the heatup transient. Additionally, the temperature difference between water and metal were not great for the water/rock runs (order of 10°F) while the difference was somewhat larger for the water runs. Thus the system might be represented by only one lumped mass. This representation is convenient when evaluating the system effective mass and the derivations are presented in the following.

Adding Eqs. (A.4a) and (A.4b) with the understanding that $S_1$ is continuously and $S_2$ is "off" and using the continuity equation to cancel the last two terms in Eq. (A.4a), there results

$$(M_w C_1 + M_r C_r)\frac{dT_1}{dt} - M_2 C_2 \frac{dT_2}{dt} + h_2 A_2 (T_2 - T_\infty) = S_1 .$$

Assuming $dT_1/dt = dT_2/dt$ and letting $T_1 = T_2 = T$ there results after introduction of the temperature variable $\theta = T - T_\infty$,

$$MC \frac{d\theta}{dt} + h_2 A_2 \theta = S_1 , \qquad \text{(A. 16)}$$

where the total system heat capacitance MC is given by

$$MC \triangleq M_w C_1 + M_r C_r + M_2 C_2 \qquad \text{(A. 17)}$$

## APPENDIX B

## DERIVATIONS FOR DATA REDUCTION PROCEDURES

### Derivations for Specific External Energy Transfer Parameter

Consider the annular control volume enclosing the steel chimney with connecting inlet and outlet lines and insulation. This control volume by definition excludes the water/rock system contained inside the chimney and in the inlet/outlet piping. It is of interest to determine the net energy transfer from the chimney wall to the water/rock system ("wall effect"). There are four energy terms involved:

1. Heat losses from the chimney of magnitude $h_2A_2\theta_2$ (Btu).
2. Energy storage in the chimney metal of magnitude $M_2C_2\theta_2$ (Btu).
3. Net rate of energy transfer from the chimney system to the water/rock system denoted by $\dot{Q}_m$ (Btu/hr).
4. Electrical energy supply by the tape heaters on the chimney outside surface denoted by $S_2$ (Btu/hr).

An energy balance on the chimney control volume yields the equation

$$\frac{\partial}{\partial t}(M_2C_2\theta_2) + h_2A_2\theta_2 + \dot{Q}_m = S_2 \quad . \tag{B.1}$$

A mean value of $Q_m$ between distinct times $t_1$ and $t_2$ can be obtained when the mean values of $\theta_2$, $C_2$ and $S_2$ in this time interval are available. Solving Eq. (B.1) for $Q_m$ yields

$$(\bar{\dot{Q}}_m) \cong \bar{S}_2 - M_2 \frac{(C_2\theta_2)_2 - (C_2\theta_2)_1}{t_2 - t_1} - h_2A_2\bar{\theta}_2 \quad . \tag{B.2}$$

The total net energy transfer from the chimney to the water/rock system can be computed by integrating Eq. (B.1),

$$\int_0^{t_f} \dot{Q}_m dt = Q_m = \int_0^{t_f} S_2 dt + M_2 \int_{\theta_{2_f}}^{\theta_{2_o}} d(C_2\theta_2) - h_2A_2 \int_0^{t_f} \theta_2 dt \quad . \tag{B.3}$$

Derivations for Condenser Heat Balance

A diagram of the condenser showing locations of thermocouples and the notation to be used in the following derivation is shown in Fig. B.1. The condenser and the short piping sections carrying hot fluids are well insulated. Therefore, it is assumed that the heat losses are negligible. The energy balance based on Eq. (A.2) then becomes, neglecting the rate of change of storage because of the small mass involved,

$$\dot{m}_c(i_{C,out} - i_{C,in}) = \dot{m}_p(i_{H,in} - i_{H,out}) .$$

It is convenient to use the temperature measurements on the cool side and using the mean specific heat for water in the temperature range or interest there results

$$\dot{m}_c \bar{C}_p(T_{C,out} - T_{C,in}) = \dot{m}_p(i_{H,in} - i_{H,out}) .$$

All quantities here are known from measurements except $i_{H,in}$ which is the chimney exit enthalpy. Thus,

$$i_e = i_{H,in} = i_{H,out} + \frac{\dot{m}_c}{\dot{m}_p} \bar{C}_p(T_{C,out} - T_{C,in}) . \qquad (B.4)$$

Derivations for Chimney Flash Front Location

The sight glass installed on the chimney for flash front location observation is not as well insulated as the chimney itself and consequently the temperature of the water in the sight glass tends to remain lower than in the chimney. Thus, the observed liquid level is not necessarily the true flash front position due to the density difference of the two water columns. A density correction to the observed measurement is derived using the notation shown on Fig. B.2. At point (1) the pressure due to the two water columns is equal and therefore

$$\frac{H - \ell'}{v_{SG}} = \frac{H - \ell}{v_L}$$

Solving this relationship for the corrected level $\ell$, there results in dimensionless fo m

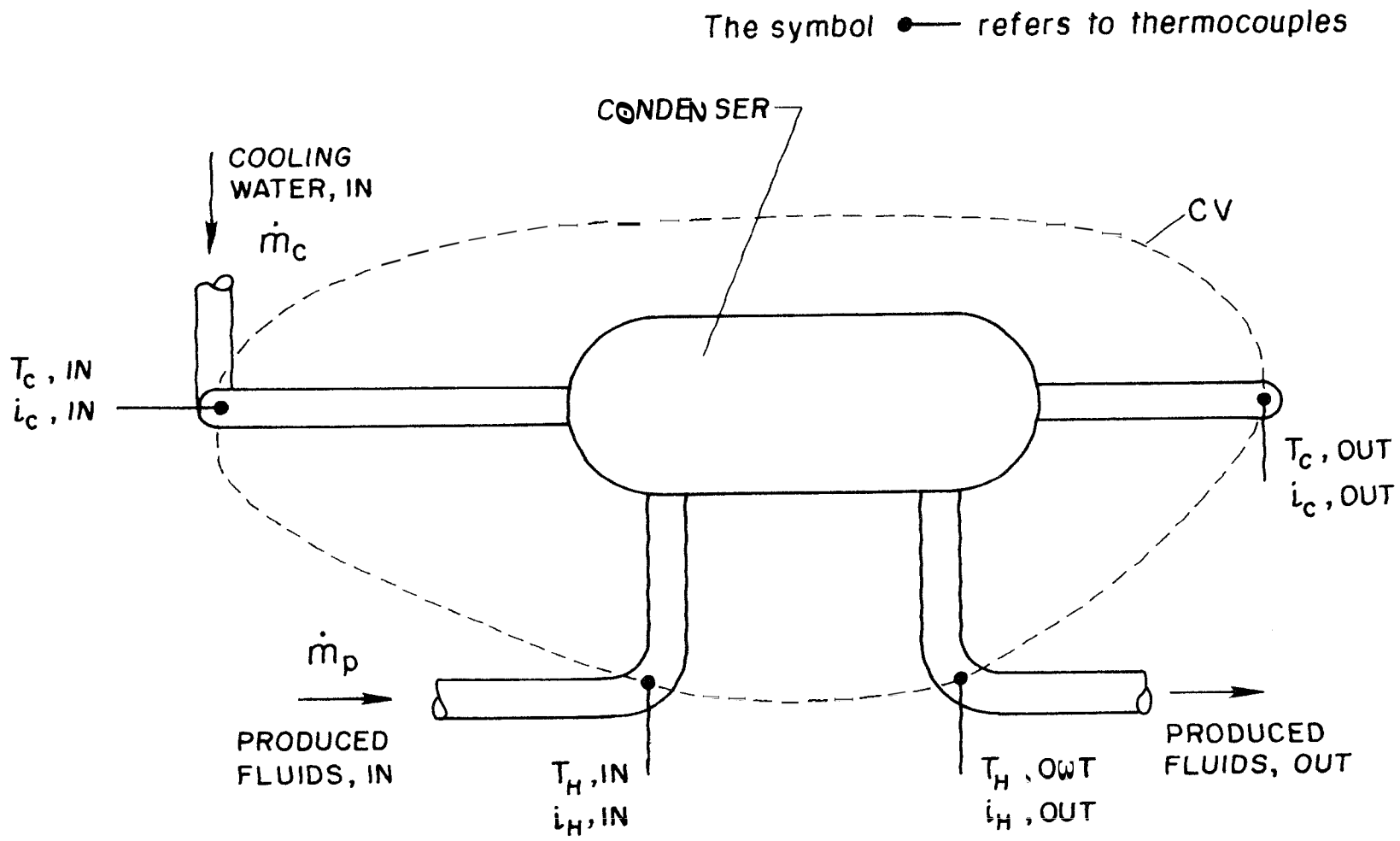


Figure B.1 Control volume for condenser heat balance

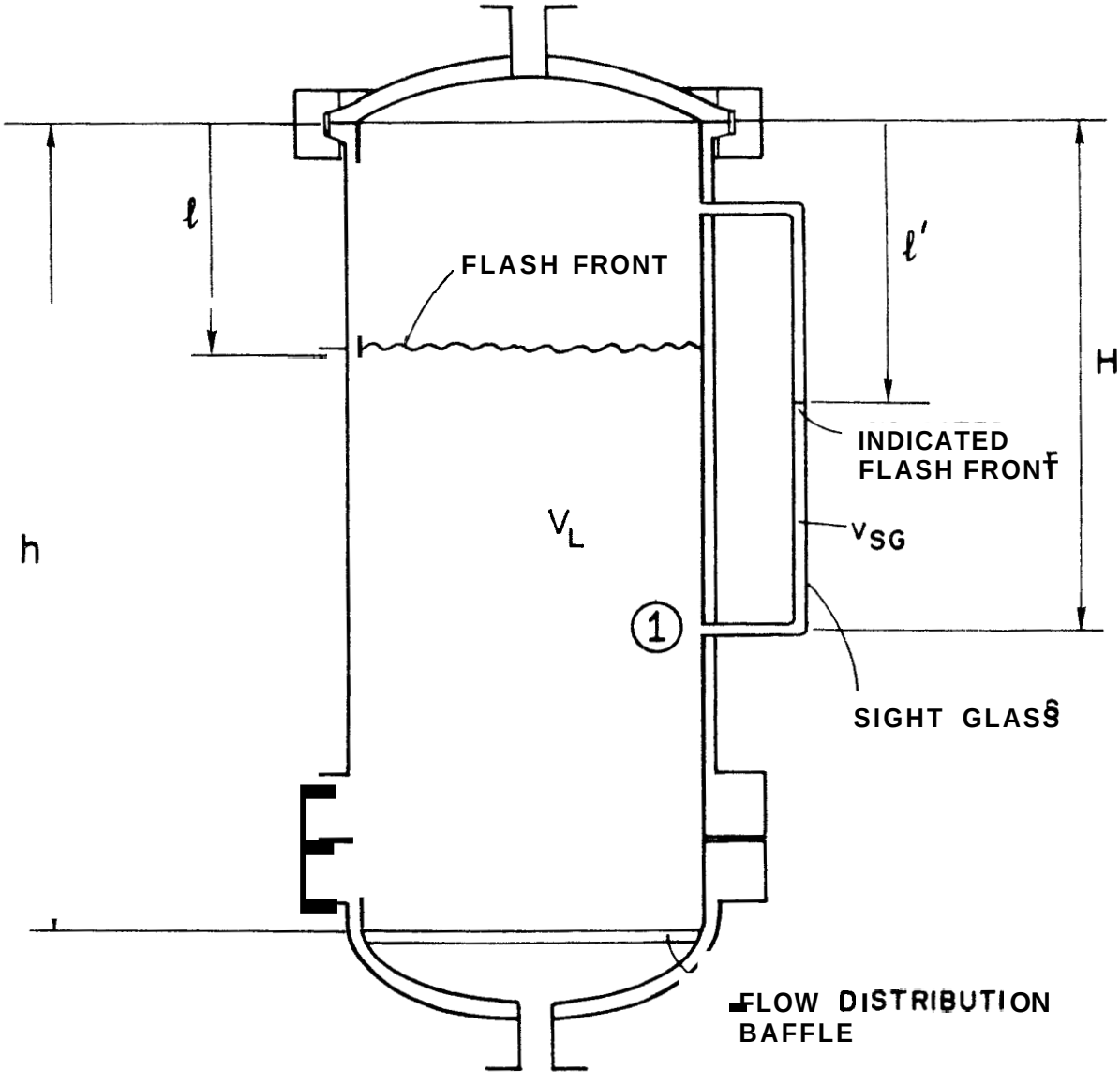


Figure **B.2** Diagram of chimney and sight glass showing nomenclature for level density correction

$$\frac{\ell}{h} = \left(1 - \frac{v_L}{v_{SG}}\right)\frac{H}{h} + \frac{v_L}{v_{SG}}\frac{\ell'}{h} \quad . \tag{B.5}$$

Derivations for Void/Steam Quality Relationship

A diagram of the chimney and connecting inlet/outlet piping is shown on Fig. B.3. The notation used for the various volumes contained between the isolation values are also indicated on the diagram. The total volume containing either steam or liquid is given by

$$V = V_d + V_{sc} + V_c\varphi + V_i = V_g + V_f \quad . \tag{B.6}$$

The volume of the space occupied by steam only is

$$V_g = V_d + V_{sc} + V_c\varphi\frac{\ell}{h} \quad . \tag{B.7}$$

Using these in the definition of the void fraction (Eq. (5.8)) there results

$$\alpha = (V_d + V_{sc} + V_c\varphi\frac{\ell}{h})/V \quad . \tag{B.8}$$

A void/quality relationship can now be derived. The mass of liquids present in the chimney in terms of $V_f$ and the specific volume is

$$M_f = V_f/v_L \quad .$$

Use this expression in the definition of steam quality (Eq. (5.7)) which yields

$$X = 1 - \frac{V_f}{v_L M_w} \quad ,$$

or

$$V_f = (1 - x)\, v_L M_w \quad .$$

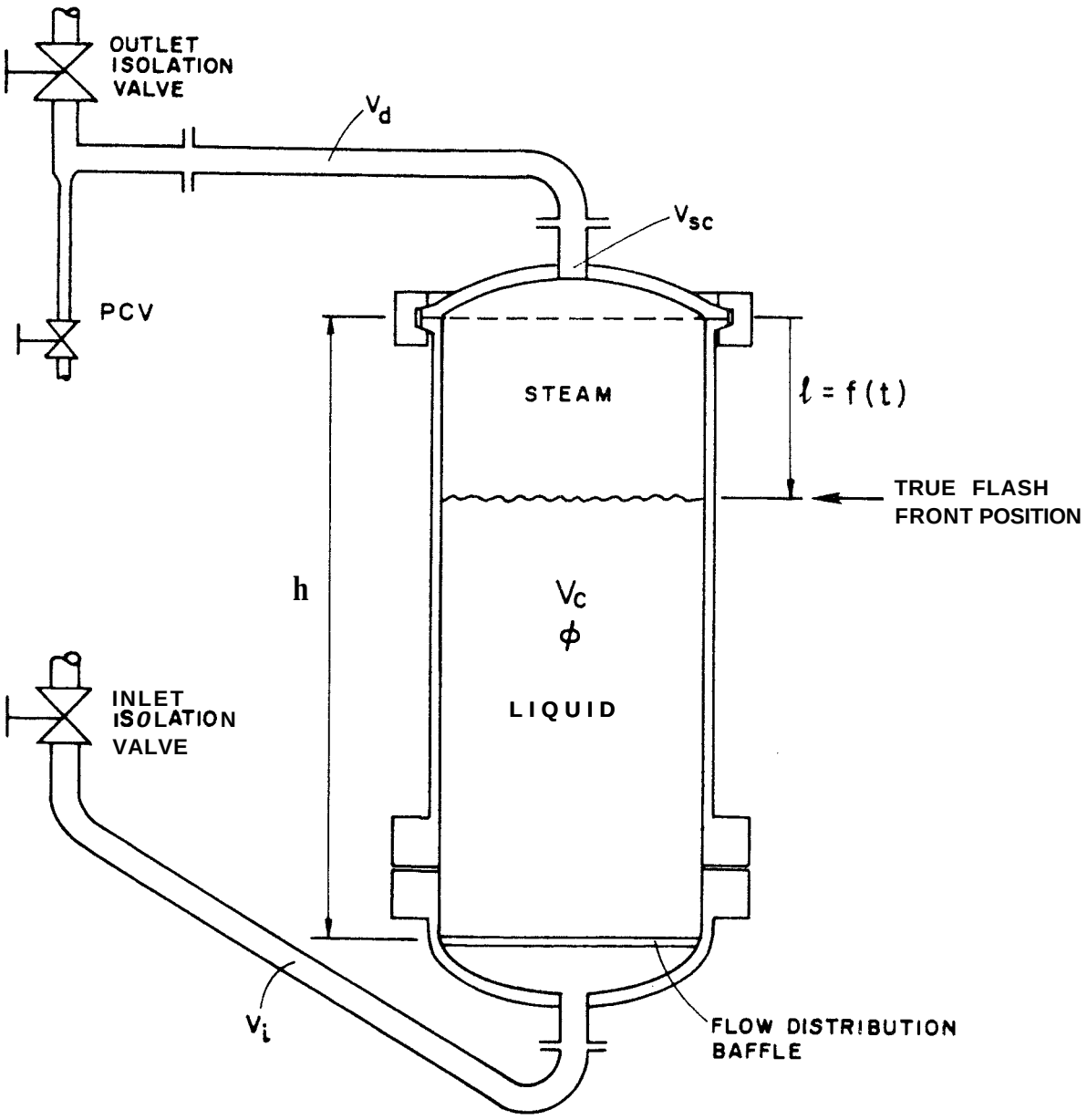


Figure B.3 Diagram of chimney and inlet/outlet piping showing nomenclature used for level analysis

Substitute this into the definition of the void fraction (Eq. (5.8)) and get

$$\alpha = 1 - \frac{(1 - x)\, v_L M_w}{V} \quad .$$

Dividing through by the initial mass of water in the system, $(M_w)_o$, and redefining variables, the void/quality relationship is obtained:

$$\alpha = 1 - \frac{v_L}{v_o} (1 - x)\, M_w^* \quad . \tag{B.9}$$

An expression for the $\ell/h$ ratio can be derived using the notation of Fig. B.3. The total amount of water (steam and liquid phases) can be expressed as

$$M_w = \frac{V_d}{(v_G)_d} + \frac{V_{sc}}{(v_G)_{sc}} + \frac{V_c \varphi}{(v_G)_c} \frac{\ell}{h} + \frac{V_c \varphi}{(v_L)_c} \frac{h - \ell}{h} + \frac{V_i}{(v_L)_i} \quad ,$$

where the $v_G$'s are the mean specific volumes for the steam in the various steam spaces and the $v_L$'s have a similar meaning for the liquid spaces. One can solve this relationship for the $\ell/h$ ratio which yields after introducing the mass fraction $M_w^*$,

$$\ell/h = \left[\frac{V_d}{V_c \varphi} \frac{1}{(v_G)_d} + \frac{V_{sc}}{V_c \varphi} \frac{1}{(v_G)_{sc}} + \frac{1}{(v_L)_c} + \frac{V_i}{V_c \varphi} \frac{1}{(v_L)_i} - \frac{M_w^*}{V_c \varphi / (M_w)_o}\right] \frac{(v_L)_c}{1 - (v_L/v_G)_c} \quad .$$

A simplification of this expression can be made if it is assumed that the steam in all steam spaces is saturated and all liquid is saturated. The previous expression then becomes

$$\ell/h = \left[\left(\frac{V_d}{V_c \varphi} + \frac{V_{sc}}{V_c \varphi}\right) \frac{1}{v_g} + \left(1 + \frac{V_i}{V_c \varphi}\right) \frac{1}{v_f} - \frac{M_w^*}{V_c \varphi / (M_w)_o}\right] \frac{v_f}{1 - (v_f/v_g)} \quad . \tag{B.11}$$

It is recognized that errors may be introduced by this approach since there is considerable amount of moisture due to condensation in the outlet line.

## REFERENCES


Atkinson, Charles H. and Ward, Don C. "Project Gasbuggey: Status Report," J. Petrol. Technol., 19:1319-1324, October 1967.

Goldsmith, Alexander, Waterman, Thomas E., and Hirschhorn, Harry J. Handbook of Thermophysical Properties of Solid Materials, Vol. 2. The Macmillan Company, 1961.

Griffiths, J. C. Scientific Method in Analysis of Sediments. McGraw-Hill Book Co., 1967.

Kline, S. J. and McClintock, F. A. "The Description of Uncertainties in Single Sample Experiments," Mechanical Engineering:,75, 1953, p. 3.

Kreith, F. Principles of Heat Transfer, 2nd ed. International Textbook Co., 1965.

Kruger, Paul and Otte, Carel (eds.). Geothermal Energy, Resources, Production, Stimulation. Stanford University Press, 1973.

Kruger, P., and Ramey, H. J. Stimulation of Geothermal Aquifers, Progress Report No, 1. Advanced Technology Dept., RANN, National Science Foundation, Grant No. GI-34925, March 1973.

Kruger, P., and Ramey, H. J. Stimulation and Reservoir Engineering of Geothermal Resources, SGP-TR-1. Advanced Technology Dept., RANN, National Science Foundation, Gront No. GI-34925, June 1974.

Krumbein, W. C. "Measurement and Geological Significance of Shape and Roundness of Sedimentary Particles," J. Sediment Petrol., 11:64-72, 1941.

Pittijohn, F. J. Sedimentary Rocks, 2nd ed. Harper and Bros., 1951.